

FREE VIBRATIONS OF CURVED BOX GIRDERS

by

Mohammad Myassar Tabba, B.Sc.(Civil Eng.)

A THESIS

submitted to

The FACULTY OF GRADUATE STUDIES AND RESEARCH
in partial fulfilment of the requirements
for the Degree of Master of Engineering

Department of Civil Engineering
and Applied Mechanics
McGill University,
Montreal, Canada.

July 1972

TO

MY

PARENTS

'There are strings,' said Mr. Tappertit,
'in the human heart that had better not
to be vibrated.'

- Charles Dickens -

TABLE OF CONTENTS

ABSTRACT,	i
RESUME,	ii
ACKNOWLEDGMENTS,	iii
LIST OF FIGURES,	iv
LIST OF TABLES,	vi
NOMENCLATURE,	vii

Chapter

1

1-1	Introduction,	1
1-2	Review of Previous Work,	3
a	Straight thin walled girders,	4
b	Curved solid girders and rings,	4
c	Thin walled curved girders,	5
1-3	Scope of the Work,	6

2 THEORETICAL ANALYSIS, 8

2-1	Mathematical Model,	8
2-2	Equilibrium Equations,	10
2-3	Elasto-Statical Relationships,	12
2-4	Inertia Forces,	15
2-5	The Warping Function,	17
2-6	Displacement Functions and Boundary Conditions,	20
2-7	The Frequency Equation,	24

Chapter

- 2-8 Eigen Functions, 29
- 2-9 Orthogonality of Eigenfunctions, 31
- 2-10 Special Cases, 33
- 2-11 Parametric Study, 36
- 3 EXPERIMENTAL PROGRAM, 41
 - 3-1 Design, Description and Febrication of Models, 41
 - 3-1-1 Description of the models, 42
 - 3-1-2 Material properties, 44
 - 3-1-3 Fabrication of the models, 48
 - 3-2 Dynamic Model Tests, 49
 - 3-2-1 The exciting system, 51
 - 3-2-2 Pickup system, 53
 - 3-2-3 Display system, 54
 - 3-2-4 The resonance criteria, 54
 - 3-2-5 Experimental procedure, 56
 - 3-2-6 Experimental results, 59
- 4 ANALYSIS OF TEST RESULTS, 61
 - 4-1-1 Geometric properties of models, 61
 - 4-1-2 Mechanical properties of models, 63
 - 4-2 Natural Frequencies and Modal Shapes, 65
- 5 DISCUSSION, SUMMARY AND CONCLUSIONS, 70
 - 5-1 Limitations of the Results, 70
 - 5-2 Summary, 71
 - 5-3 Conclusions, 73

REFERENCES, 74

FIGURES, 80

Appendix I Warping in Box Girders with Overhangs, 120

Appendix II FORTRAN IV Program, 124

FREE VIBRATIONS OF CURVED BOX GIRDERS

by

M. Myassar Tabba

Department of Civil Engineering
and Applied Mechanics
McGill University
Montreal, P.Q.

M.Eng. Thesis
July 1972

ABSTRACT

The problem of coupled free vibrations of curved thin walled girders of asymmetric cross-section is examined in this thesis. The general governing differential equations are derived for quadruple coupling between the two flexural, tangential and torsional vibrations.

An approximate solution for the case of triple coupling between the two flexural and the torsional vibrations is given for a simply supported girder, assuming non-deformable cross-sections and uniform specific gravity of the material of the box, accounting for warping but neglecting axial forces and rotary inertia. The frequency equation and eigenfunctions are given with the orthogonality condition satisfied. A parametric study is conducted to investigate the effect of various geometric parameters on the natural frequencies.

An experimental investigation was carried out to compare the behavior of two curved box girder models with theory. The first model had a single cell cross-section symmetric with respect to the vertical axis. The second had an asymmetric two cell section. Reasonable agreement between experimental values of the first four natural frequencies and modal shapes and those predicted by theory was obtained.

VIBRATIONS LIBRES DE POUTRES EN CAISSON COURBES

M. Myassar Tabba

Département de génie civil
et de mécanique appliquée
Montréal, P.Q.

Thèse de maîtrise
Juillet 1972

RESUMÉ

Le problème des vibrations libres couplées de poutres courbes à parois minces, et de section transversale asymétrique est examiné dans le présent ouvrage. Les équations différentielles du problème sont dérivées pour un couplage quadruple entre les deux vibrations de flexion, ainsi que celles de torsion et tangentielle.

Une solution approchée est donnée dans le cas d'un couplage triple entre les deux vibrations de flexion et celle de torsion, pour le cas d'une poutre simplement appuyée, en supposant que les sections transversales sont indéformables. Il est tenu compte du voilement des sections transversales, mais les forces axiales et l'inertie de rotation ont été négligées. L'équation aux fréquences et les fonctions propres sont données et la condition d'orthogonalité est satisfaite. Une étude a été réalisée pour évaluer l'influence de divers paramètres géométriques sur les fréquences propres.

Une étude expérimentale a également été conduite pour comparer à la théorie le comportement de deux modèles de poutres en caisson courbes. Le premier modèle consistait en un caisson unique, symétrique par rapport à un axe vertical. Le deuxième modèle consistait en un caisson double et asymétrique.

Les résultats obtenus pour les quatre premières fréquences propres et les modes de vibration correspondants ont confirmé raisonnablement ceux prédits par la théorie.

ACKNOWLEDGMENTS

The author would like to thank Professor Carl J. Turkstra of the Department of Civil Engineering and Applied Mechanics, who supervised this work, for his encouragement and helpful suggestions.

He wishes to thank Mr. Reinhard Schutz for translating an invaluable paper "Ref.(11)" from German, the Translations Section of the National Science Library, NRC, Ottawa for translating the aforementioned and another paper "Ref.(10)" from German, Dr. Usen E. Eka who proofread Chapter Two, Dr. René Tinawi who prepared the finite element program used in Appendix I, the staff of the Civil Engineering Laboratory for their hand, Mr. George Dedic of the Instruments Laboratory, Department of Mechanical Engineering, for his help in solving some electronic problems, all fellow graduate students, particularly Mr. Adel Fam for his inspiration and valuable discussions, and Margaret Powell for an excellent typing of the manuscript.

He also wishes to acknowledge the financial assistance of the National Research Council of Canada.

LIST OF FIGURES

Figure

- 2.1 Idealized Model of a Simply Supported Curved Asymmetric Box Girder, 80
- 2.2 Forces acting on an Element of a Curved Girder, 80
- 2.3 Net Displacements of any Point on the Cross-Section of a Thin walled Girder, 81
- 2.4-13 First and Second Modes coupled Natural Frequencies of Curved Girders of various Geometric Properties, 83-100
- 3.1 General Plan and Cross-Sectional Dimensions of Model A, 101
- 3.2 General Plan and Cross-Sectional Dimensions of Model B, 102
- 3.3 General View of Model B, 103
- 3.4 Left Support of Model B, 103
- 3.5 Right Support of Model B, 104
- 3.6 Shaker Head and Attachment to the Model, 104
- 3.7 Roller Point Support, 105
- 3.8 Fixed Point Support, 105
- 3.9 Stress Strain Creep Diagram of Plexiglas, 106
- 3.10 Correction Factor of the Modulus of Elasticity vs. Frequency for Plexiglas, 107
- 3.11 Curved Webs mounted on special Aluminum Frameworks, 108
- 3.12 Curved Webs glued to the Upper Deck, 108
- 3.13 Block Diagram of Experimental Setup, 109
- 3.14 The Shaker, Load Cell and their Attachment to the Model, 110
- 3.15 Circuitry of Load Cell, 110
- 3.16 Calibration of Transducer T-3 with Channel 6 of the U-V Recorder, 111

Figure

- 3.17 Load Cell Calibration Graph, 112
- 3.18,19 Equipment used in the Experimental Setup, 113
- 3.20 Typical Records, 114
- 4.1 Warping Displacement Diagrams of Box Models, 115
- 4.2, 3, First, Second, Third and Fourth Modal Shapes of the
4, 5 Upper Deck of Model B, 116, 117, 118, 119
- I Finite Element Analysis of Warping Displacements in
a Box Girder with Overhangs, 123

LIST OF TABLES

Table

- | | |
|------------|---|
| 2-1 | Values of various Parameters for Cases examined in the Parametric Study, 37 |
| 3-1 | Test Results of Tension Coupons, 45 |
| 3-2 | Experimental Values of the first Four Natural Frequencies of Models A and B, 59 |
| 4-1 | Physical Properties of Models A and B, 64 |
| 4-2(A & B) | Natural Frequencies and Amplitudes of Modal Shapes of Models A and B respectively, 66, 67 |
| 4-3 | Corrected Theoretical Natural Frequencies vs. Experimental Values, 68 |

NOMENCLATURE

A	Area of the cross-section (material only)
B	Bimoment
E	Modulus of elasticity
E_c	Modulus of elasticity when creep terminates
E_d	Dynamic modulus of elasticity
f	Warping function
G	Shear modulus
H	Twisting moment
I_o	Polar moment of inertia with respect to the shear center
I_p	Polar moment of inertia with respect to the centroid
I_w	Warping constant (sectorial moment of inertia)
I_x, I_y	Moments of inertia about the x and y axes respectively
I_{xy}	Product of inertia about the x and y axes
K_t	St.Venant's torsion constant
ℓ	Length of the curved girder along the centroidal axis
M_x, M_y	Bending moments with respect to the x and y axes respectively
N	Normal force acting through the centroid
P_x, P_y, P_z, P_ϕ	Uniformly distributed external loads in the x , y , z , directions and uniformly distributed twisting moment

\vec{P}_i	State vector of any point on the girder vibrating in the i th mode.
q	Indeterminate shear flow in the box
$\vec{q}, \vec{r}, \vec{s}$	Base vectors mutually orthogonal and parallel to the x, y, z axes respectively.
Q_x, Q_y	Shear forces acting at the shear center in the x and y directions
r_x	$\frac{1}{I_x} \int y^2 x \, dA$
r_y	$\frac{1}{I_y} \int x^2 y \, dA$
R	Radius of curvature of the girder
t	Time
u, v, w	Displacements of the shear center in the $x, -y$ and z directions respectively
U_i, V_i	Amplitudes of the i th modal displacements in the x and $-y$ directions respectively
w_s	Longitudinal displacement of a point on the wall's centerline
\hat{w}	Sectorial coordinate of a point on the wall's centerline
w_{iz}	Amplitude of axial (tangential) displacement of a point located at section z and vibrating in the i th mode
x, y	Orthogonal centroidal axes, radial in-plane of curvature and normal to the plane of curvature respectively
x_0, y_0	Coordinates of the shear center

z, z_1	Curved axes with origin at the left support, mutually orthogonal to the x and y axes and passing through the centroids and shear centers respectively
α	Correction factor of the calculated frequency to account for the dynamic modulus of elasticity
α_1	Central angle
β	I_{xy}/I_x
γ	I_{xy}/I_y
δ	Wall's thickness
δ_x	x_o/R
δ_y	y_o/R
δ_{ui}, δ_{vi}	Horizontal and vertical displacements of any point located on the wall of the girder's cross-section due to an angle of twist ϕ_i in the i th mode
δ_{ij}	The Kronecker delta
η	$1 - \frac{1}{R^2 \theta_i^2}$ Mode - Curvature Index
ϕ	Angle of twist of the cross-section measured clockwise from the $+y$ direction
ϕ_i	Amplitude of angle of twist of a cross-section vibrating in the i th mode
μ	$1 - K_t/I_p$
ω_i	The i th coupled natural frequency of the curved girder
$\omega_{ui}, \omega_{vi}, \omega_{\phi i}$	Natural frequencies of the i th mode of vibration in the u , v and ϕ directions of an equivalent straight

girder of length ℓ and whose cross-section is doubly symmetric

Ω_j Area enclosed by the wall's center-line of the j th cell.

ψ $1 - \beta \gamma = 1 - \frac{(I_{xy})^2}{I_x I_y}$ Symmetry Index

ρ Mass per unit volume of the material used

ρ_x r_x/R

ρ_y r_y/R

θ_i $\frac{i\pi}{\ell}$ where i is the mode number

$(\)'$ Differentiation with respect to z

$(\)^\cdot$ Differentiation with respect to t

CHAPTER 1

1-1 Introduction

In recent years thin walled curved beams and girders have been used extensively as structural members in bridges, ships and aircrafts. Thin walled box sections possess relatively high torsional and warping rigidities and as a result are suited for long spans, large curvatures, or where large torsional moments act on a girder.

The theoretical and experimental investigation reported in this work deals with the free vibrations of simply supported curved girders with thin walled asymmetrical cross sections. Solutions to several special cases such as:

- i] curved box girders of symmetric cross section with respect to one or two axes,
- ii] curved bars of solid section,
- iii] curved girders of thin walled open cross section,
- iv] straight girders of box or open symmetric or asymmetric section,

can be obtained from the general theory. Analytical solutions for these special cases have been obtained previously, but experimental verification was undertaken to check several simplifying assumptions.

Asymmetry of the cross section with respect to the horizontal axis may arise in bridge design when the upper deck of the section is made wider than the bottom deck to allow for sufficient traffic lanes. If exterior webs are thicker than inner webs due to differences in span,

asymmetry with respect to the vertical axis is introduced.

The free vibrations of a straight doubly symmetric girder in bending and torsion are uncoupled so that the girder may vibrate in either vertical or horizontal flexural modes without vibrating in the torsional mode. In this case the shear center coincides with the centroid of the cross section and in a bending mode inertia forces which are effectively applied at the centroid of the section do not cause twist.

If there is only one axis of symmetry of the cross section then flexural vibrations in the direction of this axis will be independent of other vibrations, and coupling will exist only between torsional vibrations and flexural vibrations in the other direction. Due to a shift in the position of the shear center along the axis of symmetry the bending inertia forces generate a torque as well as bending moments.

If the cross section has no centroidal axes of symmetry, a case of triple coupling arises, i.e. flexural vibrations in one direction are coupled to those in the other direction and to torsional vibrations. In this case the shear center is shifted from the centroidal axes in two directions, and bending inertia forces in both directions cause a twisting moment about the shear center.

It can be seen that coupling of vibrations in straight girders is dependent on the geometric properties of the cross-section. Any change in the properties of the girder along the axis may also result in coupling.

For girders curved in plan with doubly symmetrical cross-section, triple coupling between vibrations normal to the plane of curvature, torsional vibrations and tangential vibrations occurs due to the curvature of the girder's axis. Flexural vibrations in the plane of curvature are independent of the others.

If the cross-section of the curved girders has only one centroidal axis of symmetry normal to the plane of curvature, then a case of quadruple coupling prevails between the torsional, and tangential vibrations and the two flexural modes. Moreover if the cross-section has no centroidal axes of symmetry in any direction, quadruple coupling also occurs. However, coupling between tangential vibrations and components of vibration in other directions is weak for low frequencies and its effect on the lower modes may be negligible. For this reason many investigators do not consider coupling of the tangential vibrations when dealing with out of plane vibrations.

1-2 Review of Previous Work

Extensive research has been performed on the static behaviour of thin walled girders. The work of Vlasov (40)* on thin walled beams is substantial and widely recognized. Of particular interest to the present work are the elastostatical relationships for curved girders which were developed by Vlasov. However Dabrowski (9) showed that several terms were omitted in Vlasov's derivation which might be significant in some cases. Dabrowski (10, 11) later extended his work to include open and closed thin walled girders and obtained solutions for

*

Numbers in brackets refer to References.

different loading conditions.

Several authors have investigated the dynamic response of thin walled girders. Only those dealing with free vibrations of solid or thin walled straight or curved girders are reviewed here.

(a) Straight thin walled girders - The first attempt to examine the coupled flexural-torsional vibrations of a simply supported beam was by Timoshenko (37), who solved the case of double coupling of a straight thin walled beam with one axis of symmetry. Federhofer (13) derived and discussed differential equations for the general case of asymmetric cross-section. Vlasov (40) obtained a solution for the case of triple coupling in a simply supported girder with asymmetrical cross-section. Gere and Lin (18) also solved the general case of triple coupling of a straight thin walled girder having an asymmetrical cross-section and determined the natural frequencies of simply supported, fixed end and cantilever beams. An exact solution of the general governing differential equations was given for the case of a simply supported girder only. The Rayleigh-Ritz method was used to derive approximate expressions for other end conditions.

(b) Curved solid girders and rings - The problem of free vibrations of curved bars and rings has been studied extensively and only a few major developments are mentioned here. Lamb determined the frequency equation of unconstrained complete elastic rings using the inextensional deflection theory. Love (27) quoted Lamb's work and extended it to find the eigenvalues and eigenfunctions corresponding to torsional and flexural vibrations in and out of the plane of curvature.

Lang (25) derived the eigenvalues and eigenfunctions for free in-plane vibrations of complete and incomplete elastic rings, considering both extensional and inextensional deformation theories. He verified the inextensional theory experimentally. Volterra (41, 42, 43) in a series of papers, formulated and solved the equations of motion of a curved solid elastic bar using the so-called "Method of Internal Constraints". Shear deformations and rotary inertia were considered for doubly symmetric cross-sections. Later, Volterra and Morell (44, 45) used the Rayleigh-Ritz method to determine the lowest natural frequency for fixed elastic arcs vibrating out of their plane of curvature. Arcs of various centroidal layouts (circle, cycloid, catenary, and parabola) were analyzed. Reddy (34) used the flexibility matrix method assuming lumped masses to solve the problem of free vibrations of any combination of straight and curved bars.

(c) Thin walled curved girders - Yonezawa (47) analyzed the free vibrations of curved simply supported fan-shaped plates and under static uniform loads. Using the theory of orthotropic plates he formulated the differential equations, gave the exact and an approximate solution, and investigated the effect of several geometric parameters on natural frequencies.

Culver (8) obtained the exact solution for the problem of free vibrations of a simply supported curved girder having doubly symmetric cross-section. He also used the Rayleigh-Ritz method to obtain approximate solutions for the cases of fixed-fixed or fixed-simply supported ends. Tan and Shore (36) investigated the dynamic response of curved

girders of doubly symmetric cross-section under constant moving loads, and examined the case of free vibrations assuming flexural damping.

Christiano (6, 7) investigated the dynamic response of a curved, simply-supported thin walled girder, having a vertical axis of symmetry under sprung moving load. He also solved the problem of free vibrations and examined the effect of some geometric parameters.

Oestel (31) obtained a solution to the problem of free and forced vibrations of a two-span curved girder having a doubly symmetric cross-section. Lagrange's equations were used together with Lagrange multipliers to account for constraints at the intermediate support. Komatsu and Nakai (23) solved the general case of triple coupling for a curved girder of asymmetric cross-section. Coordinates were transformed to the principal axes of the cross-section to simplify the elastostatical equations. Field tests on two bridges excited by a 20-ton truck travelling at various speeds, another bridge excited by a shaker and laboratory tests on a model showed reasonable agreement between theory and experiment according to the authors.

1-3 Scope of the Work

The investigation reported in this work is divided into two parts theoretical and experimental.

The theoretical analysis examines the free vibrations (natural frequencies and modal functions) of simply supported curved girders, having thin walled geometrically asymmetrical cross-section. Solutions for several special cases such as straight or curved girders of thin

walled or solid, open or closed, uni or doubly symmetrical cross-section, can be obtained from the general case. It is assumed that both supports allow warping and that one support permits tangential displacements. Damping, rotary inertia and shear deformations are neglected. The cross-section is assumed to be non-deformable and the center of gravity coincides with the centroid. Local free vibrations of the constituent members or of a part of the span (upper deck, lower deck, torsional vibrations between the diaphragms) are not considered in this study.

In the experimental investigation two curved box girder models were tested under a concentrated dynamic load. The first model was a single box section uni-symmetrical with respect to the vertical centroidal axis, the second model was a two cell section of asymmetric cross-section. Resonant frequencies were isolated by a trial and error procedure based on frequency sweep tests and a series of shaker positions.

CHAPTER 2

THEORETICAL ANALYSIS

2-1 Mathematical Model

The structure under consideration is a single span simply supported circular curved girder having a constant asymmetrical cross-section (Fig.2.1), which can be a multicell box, single cell box, open or solid. The geometry of the cross-section affects only the cross-sectional properties but not the derivations given hereafter.

The cross-section is assumed to be non-deformable, which implies that there is a sufficient number of diaphragms, infinitely rigid in their own plane but flexible out of their plane. The girder is assumed to be supported at two point supports, the left one is a hinge and the right one is a roller. The material is assumed elastic and homogeneous. Damping is neglected since its effect on natural frequencies and modal shapes is generally small.

The notation adopted is that of Christiano (6) while the sign conventions are identical to those of Dabrowski (11). The position of any point in the girder is defined with respect to an orthogonal set of axes, x , y , z as shown on Fig.2.1, with the origin of the z axis at the centroid of the lefthand support. Axes x and y are sliding axes with origin at the z axis, in plane and normal to the plane of curvature respectively.

The hinge at the left support will allow warping of the cross-section and rotation about the x and y axes, but prevents movement

in the x , y and z directions at the shear center or twist ϕ of the whole cross-section. The roller at the right support provides similar constraints except that movement in the z direction is permitted.

For an asymmetrical cross-section, the shear center has coordinates x_0 , y_0 measured from the center of gravity of the cross-section (Fig. 2.2). The centroid and center of gravity of any section are assumed coincidental. The displacements of the shear center are defined as u , v , w in the x , $-y$, z_1 directions respectively. An angle of twist ϕ measured clockwise from the y axis is also defined. The center of twist is assumed coincident with the shear center.

The external distributed loads are p_x , p_y , p_z , in the x , y , z directions plus a distributed torque p_ϕ , all applied along the axis of the shear centers z_1 . The internal stress resultants are the shear forces Q_x , Q_y , and twisting moment H applied along the axis z_1 , as well as a normal force N and bending moments M_x , M_y applied along the centroidal z axis. Forces acting on an infinitesimal element dz of radius of curvature R are shown in Fig. 2.2. The bimoment B which is statically equivalent to zero is not shown.

The cross-section which is generally asymmetric has moments of inertia I_x , I_y with respect to the x and y axes, a product of inertia I_{xy} , a polar moment of inertia I_p with respect to the centroid, cross-sectional area A , a St.Venant's torsion constant K_t , and a warping constant I_w .

2-2 Equilibrium Equations

Consider the equilibrium of an infinitesimal element of length $dz = R d\alpha$, with $\sin d\alpha \approx \frac{dz}{R}$.

Summation of forces in the x , y and z directions yields:

$$Q'_x + \frac{N}{R} + p_x = 0 \quad (1-a)$$

$$Q'_y + p_y = 0 \quad (1-b)$$

$$N' - \frac{Q_x}{R} + p_z = 0 \quad (1-c)$$

respectively, where primes imply differentiation with respect to z .

Summation of moments about the x , y and z axes give:

$$M'_x + \frac{1}{R}(H + Q_x y_0) - Q_y - p_z y_0 = 0 \quad (1-d)$$

$$M'_y - Q_x + p_z x_0 = 0 \quad (1-e)$$

$$H' - \frac{M_x}{R} + \frac{N}{R} y_0 + p_\phi = 0 \quad (1-f)$$

respectively. Only quantities of the first order are included in Eqs.(1).

From Eq.(1-e):

$$Q_x = p_z x_o + M_y' \quad (1-g)$$

Differentiation of Eq.(1-d) yields:

$$M_x'' + \frac{1}{R}(H' + Q_x' y_o) - Q_y' - p_z' y_o = 0 \quad (1-h)$$

Eqs.(1-a) and (1-b) lead to:

$$Q_x' = \frac{-N}{R} - p_x \quad Q_y' = -p_y$$

which when substituted into Eq.(1-h) yields:

$$M_x'' + \frac{1}{R}(H' - \frac{N}{R} y_o - p_x y_o) + p_y - p_z' y_o = 0$$

Substituting Q_x from Eq.(1-g) into Eqs.(1-a), (1-c) and (1-f):

$$p_z' x_o + M_y'' + \frac{N}{R} + p_x = 0$$

$$N' - \frac{1}{R}(p_z x_o + M_y') + p_z = 0$$

$$H' - \frac{M_x}{R} + \frac{N}{R} y_o + p_\phi = 0$$

Finally the six basic equilibrium equations are reduced to the following four equations:

$$N' - \frac{M_y'}{R} + p_z \left(1 - \frac{x_0}{R}\right) = 0 \quad (2-a)$$

$$M_x'' + \frac{1}{R} \left(H' - \frac{N}{R} y_0 - p_x y_0 \right) - p_z' y_0 + p_y = 0 \quad (2-b)$$

$$M_y'' + \frac{N}{R} + p_z' x_0 + p_x = 0 \quad (2-c)$$

$$H' - \frac{M_x}{R} + \frac{N}{R} y_0 + p_\phi = 0 \quad (2-d)$$

This set of four differential equations describes the equilibrium of an element dz . Eq.(2-a) represents equilibrium in the z -direction.

2-3 Elasto-Statical Relationships

Dabrowski (11) gives the following force-deformation relationships for a curved girder of asymmetric section:

$$M_x = -E \left[I_x \left(v'' - \frac{\phi}{R} \right) - I_{xy} \left(u'' + \frac{u}{R^2} \right) + \left(I_{xy} y_0 - \int_A y^2 x dA \right) \frac{\phi}{R^2} \right] \quad (3-a)$$

$$M_y = -E \left[I_y \left(u'' + \frac{u}{R^2} \right) - I_{xy} \left(v'' - \frac{\phi}{R} \right) - \left(I_y y_0 - \int_A x^2 y dA \right) \frac{\phi}{R^2} \right] \quad (3-b)$$

$$N = EA \left(w' - \frac{u - \phi y_0}{R} \right) - EI_{xy} \frac{\phi}{R^2} \quad (3-c)$$

$$H = \frac{-1}{\mu} (EI_w f''' - \mu GK_t f') \quad (3-d)$$

$$B = -EI_w f'' \quad (3-e)$$

The warping function $f = f(z)$ is defined by $W_s = -f' \hat{w}$ where W_s is the longitudinal displacement of a point on the wall's center-line and \hat{w} is the sectorial coordinate of the point considered.

By definition:

$$\mu = 1 - (K_t/I_p) \quad (4-a)$$

As measures of the asymmetry of cross-section, the parameters r_x and r_y can be defined as:

$$r_x = \frac{1}{I_x} \int y^2 x \, dA \quad (4-b)$$

$$r_y = \frac{1}{I_y} \int x^2 y \, dA \quad (4-c)$$

where $r_x = 0$ in case of symmetry about the y-axis and $r_y = 0$ in case of symmetry about the x-axis.

Substituting Eqs.(3-a), (3-b), (3-c), (3-d) and Eqs.(4-b), (4-c) into Eqs.(2-a), (2-b), (2-c), (2-d) yields:

$$\left[\frac{EI_y}{R} u''' + \frac{EI_y}{R^3} u' - \frac{EA}{R} u' \right] - \frac{EI_{xy}}{R} v''' + \left[\left(EA \frac{y_0}{R} - EI_y \frac{y_0}{R^3} + EI_y \frac{r_y}{R^3} \right) \phi' \right] + EA w'' + p_z \left(1 - \frac{x_0}{R} \right) = 0 \quad (5-a)$$

$$\left[EI_{xy} \left(u^{iv} + \frac{u''}{R^2} \right) + EA \frac{y_0}{R^3} u \right] - EI_x v^{iv} + \left[\left(\frac{EI_x}{R} + EI_x \frac{r_x}{R^2} - EI_{xy} \frac{y_0}{R^2} \right) \phi'' \right] + \left(EI_{xy} \frac{y_0}{R^4} - EA \frac{y_0^2}{R^3} \right) \phi - \left[\frac{1}{\mu R} (EI_w f^{iv} - \mu GK_t f'') \right] - EA \frac{y_0}{R^2} w' - p_x \frac{y_0}{R} - p_z y_0 + p_y = 0 \quad (5-b)$$

$$\left[EI_y \left(u^{iv} + \frac{u''}{R^2} \right) + \frac{EA}{R^2} u \right] - EI_{xy} v^{iv} + \left[EI_{xy} \frac{\phi''}{R} - \frac{E}{R^2} (I_y y_0 - r_y I_y) \phi'' \right] + \left(\frac{EI_{xy}}{R^3} - EA \frac{y_0}{R^2} \right) \phi - \frac{EA}{R} w' - p_z x_0 - p_x = 0 \quad (5-c)$$

$$\left[- \frac{EI_{xy}}{R} \left(u'' + \frac{u}{R^2} \right) - EA \frac{y_0}{R^2} u \right] + \frac{EI_x}{R} v'' + \left[\left(- \frac{EI_x}{R^2} - EI_{xy} \frac{y_0}{R^3} + EA \frac{y_0^2}{R^2} \right) \phi \right] + EI_{xy} \frac{y_0}{R^3} - EI_x \frac{r_x}{R^3} \phi - \left[\frac{1}{\mu} (EI_w f^{iv} - \mu GK_t f'') \right] + EA \frac{y_0}{R} w' + p_\phi = 0 \quad (5-d)$$

Eqs.(5) are the governing differential equations of equilibrium of a general curved thin walled girder element subjected to any loading

system acting along the axis of the shear center.

2-4 Inertia Forces

When the girder undergoes free vibrations, the external loads are equal to the inertia forces resulting from accelerations \ddot{u} , \ddot{v} , $\ddot{\phi}$, and \ddot{w} . * The inertia forces p_x , p_y , p_z act through the section's centroid, giving rise to a twisting moment about the shear center axis z_1 as shown in Fig.2.3-a.

Using D'Alembert's principle one can write:

$$p_x = -\rho A \frac{\partial^2}{\partial t^2} (u - y_o \phi) \quad (6-a)$$

$$p_y = -\rho A \frac{\partial^2}{\partial t^2} (v - x_o \phi) \quad (6-b)$$

$$p_z = -\rho A \frac{\partial^2 w}{\partial t^2} \quad (6-c)$$

$$p_\phi = -\rho I_p \frac{\partial^2 \phi}{\partial t^2} + \rho A y_o \frac{\partial^2}{\partial t^2} (u - y_o \phi) + \rho A x_o \frac{\partial^2}{\partial t^2} (v - x_o \phi) \quad (6-d)$$

where ρ - is the mass per unit volume of the material used.

I_p - is the polar moment of inertia about the centroid.

*

If rotary inertia is to be considered for a more refined analysis, then it should be included at this stage.

Substituting Eqs.(6) into Eqs.(5):

$$\left[\frac{EI_y}{R} u''' + \frac{EI_y}{R^3} u' - \frac{EA}{R} u' \right] - \frac{EI_{xy}}{R} v''' + \left[\left(\frac{EA y_0}{R} - EI_y \frac{y_0}{R^3} + EI_y \frac{r_y}{R} \right) \phi' \right] + \left[EA w'' - \rho A \left(1 - \frac{x_0}{R} \right) \ddot{w} \right] = 0 \quad (7-a)$$

$$\left[EI_{xy} (u^{iv} + \frac{u''}{R^2}) + \frac{EA y_0}{R^3} u' \right] - EI_x v^{iv} + \left[\left(\frac{EI_x}{R} + EI_x \frac{r_x}{R^2} - EI_{xy} \frac{y_0}{R^2} \right) \phi'' \right] + \left(EI_{xy} \frac{y_0}{R^4} - EA \frac{y_0^2}{R^3} \right) \phi - \left[\frac{1}{\mu R} (EI_w f^{iv} - \mu GK_t f'') \right] - EA \frac{y_0}{R^2} w' + \rho A \frac{y_0}{R} (\ddot{u} - y_0 \ddot{\phi}) + \rho A y_0 \frac{\partial \ddot{w}}{\partial z} - \rho A (\ddot{v} - x_0 \ddot{\phi}) = 0 \quad (7-b)$$

$$\left[EI_y (u^{iv} + \frac{u''}{R^2}) + \frac{EA}{R^2} u' \right] - EI_{xy} v^{iv} + \left[\frac{EI_{xy}}{R} \phi'' - \frac{EI_y}{R^2} (y_0 - r_y) \phi'' \right] + \left(\frac{EI_{xy}}{R^3} - EA \frac{y_0}{R^2} \right) \phi - \frac{EA}{R} w' + \rho A x_0 \frac{\partial \ddot{w}}{\partial z} + \rho A (\ddot{u} - y_0 \ddot{\phi}) = 0 \quad (7-c)$$

$$\left[\frac{-EI_{xy}}{R} (u'' + \frac{u}{R^2}) - EA \frac{y_0}{R^2} u \right] + \frac{EI_x}{R} v'' + \left[\left(\frac{-EI_x}{R^2} + EA \frac{y_0^2}{R^2} - EI \frac{r_x}{R} \right) \phi \right] - \left[\frac{1}{\mu} (EI_w f^{iv} - \mu GK_t f'') \right] + EA \frac{y_0}{R} w' - \rho I_0 \ddot{\phi} + \rho A y_0 \ddot{u} + \rho A x_0 \ddot{v} = 0 \quad (7-d)$$

where the dot superscript (·) represents partial derivative with respect to time t, and $I_0 = I_p + A(x_0^2 + y_0^2)$ is the polar moment of inertia about the shear center.

2-5 The Warping Function f

The warping function $f = f(z)$ as defined by Dabrowski (11) is given in section 2-3. In the general case of restrained warping, f can be assumed to have the form $f = au + bv + c\phi + dw$, where a, b, c, d are operators. However, Dabrowski (11) has shown that in the case of unrestrained warping, f will have the form:

$$f = \frac{v}{R} + \phi \quad (7-e)$$

Eq.(7-e) was assumed by Christiano (6, 7) in the analysis of dynamic response of curved girders of open thin walled sections (where warping is more important) and is adopted here.

Substituting Eq.(7-e) into Eqs.(7-a), (7-b), (7-c), (7-d):

$$\begin{aligned} & \left[\frac{EI_y}{R} (u'''' + \frac{u''}{R^2}) - \frac{EA}{R} u' \right] - \frac{EI_{xy}}{R} v'''' + \left[(EA \frac{y_0}{R} - EI_y \frac{y_0}{R^3} + EI_y \frac{r_y}{R^3}) \phi' \right] \\ & + \left[EAw'' - \rho A (1 - \frac{x_0}{R}) \ddot{w} \right] = 0 \end{aligned} \quad (8-a)$$

$$\begin{aligned} & \left[EI_{xy} (u^{iv} + \frac{u''}{R^2}) + EA \frac{y_0}{R^3} u \right] + \left[-EI_x v^{iv} - \frac{EI_w}{\mu R^2} v^{iv} + \frac{GK_t}{R^2} v'' \right] \\ & + \left[-\frac{EI_w}{\mu R} \phi^{iv} + (\frac{EI_x}{R} + \frac{GK_t}{R} + EI_x \frac{r_x}{R^2} - EI_{xy} \frac{y_0}{R^2}) \phi'' + (EI_{xy} \frac{y_0}{R^4} - EA \frac{y_0^2}{R^3}) \phi \right] \\ & - EA \frac{y_0}{R^2} w' + \rho A \frac{y_0}{R} (\ddot{u} - y_0 \ddot{\phi}) + \rho A y_0 \frac{\partial \ddot{w}}{\partial z} - \rho A (\ddot{v} - x_0 \ddot{\phi}) = 0 \end{aligned} \quad (8-b)$$

$$\left[EI_y (u^{iv} + \frac{u''}{R^2}) + \frac{EA}{R^2} u \right] - EI_{xy} v^{iv} + \left[EI_{xy} \frac{\phi''}{R} - \frac{EI_y}{R^2} (y_0 - r_y) \phi'' \right. \\ \left. + (\frac{EI_{xy}}{R^3} - EA \frac{y_0}{R^2}) \phi \right] - \frac{EA}{R} w' + \rho A x_0 \frac{\partial^2 w}{\partial z^2} + \rho A (\ddot{u} - y_0 \ddot{\phi}) = 0 \quad (8-c)$$

$$\left[-\frac{EI_{xy}}{R} (u'' + \frac{u}{R^2}) - EA \frac{y_0}{R^2} u \right] + \left[-\frac{EI_w}{\mu R} v^{iv} + \frac{EI_x}{R} v'' + \frac{GK_t}{R} v'' \right] + \left[-\frac{EI_w}{\mu} \phi^{iv} \right. \\ \left. + GK_t \phi'' + (\frac{EI_x}{R^2} + EA \frac{y_0^2}{R^2} - EI_x \frac{r_x}{R^3}) \phi \right] + EA \frac{y_0}{R} w' - \rho I_0 \ddot{\phi} + \rho A y_0 \ddot{u} + \rho A x_0 \ddot{v} = 0 \quad (8-d)$$

These four coupled partial differential equations with constant coefficients are of order 4 in u , v , ϕ and order 2 in w for the variable z , and of order 2 in u , v , ϕ and w for the variable t .

If coupling due to axial vibrations in the z -direction is to be considered, Eqs.(8) must be solved. However, coupling between axial vibrations in the w -direction and those in the u , v , and ϕ is weak, as can be witnessed from Eq.(5) where the terms containing p_z , \dot{p}_z are of second order. On the other hand, the uncoupled axial natural frequencies of an equivalent straight girder are much larger than those of flexural and torsional vibrations. Hence it can be concluded that the coupling effect of axial vibrations on the lower modes will be small and one can neglect terms containing p_z and \dot{p}_z , and assume that the normal force N at any section is negligible.

With this assumption Eq.(8-a), which represents equilibrium of axial forces in the z-direction is uncoupled from the other three equations. With the assumption of $N = 0$, Eq.(3-c) reduces to:

$$w' = \frac{u}{R} + \left(\frac{I_{xy}}{AR^2} - \frac{y_0}{R} \right) \phi \quad (9-a)$$

The axial displacement w of a point on the shear center located at a distance z from the origin is:

$$w = \frac{1}{R} \int_0^z u \, dz + \left(\frac{I_{xy}}{AR^2} - \frac{y_0}{R} \right) \int_0^z \phi \, dz \quad (9-b)$$

Substituting Eq.(9-a) into Eqs.(8-b), (8-c), (8-d) and rearranging one obtains:

$$\left[EI_{xy} (u^{iv} + \frac{u''}{R^2}) + \rho A \frac{y_0}{R} \ddot{u} \right] + \left[- (EI_x + \frac{EI_w}{\mu R^2}) v^{iv} + \frac{GK_t}{R^2} v'' - \rho A \ddot{v} \right] + \left[- \frac{EI_w}{\mu R} \phi^{iv} + \left(\frac{EI_x}{R} + \frac{GK_t}{R} + EI_x \frac{r_x}{R^2} - EI_{xy} \frac{y_0}{R^2} \right) \phi'' - \left(\frac{\rho A}{R} y_0^2 - \rho A x_0 \right) \ddot{\phi} \right] = 0 \quad (10-a)$$

$$\left[EI_y (u^{iv} + \frac{u''}{R^2}) + \rho A \ddot{u} \right] - EI_{xy} v^{iv} + \left[\left(\frac{EI_{xy}}{R} - EI_y \frac{y_0}{R^2} + EI_y \frac{r_y}{R^2} \right) \phi'' - \rho A y_0 \ddot{\phi} \right] = 0 \quad (10-b)$$

$$\left[- \frac{EI_{xy}}{R} (u'' + \frac{u}{R^2}) + \rho A y_0 \ddot{u} \right] + \left[- \frac{EI_w}{\mu R} v^{iv} + \left(\frac{EI_x}{R} + \frac{GK_t}{R} \right) v'' + \rho A x_0 \ddot{v} \right] + \left[- \frac{EI_w}{\mu} \phi^{iv} + GK_t \phi'' + \left(- \frac{EI_x}{R^2} - EI_x \frac{r_x}{R^3} + \frac{EI_{xy} y_0}{R^3} \right) \phi - \rho I_0 \ddot{\phi} \right] = 0 \quad (10-c)$$

It can be seen that the assumption of $N = 0$ was used to uncouple the axial displacement w from u , v , and ϕ . Eqs.(10) are three coupled partial differential equations with three unknown displacement functions u , v , and ϕ of the fourth and second order differentials with respect to the variables z and t .

2-6 Displacement Functions and Boundary Conditions

To permit a separation of variables in solving Eqs.(10), the displacement functions can be separated into two functions, a function of location z and a function of time t . In the general case of vibration, the displacement function can be taken as a Fourier Series over an infinite number of natural modes, i.e.:

$$u(z, t) = \sum_{i=1}^{\infty} \bar{u}_i(t) \tilde{u}_i(z) \quad (11-a)$$

$$v(z, t) = \sum_{i=1}^{\infty} \bar{v}_i(t) \tilde{v}_i(z) \quad (11-b)$$

$$\phi(z, t) = \sum_{i=1}^{\infty} \bar{\phi}_i(t) \tilde{\phi}_i(z) \quad (11-c)$$

For the particular case of free vibrations, only one mode is excited and there is no need to sum all components of other modes. Hence in any pure modal vibration:

$$u_i(z, t) = \bar{u}_i(t) \tilde{u}_i(z) \quad (12-a)$$

$$v_i(z, t) = \bar{v}_i(t) \tilde{v}_i(z) \quad (12-b)$$

$$\phi_i(z, t) = \bar{\phi}_i(t) \tilde{\phi}_i(z) \quad (12-c)$$

In accordance with the conventional procedure for finding natural frequencies the time functions are taken in the form:

$$\bar{u}_i(t) = \sin \omega_i t \quad (13-a)$$

$$\bar{v}_i(t) = \sin \omega_i t \quad (13-b)$$

$$\bar{\phi}_i(t) = \sin \omega_i t \quad (13-c)$$

Since Eqs.(10) contain derivatives of u , v and ϕ with respect to z of the fourth order, four boundary conditions on each displacement function are required. Under the assumed support conditions, transverse displacements u , v and twist ϕ are prevented at both supports, i.e.:

$$u(o, t) = u(l, t) = 0 \quad \text{or} \quad \tilde{u}_i(o) = \tilde{u}_i(l) = 0 \quad (14-a)$$

$$v(o, t) = v(l, t) = 0 \quad \text{or} \quad \tilde{v}_i(o) = \tilde{v}_i(l) = 0 \quad (14-b)$$

$$\phi(o, t) = \phi(l, t) = 0 \quad \text{or} \quad \tilde{\phi}_i(o) = \tilde{\phi}_i(l) = 0 \quad (14-c)$$

Since bending moments M_x , M_y vanish at both supports:

$$u''(o, t) = u''(l, t) = 0 \quad \text{or} \quad \tilde{u}_i''(o) = \tilde{u}_i''(l) = 0 \quad (14-d)$$

$$v''(o, t) = v''(l, t) = 0 \quad \text{or} \quad \tilde{v}_i''(o) = \tilde{v}_i''(l) = 0 \quad (14-e)$$

from Eqs.(3-a), (3-b).

The cross-sections at both supports are free to warp and so the axial stress σ due to bimoment B

$$\sigma = \frac{B}{I_w} \hat{w} \quad (14-f)$$

must vanish. Eq.(14-f) implies that B must vanish as well at the supports. From (3-e) and (7-e)

$$B = -EI_w \left(\phi'' + \frac{v}{R} \right)$$

Recalling (14-e), it can be concluded that

$$\phi''(0, t) = \phi''(\ell, t) = 0 \quad \text{or} \quad \tilde{\phi}_i''(0) = \tilde{\phi}_i''(\ell) = 0 \quad (14-g)$$

Displacement w in the axial direction is prevented at $z = 0$ and permitted at $z = \ell$

$$w(0, t) = w'(\ell, t) = 0 \quad (14-h)$$

All of conditions (14-a), (14-b), (14-c), (14-d), (14-e), (14-g), (14-h) together with Eq.(9-b) can be met by selecting

$$\tilde{u}_i(z) = U_i \sin \theta_i z \quad (14-i)$$

$$\tilde{v}_i(z) = V_i \sin \theta_i z \quad (14-j)$$

$$\tilde{\phi}_i(z) = \Phi_i \sin \theta_i z \quad (14-k)$$

where

$$\theta_i = \frac{i\pi}{\ell} \quad (14-l)$$

and U_i , V_i , Φ_i , are amplitudes of vibration of the i^{th} mode in the x , $-y$ and ϕ directions respectively.

Substituting Eqs.(13) and (14-i), (14-j), (14-k) into Eqs.(12)

$$u_i(z, t) = U_i \sin \omega_i t \sin \theta_i z \quad (15-a)$$

$$v_i(z, t) = V_i \sin \omega_i t \sin \theta_i z \quad (15-b)$$

$$\phi_i(z, t) = \Phi_i \sin \omega_i t \sin \theta_i z \quad (15-c)$$

Substituting Eqs.(15) into Eqs.(10) one obtains

$$\begin{aligned} & \left[EI_{xy} \left(\theta_i^2 - \frac{1}{R^2} \right) \theta_i^2 - \rho A \frac{y_0^2}{R} \omega_i^2 \right] U_i + \left[- \left(EI_x + \frac{EI_w}{\mu R^2} \right) \theta_i^4 - \frac{GK_t}{R^2} \theta_i^2 \right. \\ & + \rho A \omega_i^2 \left. \right] V_i + \left[- \frac{EI_w}{\mu R} \theta_i^4 - \left(\frac{EI_x}{R} + \frac{GK_t}{R} + EI_x \frac{r_x^2}{R^2} - EI_{xy} \frac{y_0}{R^2} \right) \theta_i^2 \right. \\ & + \left. \left(\frac{y_0^2}{R} - x_0 \right) \rho A \omega_i^2 \right] \Phi_i = 0 \end{aligned} \quad (16-a)$$

$$\begin{aligned} & \left[EI_y \theta_i^2 \left(\theta_i^2 - \frac{1}{R^2} \right) - \rho A \omega_i^2 \right] U_i - EI_{xy} \theta_i^4 V_i - \left[\left(\frac{EI_{xy}}{R} - EI_y \frac{y_0}{R^2} + EI_y \frac{r_y^2}{R^2} \right) \theta_i^2 \right. \\ & - \left. \rho A y_0 \omega_i^2 \right] \Phi_i = 0 \end{aligned} \quad (16-b)$$

$$\begin{aligned} & \left[\frac{EI_{xy}}{R} \left(\theta_i^2 - \frac{1}{R^2} \right) - \rho A y_0 \omega_i^2 \right] U_i - \left[\frac{EI_w}{\mu R} \theta_i^4 + \left(EI_x + GK_t \right) \frac{\theta_i^2}{R} + \rho A x_0 \omega_i^2 \right] V_i \\ & + \left[- \frac{EI_w}{\mu} \theta_i^4 - GK_t \theta_i^2 + \left(- \frac{EI_x}{R^2} - EI_x \frac{r_x^2}{R^3} + EI_{xy} \frac{y_0}{R^3} \right) + \rho I_o \omega_i^2 \right] \Phi_i = 0 \end{aligned} \quad (16-c)$$

2-7 The Frequency Equation

Let us now introduce the expressions of natural frequencies ω_{ui} , ω_{vi} , $\omega_{\phi i}$ of an equivalent straight girder of length l whose

geometry does not lead to modal coupling. Gere and Lin (19) give the following expressions, which are valid for any boundary conditions:

$$\bar{\omega}_{ui}^2 = \frac{EI_y \int_0^l \left(\frac{d^2 \tilde{u}_i}{dz^2} \right)^2 dz}{\rho A \int_0^l \tilde{u}_i^2 dz}$$

$$\bar{\omega}_{vi}^2 = \frac{EI_x \int_0^l \left(\frac{d^2 \tilde{v}_i}{dz^2} \right)^2 dz}{\rho A \int_0^l \tilde{v}_i^2 dz}$$

$$\bar{\omega}_{\phi i}^2 = \frac{EI_w \int_0^l \left(\frac{d^2 \tilde{\phi}_i}{dz^2} \right)^2 dz + \mu GK_t \int_0^l \left(\frac{d \tilde{\phi}_i}{dz} \right)^2 dz}{\mu \rho I_o \int_0^l \tilde{\phi}_i^2 dz}$$

Substituting Eqs.(14-i), (14-j), (14-k), (14-l) into the previous expressions yields:

$$\bar{\omega}_{ui}^2 = \frac{EI_y}{\rho A} \theta_i^4 \quad (17-a)$$

$$\bar{\omega}_{vi}^2 = \frac{EI_x}{\rho A} \theta_i^4 \quad (17-b)$$

$$\bar{\omega}_{\phi i}^2 = \frac{EI_w \theta_i^4 + \mu GK_t \theta_i^2}{\mu \rho I_o} \quad (17-c)$$

Let us introduce the dimensionless quantities β and γ :

$$\beta = \frac{I_{xy}}{I_x} \quad \gamma = \frac{I_{xy}}{I_y} \quad (18)$$

Equations (16) can be written in matrix form as:

$$\begin{bmatrix} L_{11} & L_{12} & L_{13} \\ L_{21} & L_{22} & L_{23} \\ L_{31} & L_{32} & L_{33} \end{bmatrix} \begin{bmatrix} U_i \\ V_i \\ \Phi_i \end{bmatrix} = \begin{bmatrix} 0 \\ 0 \\ 0 \end{bmatrix} \quad (19)$$

Where L_{ij} can be written after substituting (17-a), (17-b), (17-c) and (18) as:

$$\begin{aligned} L_{11} &= \beta \left(1 - \frac{1}{R^2 \theta_i^2} \right) - \frac{y_0}{R} \left(\frac{\omega_i}{\omega_{vi}} \right)^2 \\ L_{12} &= -1 - \frac{I_0}{AR^2} \left(\frac{\omega_{\phi i}}{\omega_{vi}} \right)^2 + \left(\frac{\omega_i}{\omega_{vi}} \right)^2 \\ L_{13} &= -\frac{I_0}{AR} \left(\frac{\omega_{\phi}}{\omega_{vi}} \right)^2 - \frac{1}{R \theta_i^2} \left(1 + \frac{r_x}{R} \right) + \frac{\beta y_0}{R^2 \theta_i^2} + \left(\frac{y_0^2}{R} - x_0 \right) \left(\frac{\omega_i}{\omega_{vi}} \right)^2 \\ L_{21} &= \left(1 - \frac{1}{R^2 \theta_i^2} \right) \left(\frac{\omega_{ui}}{\omega_{vi}} \right)^2 - \left(\frac{\omega_i}{\omega_{vi}} \right)^2 \\ L_{22} &= -\gamma \left(\frac{\omega_{ui}}{\omega_{vi}} \right)^2 \end{aligned}$$

$$\begin{aligned}
 L_{23} &= \left(\frac{-\gamma}{R\theta_i^2} + \frac{y_0}{R^2\theta_i^2} - \frac{r_y}{R^2\theta_i^2} \right) \left(\frac{\omega_i}{\omega_{vi}} \right)^2 + y_0 \left(\frac{\omega_i}{\omega_{vi}} \right)^2 \\
 L_{31} &= \frac{\beta}{R\theta_i^2} \left(1 - \frac{1}{R^2\theta_i^2} \right) - y_0 \left(\frac{\omega_i}{\omega_{vi}} \right)^2 \\
 L_{32} &= \frac{-I_0}{AR} \left(\frac{\omega_i}{\omega_{vi}} \right)^2 - \frac{1}{R\theta_i^2} - x_0 \left(\frac{\omega_i}{\omega_{vi}} \right)^2 \\
 L_{33} &= \frac{-I_0}{A} \left(\frac{\omega_i}{\omega_{vi}} \right)^2 + \frac{I_0}{A} \left(\frac{\omega_i}{\omega_{vi}} \right)^2 - \frac{1}{R^2\theta_i^4} \left(1 + \frac{r_x}{R} - \beta \frac{y_0}{R} \right)
 \end{aligned} \tag{20}$$

For a non-trivial solution of Eq.(19), the determinant of [L] must vanish, or:

$$\det.[L] = 0 \tag{21}$$

A symmetry index ψ can be defined by:

$$\psi = 1 - \beta \gamma = 1 - \frac{I_{xy}^2}{I_x I_y} \tag{22-a}$$

and is a measure of symmetry of the moments of inertia with respect to the x and y axes. Obviously $\psi = 1$ in the case of single or double symmetry of the cross-section. Another useful measure, a mode-curvature index η can be defined by:

$$\eta = 1 - \frac{1}{R^2\theta_i^2} \tag{22-b}$$

The mode-curvature index η is dependent upon the mode number i and radius of curvature R , with $\eta = 1$ for straight girders. To non-dimensionalize the frequency equation the parameters ρ_x , ρ_y , δ_x , and

δ_y , can be defined by:

$$\rho_x = \frac{r_x}{R} \quad \rho_y = \frac{r_y}{R} \quad (22-c)$$

$$\delta_x = \frac{x_0}{R} \quad \delta_y = \frac{y_0}{R} \quad (22-d)$$

Substituting L_{ij} from Eq.(20) into Eq.(21) and taking into account (22-a), (22-b), (22-c), (22-d) the frequency equation becomes:

$$\begin{aligned} & \left(\frac{\omega_i}{\omega_{vi}} \right)^6 + \left[\gamma \delta_y \left(\frac{I_0}{I_p} - \frac{AR^2}{I_p} \delta_y^2 \right) + \frac{AR^2}{I_p} \delta_x \delta_y \gamma \left(1 + \frac{1}{R^2 \theta_i^2} \right) - \frac{AR^2}{I_p} \delta_x \delta_y \right. \\ & \left. \left(\delta_y - \frac{\rho_y}{R^2 \theta_i^2} \right) + \frac{A\gamma}{I_p \theta_i^2} \delta_y - \frac{A}{I_p \theta_i^2} \delta_y (\delta_y - \rho_y) - \eta \left(\frac{I_0}{I_p} - \frac{AR^2}{I_p} \delta_x^2 \right) \right] \\ & \left(\frac{\omega_{ui}}{\omega_{vi}} \right)^2 \left(\frac{\omega_i}{\omega_{vi}} \right)^4 - \frac{I_0}{I_p} \left[1 + 2\delta_x + \frac{I_0}{AR^2} - \delta_y^2 \right] \left(\frac{\omega_{\phi i}}{\omega_{vi}} \right)^2 \left(\frac{\omega_i}{\omega_{vi}} \right)^4 + \left\{ \frac{AR^2}{I_p} \beta \delta_x \delta_y \right. \\ & \left. - \left(\frac{I_0}{I_p} - \frac{AR^2}{I_p} \delta_y^2 \right) - \frac{A}{I_p \theta_i^2} \left[-\beta \delta_y + 2\delta_x + \frac{1}{R^2 \theta_i^2} + \rho_x \left(\delta_x + \frac{1}{R^2 \theta_i^2} \right) \right] \right\} \\ & \left(\frac{\omega_i}{\omega_{vi}} \right)^4 + \left[\frac{I_0}{I_p} \eta \psi + \frac{2A}{I_p \theta_i^2} (\delta_x \eta \psi + \delta_y \gamma) + \frac{A}{I_p \theta_i^2} \gamma \rho_x \delta_y - \frac{A}{I_p \theta_i^2} \beta \eta \rho_y \right. \\ & \left. \left(\delta_x + \frac{1}{R^2 \theta_i^2} \right) - \frac{A}{I_p \theta_i^2} \delta_y^2 (1 + \eta \psi + \frac{\psi}{R^2 \theta_i^2} + \gamma \beta) + \frac{A}{I_p \theta_i^2} \rho_y \delta_y \left(1 + \frac{1}{R^2 \theta_i^2} \right) \right. \\ & \left. + \frac{A}{I_p R^2 \theta_i^4} \eta \psi + \frac{A}{I_p \theta_i^2} \rho_x \eta \left(\delta_x + \frac{1}{R^2 \theta_i^2} \right) \right] \left(\frac{\omega_{ui}}{\omega_{vi}} \right)^2 \left(\frac{\omega_i}{\omega_{vi}} \right)^2 + \left[\frac{I_0}{I_p} \eta (1 + \beta \delta_y) \right. \\ & \left. - \frac{I_0}{I_p} \frac{\eta}{R^2 \theta_i^2} (\rho_x - \beta \delta_y) \right] \left(\frac{\omega_{\phi i}}{\omega_{vi}} \right)^2 \left(\frac{\omega_i}{\omega_{vi}} \right)^2 + \left[\frac{I_0}{I_p} \eta (2\delta_x - \delta_y^2) - \frac{I_0}{I_p} \eta \left(\frac{I_0}{AR^2} + 1 \right) \right] \left(\frac{\omega_{ui}}{\omega_{vi}} \right)^2 \\ & \left(\frac{\omega_{\phi i}}{\omega_{vi}} \right)^2 \left(\frac{\omega_i}{\omega_{vi}} \right)^2 + \frac{I_0}{I_p} \eta \left[\frac{\rho_x \eta}{R^2 \theta_i^2} - \frac{\beta \rho_y \eta}{R^2 \theta_i^2} - \eta^2 \psi \right] \left(\frac{\omega_{ui}}{\omega_{vi}} \right)^2 \left(\frac{\omega_{\phi i}}{\omega_{vi}} \right)^2 = 0 \quad (23) \end{aligned}$$

Eq.(23) is the frequency equation. It is cubic in the unknown ω_i^2 and can be solved to furnish a set of three positive roots corresponding to a given mode number i . A set of three such roots represent different coupling patterns between U_i , V_i , and Φ_i , but they all have the same longitudinal distribution, which is sinusoidal as given by Eqs.(15).

A computer program for solving Eq.(23) is given in Appendix II. Further details and numerical examples are given in Chapter 4.

2-8 Eigen Functions

Having found the eigenvalues ω_i , from the roots of the frequency Equation (23), one can obtain the relative values of the amplitudes of vibration U_i , V_i , and Φ_i from Eq.(19). Since Eq.(19) represents a set of three homogeneous dependent linear equations, it is only possible to get relative values of modal displacements. For ease of computations unit amplitude can be assigned to one modal amplitude such as V_i , and the amplitudes of U_i , and Φ_i computed.

From the first and second rows in Eq.(19), one can write:

$$\Phi_i = \frac{\begin{pmatrix} L_{11} & L_{22} & -L_{12} & L_{21} \end{pmatrix}}{\begin{pmatrix} L_{21} & L_{13} & -L_{11} & L_{23} \end{pmatrix}} V_i \quad (24)$$

$$U_i = - \frac{(L_{22} V_i + L_{23} \Phi_i)}{L_{21}} \quad (25)$$

Recalling that the axial displacement w of a point on the shear

center located at a distance z from the origin is given by Eq.(9-b):

$$w = \frac{1}{R} \int_0^z u \, dz + \left(\frac{I_{xy}}{AR^2} - \frac{y_0}{R} \right) \int_0^z \phi \, dz \quad (9-b)$$

and substituting for u , ϕ from Eqs.(15):

$$\begin{aligned} w &= \frac{U_i}{R} \sin \omega_i t \int_0^z \sin \theta_i z \, dz + \left(\frac{I_{xy}}{AR^2} - \frac{y_0}{R} \right) \phi_i \sin \omega_i t \int_0^z \sin \theta_i z \, dz \quad (26) \\ &= - \left[\frac{U_i}{R} - \left(\frac{I_{xy}}{AR^2} - \frac{y_0}{R} \right) \phi_i \right] \frac{\sin \omega_i t}{\theta_i} \cos \theta_i z \end{aligned}$$

At the R-H support $z = \ell$, $\cos \theta_i \ell = 1$

$$w_\ell = \left[-\frac{U_i}{R} + \left(\frac{I_{xy}}{AR^2} - \frac{y_0}{R} \right) \phi_i \right] \frac{\sin \omega_i t}{\theta_i}$$

re-writing w in the form:

$$w = W_i \sin \omega_i t \cos \theta_i z \quad (27)$$

then

$$w_\ell = W_{i\ell} \sin \omega_i t$$

where

$$W_{i\ell} = \left[-\frac{U_i}{\theta_i R} + \left(\frac{I_{xy}}{AR^2} - \frac{y_0}{R} \right) \frac{\phi_i}{\theta_i} \right] \quad (28)$$

Eq.(28) describes the tangential vibration of the right support which is in phase with other components of vibration of the i th mode, and has an amplitude of $W_{i\ell}$.

2-9 Orthogonality of Eigenfunctions

Any point M of coordinates (x, y) located on the wall of the cross-section will undergo horizontal and vertical displacements $\delta u_i, \delta v_i$ with respect to the shear center (x_0, y_0) as the cross-section rotates by an angle of twist ϕ_i around the shear center, Fig.2.3-b.

The values of $\delta u_i, \delta v_i$, are:

$$\delta u_i = (x - x_0)(\cos \phi_i - 1) + (y - y_0) \sin \phi_i$$

$$\delta v_i = (x - x_0) \sin \phi_i + (y - y_0)(1 - \cos \phi_i)$$

However, since analysis is limited to small vibrations only, then one can assume $\cos \phi_i \approx 1$, $\sin \phi_i \approx \phi_i$ hence:

$$\delta u_i = (y - y_0)\phi_i \quad (29-a)$$

$$\delta v_i = (x - x_0)\phi_i \quad (29-b)$$

the position of any point M on the wall of the girder vibrating in mode i at any section z with respect to the $oxyz$ axes

can be obtained from the state vector:

$$\begin{aligned}\vec{P}_i &= \vec{U}_i + \vec{V}_i + \vec{W}_i \\ &= (u_i + \delta u_i) \vec{q} + (v_i + \delta v_i) \vec{r} + w_i \vec{s}\end{aligned}\quad (30)$$

where u_i , v_i , w_i , are the displacements of the shear center at the same longitudinal location z as that of point M . \vec{q} , \vec{r} , \vec{s} are three base vectors mutually orthogonal and parallel to the x , y , and z axes respectively.

The orthogonality condition of modes i and j can be written as:

$$\int \vec{P}_i \cdot \vec{P}_j Q dD = c \delta_{ij} \quad (31)$$

where the integral is taken over a domain D , Q is a weighting function, δ_{ij} is the Kronecker delta and c is a constant.

Substituting P_i , P_j , from Eq.(30) into Eq.(31) one obtains:

$$\begin{aligned}\int \vec{P}_i \cdot \vec{P}_j Q dZ &= \int \left[(u_i + \delta u_i) \vec{q} + (v_i + \delta v_i) \vec{r} + w_i \vec{s} \right] \\ &\quad \left[(u_j + \delta u_j) \vec{q} + (v_j + \delta v_j) \vec{r} + w_j \vec{s} \right] Q dZ\end{aligned}\quad (32)$$

The mixed terms containing $\vec{q} \cdot \vec{r}$, $\vec{q} \cdot \vec{s}$, or $\vec{r} \cdot \vec{s}$ will vanish because base vectors are orthogonal. Then Eq.(32) will reduce to the product

of like terms of base vectors, $\vec{q} \cdot \vec{q}$, $\vec{r} \cdot \vec{r}$, $\vec{s} \cdot \vec{s}$, or:

$$\int \vec{P}_i \cdot \vec{P}_j Q dz = \int \left[(u_i + \delta u_i)(u_j + \delta u_j) + (v_i + \delta v_i)(v_j + \delta v_j) + w_i w_j \right] Q dz \quad (33)$$

Recalling Eq.(15), Eqs.(29-a), (29-b) and Eq.(27), and substituting back into Eq.(33):

$$\begin{aligned} \int \vec{P}_i \cdot \vec{P}_j Q dz = & \left[u_i u_j + (y - y_0) u_i \phi_j + (y - y_0) u_j \phi_i + (y - y_0)^2 \right. \\ & \left. \phi_i \phi_j \right] + \left[v_i v_j + (x - x_0) v_i \phi_j + (x - x_0) v_j \phi_i + (x - x_0)^2 \phi_i \phi_j \right] \\ & \sin \omega_i t \sin \omega_j t \int \sin \theta_i z \sin \theta_j z Q dz + w_i w_j \sin \omega_i t \sin \omega_j t \\ & \int \cos \theta_i z \cos \theta_j z Q dz \end{aligned} \quad (34)$$

it can be seen that the righthand side of Eqs.(31) and (34) are identical.

2-10 Special Cases

Governing frequency equation for the following special cases can be determined from the general case of Eq.(23).

(a) Curved girder with cross-section having single symmetry with

respect to the y axis. Christiano (6, 7).

$$I_{xy} = 0 \qquad r_x = x_o = 0$$

$$\beta = \gamma = \rho_x = \delta_x = 0 \qquad \psi = 1$$

Triple coupling between u , v , and ϕ exists under such conditions.

- (b) Curved girder with cross-section having single symmetry with respect to the x axis.

$$I_{xy} = 0 \qquad r_y = y_o = 0$$

$$\beta = \gamma = \rho_y = \delta_y = 0 \qquad \psi = 1$$

Double coupling between v and ϕ exists but u is independent.

- (c) Curved girder with cross-section doubly symmetric with respect to x and y . Culver (8)

$$I_{xy} = 0 \qquad r_x = r_y = x_o = y_o = 0$$

$$\beta = \gamma = \rho_x = \rho_y = \delta_x = \delta_y = 0 \qquad \psi = 1$$

Double coupling between v and ϕ exists, u is independent.

- (d) Straight girder with asymmetrical cross-section. Gere and Lin (18), Vlasov (40) and Federhofer (13).

$$R \rightarrow \infty \quad \eta = 1$$

Triple coupling between u , v and ϕ prevails.

- (e) Straight girder with cross-section having single symmetry with respect to x . Timoshenko (37).

$$R \rightarrow \infty \quad I_{xy} = 0 \quad r_y = y_o = 0$$

$$\beta = \gamma = \rho_y = \delta_y = 0 \quad \eta = 1 \quad \psi = 1$$

Double coupling exists between v and ϕ but u is independent.

- (f) Straight girder with cross-section doubly symmetric with respect to x and y .

$$R \rightarrow \infty \quad I_{xy} = 0 \quad r_x = r_y = x_o = y_o = 0$$

$$\beta = \gamma = \rho_x = \rho_y = \delta_x = \delta_y = 0 \quad \eta = 1 \quad \psi = 1$$

No coupling exists and the girder can vibrate in either the u or v or ϕ directions independently.

2-11 Parametric Study

It can be seen from Eq.(23) that the following non-dimensional parameters define the required frequencies of coupled vibrations:

$$\begin{aligned} \beta &= \frac{I_{xy}}{I_x} & \gamma &= \frac{I_{xy}}{I_y} & \rho_x &= \frac{r_x}{R} & \rho_y &= \frac{r_y}{R} \\ \delta_x &= \frac{x_0}{R} & \delta_y &= \frac{y_0}{R} & \frac{AR^2}{I_p} & & \\ R^2 \theta_i^2 &= (i\pi\alpha_1)^2 & \left(\frac{\omega_{ui}}{\omega_{vi}}\right)^2 &= \frac{I_y}{I_x} & \left(\frac{\omega_{\phi i}}{\omega_{vi}}\right)^2 & & \end{aligned}$$

All the other non-dimensional parameters in Eq.(23) can be obtained from a proper combination of these parameters. These parameters are not absolutely independent but related through the geometry of the cross-section. A number of cases were examined, with uni-symmetrical, doubly-symmetrical, and asymmetrical sections with both positive and negative asymmetry included. Only high asymmetry was considered to clarify its effect on natural frequency. The basic parameters used in analysis are shown in Table 2-1.

The ratio $\frac{AR^2}{I_p}$ was assumed to take on one of the following values (100, 500, 1000, 5000, 10000). A range of values for $\frac{\omega_{\phi}}{\omega_v}$ from 0 to 5 was chosen. Given a set of the parameters from Table 2-1, a value of $\frac{AR^2}{I_p}$ and another for $\frac{\omega_{\phi}}{\omega_v}$ were selected and three roots for each of the ratios $\frac{\omega_1}{\omega_{v1}}$ and $\frac{\omega_2}{\omega_{v2}}$ were calculated from Eq.(23).

$\frac{\omega_1}{\omega_{v_1}}, \frac{\omega_2}{\omega_{v_2}}$ with $\frac{\omega_\phi}{\omega_v}$ and $\frac{AR^2}{I_p}$ were obtained. These plots are shown in Figs. 2.4, 2.5,, 2.13.

Values of Various Parameters for Cases examined in the Parametric Study

α_1	$\frac{w_u}{w_v}$	β	γ	ρ_x	ρ_y	δ_x	δ_y	Symmetry	Plot on Figure
45°	5	0	0	0	0	0	0	DS	2.4
	10	0	0	0	0	0	0	DS	2.5
		0	0	0	0.001	0	0.01	USY	2.6
		0.05	0.0005	0.001	0.001	0.01	0.01	ASP	2.7
		-0.05	-0.0005	-0.001	0.001	-0.01	0.01	ASN	2.8
90°	5	0	0	0	0	0	0	DS	2.9
		-0.05	-0.002	-0.001	0.001	-0.01	0.01	ASN	2.10
	10	0	0	0	0	0	0	DS	2.11
		0.05	0.0005	0.001	0.001	0.01	0.01	ASP	2.12
		-0.05	-0.0005	-0.001	0.001	-0.01	0.01	ASN	2.13

DS - Doubly Symmetric section; USY - Unisymmetric with respect to y-axis; ASP - Positively Asymmetric Section; ASN - Negatively Asymmetric Section (x-direction only)

Upon examining these Figures the following observations can be made:

- (a) In comparison to an equivalent straight girder, coupling between three (or less) different frequencies decreases the lowest and increases the highest of these frequencies, (Figs.2.4, 2.13), while the intermediate frequency might increase or decrease depending upon the geometry (Fig.2.10(a)). The effects of coupling decrease as the mode number increases (Figs.2.11(a) and (b)).
- (b) When $\frac{AR^2}{I_p}$ increases with α_1 fixed (i.e. the length of the girder increases) the upper and lower roots of the coupled frequencies diverge. Figs.2.5(a) and (b).
- (c) For doubly symmetric sections, the horizontal frequency will be uncoupled (Figs.2.4, 2.5, 2.9 and 2.11). This frequency is always less than the uncoupled frequency of an equivalent straight girder, and will converge to it when the central angle α_1 approaches zero and $\frac{AR^2}{I_p}$ becomes very large.
- (d) For sections uni-symmetrical with respect to the vertical axis, triple coupling arises. The effect on the first and second modes as compared to the case of double coupling is to couple the horizontal vibration and slightly decrease coupling (i.e. to increase the lower and decrease the higher frequencies) between the previously coupled vertical and torsional vibrations. Figs.2.5 and 2.6.
- (e) The effect of increasing the lateral moment of inertia with respect to the vertical one is to cause a slight diversion of the upper and lower roots of the coupled frequencies. Figs.2.4 and 2.5(a). The diversion will

be greater for small values of $\frac{AR^2}{I_p}$.

- (f) The effect on the first mode of positive asymmetry of the cross-section compared to the doubly symmetrical one is to couple the horizontal vibration and decrease coupling slightly between the previously coupled vertical and torsional vibrations. Figs.2.5(a) and 2.7(a), also Figs.2.11(a) and 2.12(a).
- (g) The effect on the second mode of positive asymmetry of the cross-section compared to the doubly symmetrical one is to couple the horizontal vibration and increase coupling (i.e. increase the higher and decrease the lower frequencies) slightly between the previously coupled vertical and torsional vibrations. Figs.2.11(b) and 2.12(b), also Figs.2.5(b) and 2.7(b).
- (h) The effect on the first mode of negative asymmetry of the cross-section compared to the doubly symmetrical one is to couple the horizontal vibration and decrease coupling - more than in (f) - between the previously coupled vertical and torsional vibrations. Figs.2.5(a) and 2.8(a), also Figs.2.11(a) and 2.13(a).
- (i) The effect on the second mode of negative asymmetry of the cross-section compared to the doubly symmetric one is to couple the horizontal vibration and decrease coupling between the previously coupled vertical and torsional vibrations for all or low ω_ϕ/ω_v ratios and increase coupling between the same two components for higher ω_ϕ/ω_v values. Figs.2.5(b) and 2.8(b), also Figs.2.11(b) and 2.13(b).
- (j) For asymmetrical cross-sections the increase in the highest frequency for any modal number can be very

- 40 -

large, particularly for higher values of $\frac{AR^2}{I_p}$ while
the decrease of the lowest value is less sensitive.

CHAPTER 3

EXPERIMENTAL PROGRAM

Laboratory tests were conducted to obtain the natural frequencies and estimate the modal shapes of the first few modes of two plexiglas models. The first model was a simply supported curved girder of single cell section symmetric with respect to the vertical centroidal axis, and the second model was also a simply supported curved girder but had a two cell asymmetric section.

The models were excited by a single shaker with a controllable frequency. Response was measured at different points in the vertical direction by six displacement transducers. A trial and error procedure was used to converge to the optimum position and orientation of the shaker. A set of resonance criteria was used to identify the modes sought.

3-1 Design, Description and Fabrication of Models

Two models denoted A and B were designed to meet the requirements of both static and dynamic tests. Both models were constructed of plexiglas with a central angle α_1 of 90° , and a length along the center line of the upper deck l of 80.2 inch. Model A had a symmetric cross-section with respect to the vertical axis, while Model B had an asymmetric cross-section. Model B was obtained by adding an eccentric web to model A. Plan and cross-sectional dimen-

sions of models A and B are given in Figs.3.1, 3.2 respectively. A general view of model B is shown in Fig.3.3.

3-1-1 Description of the models

Both models were simply supported, with the whole section extended 1 inch beyond the line of supports on each end. The line of supports consisted of two or three point supports for models A and B respectively. Point supports were located on a radial line directly under the webs.

The left-hand support was essentially a hinge since it prevented twist ϕ , vertical displacement v or horizontal displacements, u , w , but allowed rotation with respect to the x and y axes and warping of the cross-section. This was achieved by using one fixed point support and one or two roller point supports. (Fig. 3.4). The right-hand support was essentially a roller, since it prevented twist ϕ , vertical displacements v or horizontal displacement u , but allowed rotation with respect to the x and y axes, and warping of the cross-section as well as horizontal axial displacement w . (Fig.3.5).

The roller point support consisted of a plexiglas cap machined from a 1 inch thick block to a spherical surface to provide point support to the model. A soft piece of rubber was placed on top of the cap to prevent vibration of the support. The lower face of the cap was machined to a concave surface to accommodate a 1/4 inch hard nylon ball. The ball itself was mounted on top of a concave

surface machined into a supporting cylindrical bar 1 inch in diameter. (Fig.3.7). The bar was 3.25 inch long and made of plexiglas. The lower 3/4 inch was threaded and screwed into another plexiglas block 1 inch thick. These threads allow for relative adjustment of point support elevation and inclination. The lower block rested on two small cylindrical plexiglas bars 1/8 inch diameter to allow for motion in the direction desired. A concentric hole of 1/8 inch was drilled to accommodate a prestressing wire which was a flexible high strength steel wire, 1/12 inch soldered on top to a penny. A rubber pad was placed between the penny and model. The lower end of the prestressing wire was hooked to a 15 lb. hanging weight. The fixed point support was similar to the roller type except that the rollers were omitted and the bottom block fixed to the supporting beam, and a cantilever bar fixed to the supporting beam was placed in contact with the end section of the girder to restrain warping at the desired point. (Fig.3.8).

Both models had a curvature $\frac{1}{R}$ of 0.0196, a central angle of 90° , a width of upper deck of 18 inch, a ratio of upper deck width to radius of $18/51 = 0.353$, and a width of lower deck of 12 inch. All webs are 2.5 inch deep. Model A was provided with two webs located symmetrically on the cross-section at radii $r_1 = 45.125$ inch, $r_2 = 56.875$ inch as shown in Fig.3.1. Four diaphragms 1/4 inch thick were located symmetrically along the span. Model B was obtained from Model A by adding an extra web located at a radius of $r_3 = 52.00$ inch. Six diaphragms 1/4 inch thick were located at sections 0° , 15° , 35° , 55° , 75° and 90° as shown in Fig.3.2.

In order to facilitate modification of the cross-section, the two webs of Model A were glued to the upper deck, while screws were used to attach the lower deck. This design permitted addition of new webs and new diaphragms. In both models machine screws #4-40, 0.5 inch long were used to connect the diaphragms to the decks and webs.

3-1-2 Material properties

Plexiglas G of Rohm and Haas Co. was used in both models. It is well known that plastics creep under sustained loads due to their molecular structure. Moreover, the modulus of elasticity of plastics under dynamic loads is frequency dependent.

Three series of tests were performed to measure material properties. The first test was a standard tension coupon test. Eight coupons were cut from different points of the plexiglas sheets used and tested at a low strain rate of 3000 μ strains/min. up to failure. Test results are summarized in Table 3-1. The average value of Young's modulus was $E = 421$ Ksi.

Table (3-1)
Test Results of Tension Coupons

No.	Thickness inch	Ultimate Stress Ksi	Initial E Ksi	Average Tangent E at $\epsilon = 2.2$ Ksi
1	0.248	8.7	474	425
2	0.249	8.2	450	385
3	0.249	8.6	433	422
4	0.249	8.77	455	406
5	0.194	8.35	467	414
6	0.193	8.45	438	368
7	0.196	8.28	470	423
8	0.194	8.72	407	315
	Average		449	394

The second test was a static creep test under sustained loads. A simply supported plexiglas beam of span 11.00 inch, width 0.84 and height 0.252 was cut from the same sheet and tested under two equal concentrated loads located at 3.5 inch from the supports. Strains in the longitudinal and transverse directions on the compression face were measured at midspan by a TML-Rosette type pc-10. Deflections and strains were measured 0, 1, 2, 5, 10, 20, 25, 30, 35, 40 minutes after load application. The loads were then removed and the beam allowed to recover for 3-4 hours, another set of loads were applied and the procedure repeated. A stress-strain diagram after 0, 5, 15 and 40 minutes of load application is given in Fig.3.9.

This graph shows that the material exhibits slight non-linearity. Results can be approximated by two linear regions with the second region

beginning at a stress level of 800 psi. Creep effectively terminates after applying the load for 40 minutes i.e. $E_c = E_{40}$ regardless of the stress level. Poisson's ratio was calculated using the transverse strain and found to increase slightly with creep from 0.358 to 0.373 after 40 minutes for all stress levels.

The objective of the third series of tests was to establish the relationship between the dynamic modulus of elasticity E_d and the loading frequency ω . Since in dynamic loading of polymers, creep does not occur, a value of E_d higher than E_c is to be expected.

Robinson (35) utilized the resonance properties of a cantilever beam to study the dynamic mechanical properties of polymers over a wide temperature range. The same concept was used for a simply supported beam without variation in temperature. The frequency range examined was 10 - 110 cps at a temperature of approximately 70° F.

The n th resonant angular frequency of a simply supported beam is given by:

$$\omega_n = A_n \sqrt{\frac{EI}{\rho A \ell^4}} \text{ rad/sec.}$$

where

ρ = mass per unit volume of the material used.

A = cross-sectional area.

ℓ = span of the beam.

A_n = coefficient of the n th mode.

$A_1 = 9.87, \quad A_2 = 39.5, \quad A_3 = 88.9$

If ω_{nc} is the n th resonant angular frequency with $E = E_c$, then:

$$\omega_{nc} = A_n \sqrt{\frac{E_c I}{\rho A \ell^4}} \quad (35)$$

If ω is the n th resonant angular frequency assuming $E = E_d$, the dynamic modulus of elasticity then:

$$\omega_{nd} = A_n \sqrt{\frac{E_d I}{\rho A \ell^4}} \quad (36)$$

from Eqs. (35) and (36)

$$\frac{\omega_{nd}}{\omega_{nc}} = \left(\frac{E_d}{E_c}\right)^{1/2} \quad (37)$$

$$\alpha = \frac{E_d}{E_c} = \left(\frac{\omega_{nd}}{\omega_{nc}}\right)^2 \quad (38)$$

If ω_{nd} is measured experimentally, and ω_{nc} evaluated from Eq.(35), α can be calculated directly from Eq.(38). Eq.(37) implies that theoretical frequencies calculated from $E = E_c$ should be adjusted to account for the difference between E_c and E_d at that frequency. The adjusted frequency can be obtained directly from Eq.(37) as:

$$\omega_{nd} = \alpha^{1/2} \omega_{nc} \quad (39)$$

To evaluate α for the plexiglas used, a simply supported beam of width 0.73 inch and depth = 0.195 inch was tested with different spans (7,8,9,10,12,14,16,18,20,22,24 inch). The same testing procedure

used for models A and B and described in Section 3-2-5 was used to determine the natural frequencies of these beams. The values of the correction factor α were calculated as described above and are shown in Fig.3.10 plotted against frequency.

The (α, ω) curve is a characteristic of the material and indicates that α decreases rapidly as the frequency ω increases from 10 to 30 cps, and then decreases very slowly up to $\omega = 110$ cps.

3-1-3 Fabrication of the models

The upper deck and the webs were cut from a 4 x 8 ft. plexiglas sheet 1/4 inch thick and the bottom deck was cut from another 4 x 8 ft. sheet 3/16 inch thick. The webs were mounted on a mold having the required curvature and heated in a special oven up to 350⁰ F until they deflected under their own weight and assumed the required curvature. They were then clamped to the mold and cooled gradually. Forming of the webs was performed by Hickey Plastics Company of Montreal.

Special aluminum frameworks were prepared to hold the webs and give them the required curvature. (Fig.3.11.) Flat wooden studs were glued to the lower face of the upper deck along the line of the webs, to permit accurate alignment of the webs. The masking paper was then stripped and taken off along the line of the webs. (Fig.3.12.) Glue Jaybond GC-18, a polymerizable cement consisting of a base, a catalyst and a promoter purchased from Johnston Industrial Plastics of Montreal, was brushed on the contact area of the upper deck and the webs, the framework of the webs was separated and the webs clamped to

the deck. The clamps were loosened slowly after setting. The diaphragms were then attached to the webs and upper deck by screws.

The lower deck was then clamped to the upper deck and the webs, and holes (drill #39) were drilled through the lower deck and the webs manually, 4 inch apart, and threaded. Machine screws (#4-40) 0.5 inch long were installed. The 4 inch spacing provided satisfactory binding and stiffness for the whole model, and prevented crackling during dynamic tests. The actual diameter of screws #4-40 is .108 inch, thus leaving a cover of 0.142 inch in the 1/4 inch webs. Since the shearing capacity of these screws is approximately 90 lb., they can sustain a shearing stress at the joint of approximately 100 psi. A similar procedure was used in static tests of box bridge models by Macias and Van Horn (28), who reported reliable experimental results.

3-2 Dynamic Model Tests

A continuum has an infinite number of degrees of freedom and hence an infinite number of natural frequencies and modal shapes. At resonance the response of any complicated structure can be simulated by a single degree of freedom system (16).

Consider a damped single degree of freedom system, subjected to a harmonic excitation $F \sin \omega t$.

$$m\ddot{u} + c\dot{u} + Ku = F \sin \omega t \quad (40)$$

As ω approaches the natural frequency ω_i , the particular solution of Eq.(40) (i.e. the natural mode) dominates. Gauzy (16) showed that in this case there is balance between the terms of Eq.(40) such that:

$$m\ddot{u} + Ku = 0$$

$$c\dot{u} - F \sin \omega_i t = 0$$

which implies that the exciting force $F \sin \omega t$ will be in balance with the damping force $c\dot{u}$, and the system behaves exactly like a conservative system, i.e. it oscillates under inertia force $m\ddot{u}$ and a restoring spring force Ku .

Recalling the case of a continuum, one can draw a parallel with a one degree of freedom system and say that to excite a natural mode one needs an infinite number of synchronized exciters oscillating at the natural frequency and oriented such as to coincide with the modal displacement and having amplitudes large enough to feed energy at each point of the system equal to that dissipated by damping.

However, practical experience shows that satisfactory results can be obtained using a relatively small number of exciters (16), arranged such that they are:

- (a) placed at points where there are important sources of energy dissipation,
- (b) placed so as to feed a maximum amount of energy into the modal shape desired, and a minimum amount of

energy into the neighbouring modes. This is usually accomplished by installing the exciters at peak points of the modal shape sought and the nodes of the neighbouring modes,

- (c) directed in space in such a way as to produce all components of the desired modal shape with the right proportion, and not to hinder any such component.

It is worth mentioning that the circuitry and equipment necessary to operate and control a large number of shakers is extremely complicated. Lewis and Wrisley (26) in 1950 developed a system able to operate and control 24 shakers, which was used for ground vibration testing of aircrafts.

Due to equipment limitations, only one shaker was used in the experiment reported here. One shaker is sufficient to excite the first few modes (21) but this sufficiency decreases as the mode number increases. Hence discrepancies from pure modal shapes are to be expected in the higher modes.

The experimental setup consists of an exciting system, pick-ups system and a display system. Fig.3.13 shows a block diagram of the experimental setup.

3-2-1 The exciting system

The single shaker used in the experiment was an electromagnet of low impedance, manufactured by Ling Electronics, special model V50 Mk.1. It can provide a peak thrust of 48 lb. when loaded by 2.5 lb.

at 100 cps and cooled with an air blower. The maximum stroke is 0.7 inch. The shaker was mounted on a rigid base and can rotate with respect to a horizontal axis. (Fig.3.14).

The circuitry consisted of a function generator (oscillator), model HP-200 CD, which generates a sinusoidal wave of frequency range 5-600000 cps with gain control. The sinusoidal signal is amplified by a power amplifier manufactured by Ling Electronics, Model TP-300 which also has a gain control. The output signal of the amplifier drives the shaker, the frequency being controlled by the oscillator and the amplitude by the gain of the oscillator and of the amplifier.

The moving part of the shaker was connected to the model through a special attachment consisting of a load cell and a two-piece core and socket connected to a light frame surrounding the cross-section of the model. (Fig.3.6).

A description of the load cell is given in Section 3-2-2. The load cell was screwed onto the moving part of the shaker and the core of the aluminum socket tightened to the top of the load cell. This core fitted into a hollow aluminum socket, the upper part of which was solid and provided with a deep groove. (Fig.3.14). This socket was also provided with two sets of screws to tighten the core to the socket. The groove in the upper part of the socket would accommodate an aluminum blade 1/8 inch thick. A hole was also drilled in this part of the socket to match with several holes drilled in the blade at different lateral positions. A connecting screw was tightened between the socket and the blade forming a hinge-like connection. The blade was fastened

to a light aluminum framework by several screws. The framework is made of 1/2 x 1/2 aluminium angles connected together with screws, and wrap the cross-section tight in the radial direction.

3-2-2 Pickup system

Three kinds of pickups were used - displacement transducers to measure displacements of the model, an accelerometer to control displacement of the shaker, and a load cell attached to the shaker head to measure the force supplied by the shaker.

Six HP 7CDCT - 1000 displacement transducers denoted by T-1, T-2, . . . , T-6 were used. They were held in place by clamps mounted on magnetic stands. Given a certain input DC voltage the transducers produce a signal linearly proportional to the displacement of the core, due to change of electric flux around the core. The transducers are able to measure displacements in the range of ± 1.00 inch with input voltage 4-6 volts and a maximum frequency of linear response of 114 cps. These transducers were calibrated together with the oscilloscope and the UV recorder. A typical calibration graph is shown in Fig.3.16. Calibration graphs were nearly linear for all input voltages.

One accelerometer manufactured by Clevite - Model 25D21 was mounted on a screw attached to the load cell as in Fig.3.14. A charge amplifier - Model 566 (Kistler Instrument Corp.) was used to provide the necessary signal amplification.

The aluminum load cell was designed to measure small dynamic

loads from 1-2 lb. up to 25 lb. The sensitive central part of the cell was 1.0 inch in length, 0.35 inch in diameter and with a wall thickness of approximately 0.02 inch. The end sections were 0.5 inch in diameter, 0.75 inch in length and threaded from within to fit end connections. Two dynamic strain gages, type ED-DY-500 BH-350 of MicroMeasurement were attached to the wall of the central section and connected to a bridge circuit as shown in Fig.3.15. The load cell was calibrated with the oscilloscope as shown in Fig.3.17.

3-2-3 Display system

The display system, Figs.3.18, 19, consisted of two oscilloscopes used for mode probing and a U.V. Recorder to record the signal when resonance was reached. One HP-140A Scope and another HP-141A Memoscope were used to display the signals and compare their phase angles. The U.V. Recorder model S.E. 2800 is provided with 12 channels, 8 inch wide recording paper, paper speed range of 1.25 - 2000 mm./sec., and time signals for grid lines at 0.01 - 10 sec. The Galvanometers used have a limit of linear response of 160 cps. The useful frequency range of the entire experimental setup is limited by the maximum frequency of linear response of the transducers which was 114 cps.

3-2-4 The resonance criteria

Recalling the single degree of freedom system (section 3-2), if a frequency sweep test is performed then it can be shown (15, 16, 21, 26) that the response at a natural frequency will be marked by the

following phenomena:

- (a) The amplitude of response per unit exciting force will reach a maximum compared to neighboring frequencies.
- (b) The phase angle between the exciting force and the response will be $\pm \pi/2$.
- (c) The rate of change of this phase angle is rapid near the natural frequency.

The effect of damping is to reduce the amplitude of response in (a) and to reduce the rate of change of the phase angle in (c).

A continuum behaves like a single D.O.F. system near resonance with the generalization that the response of all points of the continuum will be exactly in or out of phase and orthogonal to the exciting force. However, in a complicated structure such as a box girder, secondary vibrations will arise, which in effect are local vibrations and resonances of parts of the structure such as the upper or lower deck.

Although such secondary vibrations were observed, they are beyond the scope of the present work. The use of a light frame around the cross-section of the model at the excitation station, reduced local vibrations in the vicinity of the frame. Moreover the response was measured at the junction of the webs and the upper deck since such points are nodal points in a mode of local upper deck vibrations.

3-2-5 Experimental procedure

A trial and error procedure was followed to isolate the natural frequencies of the models in the light of the resonance criteria given in section 3-2-4. The procedure began with a probe for the natural modes. If there was evidence of a natural mode, an attempt was made to purify the modal shape until a modal shape was isolated as much as possible.

The probing of natural modes began by selecting a position and orientation of the exciting force guided by the theoretical modal shape. Knowing the amplitudes of vibrations at all points the angle to the vertical of the exciting force could be calculated from simple geometry for a given transverse point of application. The longitudinal location of the point of application of the load was taken as the station of peak amplitudes as mentioned in section 3-2.

A frequency sweep test was performed for a variety of positions of the shaker. The frequency was increased gradually from 5 to 120 cps while the force signal and a displacement signal (from one of the transducers mounted on the model to measure vertical displacements at various locations) were displayed on the oscilloscope. The chop position on the oscilloscope permitted display of two simultaneous signals and a measure of their relative phase angle. The signal of the exciting force was taken as reference and signals from all the displacement transducers were compared with it simultaneously all over the range of frequency sweep. Fig.3.20b shows two signals perfectly in phase.

Another method of displaying the relative phase angle of two signals (of the same frequency) on the scope is to use Lissajous figures (3), which are the loci of the motion of a particle subjected to two orthogonal harmonic motions of the same frequency but different amplitudes and phase angles. These figures can be seen easily on the scope in the chop position by plugging one signal in the horizontal axis, and the other one in the vertical axis. Fig.3.20a shows Lissajous' figure in the general case where amplitudes and phase angles are unequal.

The frequencies at which there is a $\pm \pi/2$ phase difference between the exciting force and the displacements were recorded. Records for all the transducers for a single load position provided bands of frequencies which might include a natural frequency. A record on the U.V. recorder was taken within each frequency range to examine the shape of the dynamic response.

It is very important to note that if the excitation is not correct the criteria of section 3-2-4 do not apply for all points of the structure at the same frequency, i.e. it will not be possible to get a phase difference of $\pm \pi$ between responses of various points and a phase difference of $\pm \pi/2$ between the exciting force and response of different points.

Examination of these records provided a clue as to what the modal shape is likely to be. The next step was then to move the shaker to a new position and give it an orientation in space guided by the previous modal shapes obtained, and by the rules given in section 3-2. In general the band of frequencies was narrower in the second

trial frequency sweep. This trial and error procedure was repeated until the band-width of the frequency scatter was narrow enough to enable expedient usage of the amplitude criterion of resonance. A very careful frequency sweep was then carried out in that narrow range and the amplitudes of response were measured. Whenever the natural frequency was reached, the amplitude of responses increased rapidly for a constant exciting force. If all the resonance criteria of section 3-2-4 were satisfied at this frequency, a correct natural frequency and pure modal shape is obtained.

The preceding procedure can be used with no knowledge of the modal shapes, which be the case for complicated multi-element structures such as aircrafts. However, in the present case analytical results could be used as a guide. For example, it is clear that the optimum position to excite the first mode (which is approximately a half sine wave) is located somewhere along the midspan cross-section, but the orientation of the force is unknown due to coupling. However the modal shapes obtained from the theoretical analysis served as a check on the appropriate load position and orientation.

It was found experimentally that pure modes other than the first could not be isolated and a unique natural frequency could not be obtained with the limited facilities used. However sharply defined regions around the natural frequencies were obtained.

The displacement transducers were used to measure only the vertical amplitudes of vibration of the upper deck since measuring the horizontal amplitudes of vibration proved to be experimentally awkward

due to the coupled vertical vibrations which are perpendicular to the core of the transducers. The measurement of vertical amplitudes of two points located on the same radius of the curved girder permits a comparison of the combined vertical and torsional displacements with those predicted by the analysis given in Chapter 2, as will be seen in section 4-2.

3-2-6 Experimental results

The technique described in section 3-2-5 was used to measure the first four natural frequencies of models A and B. These frequencies fall in the range of 5-115 cps as shown in Table 3-2.

Table 3-2

Measured Natural Frequencies of the
First Four Modes of Models A and B.

Model	Natural Frequency (cps) of Mode No.			
	1	2	3	4
A	12.7	59.7	63.0	114.0
B	12.5	58.65	60.50	115.0

In Table 3-2 the modes were numbered such that the lower mode has a lower frequency but not necessarily less halfsine waves of vibration. For example modes 1, 2 and 4 correspond to one halfsine wave, while mode 3 has two halfsine waves.

The simple procedure of dropping a mass on the structure to excite the first mode was attempted with a mass of 1/2 lb. dropped from one inch at the midspan section of model B. The measured frequency was 12.7 cps.

A typical record of the forced vibration taken on the U-V recorder near the fourth mode is shown in Fig.3.20.c. Amplitudes of modal shapes measured experimentally are given in section 4-2.

CHAPTER 4

ANALYSIS OF TEST RESULTS

4-1-1 Geometric properties of models

It can be clearly seen that solving Eq.(23) and finding the modal shapes is an easy task provided that all geometric and cross-sectional properties are known. However, it is known that calculating some of these parameters (K_t , I_w , X_o , Y_o) for asymmetric box sections is tedious and usually done longhand. It is unfortunate that there are no published empirical formulae to calculate these parameters explicitly for most asymmetric cross-sectional shapes [Bleich (4) gives some such formulae for angles, channels, tees, z, and uni-symmetric I-section]. The basic definition formulae will be given here, and References (22, 24, 30, 40, 48) can be consulted for more details.

For a single-cell box with n fan-like extensions, the following formulae can be used:

$$K_t = \frac{4 \Omega^2}{\oint \frac{ds}{\delta}} + \frac{1}{3} \sum_{i=1}^n b_i \delta_i^3 \quad (41-a)$$

or

$$K_t = 4 \Omega q + \frac{1}{3} \sum_{i=1}^n b_i \delta_i^3 \quad (41-b)$$

where Ω = the area enclosed by the centerline of the box's walls.

δ_i = thickness of segment i of the box's wall or of the extension.

b_i = length of extension i of the wall.

q = indeterminate shear flow in the box.

the first term of Eqs.(41-a), (41-b) represents the contribution of the box type of behavior to the torsional constant, while the second term represents the contribution of ordinary type of torsion in the extensions. In case of an open section, only the second term is applicable.

The coordinates of the shear center (x_0, y_0) and the warping moment of inertia I_w can be calculated from the following formulae:

$$\int_A \hat{w} x \, dA = 0 \quad (42-a)$$

$$\int_A \hat{w} y \, dA = 0 \quad (42-b)$$

$$I_w = \int_A \hat{w}^2 \, dA \quad (42-c)$$

where \hat{w} = the sectorial coordinate of any point on the cross-section as defined by Vlasov (40). The origin of the sectorial coordinates can be obtained from the following condition:

$$\int_A \hat{w} \cdot dA = 0 \quad (43)$$

\hat{w} can be expressed generally as:

$$w = \int_0^s h \, ds - \frac{2}{\oint \frac{ds}{\delta}} \int_0^s \frac{ds}{\delta} = \int_0^s h \, ds - 2q \int_0^s \frac{ds}{\delta} \quad (44)$$

where h = offset of the tangent to the wall at point s , measured from sectorial pole (shear center).

The first term in Eq.(44) represents warping at point s relative to that of the origin of sectorial coordinates, the second term represents the reduction of warping caused by the indeterminate shear flow q in the box. In the case of an open thin-walled section only the first term applies.

Figs.3.1 and 3.2 give the average cross-sectional dimensions and thicknesses for models A and B respectively. The physical properties of both models were calculated as described before and listed in Table 4-1. The warping displacement diagram (sectorial coordinates) for cross-sections of models A and B is given in Fig.4.1 as obtained from Eq.(44). A discussion of warping in the overhangs is given in Appendix I.

4-1-2 Mechanical properties

It was shown in section 3-1-2 that the value E_c is different for pure tension and flexure. On the other hand, the box behavior under loads results in a combination of in-plane stresses and flexural

Table 4-1
Properties of Models A and B

Property	Model A	Model B	Property	Model A	Model B
A	8.01409 in ²	8.61620 in ²	x ₀	0	0.02515 in.
I _x	12.330796 in. ⁴	12.747827 in. ⁴	y ₀	-0.26594 in.	-0.24039 in.
I _y	188.845212 in. ⁴	190.736361 in. ⁴	K _t	31.699226 in. ⁴	31.708682 in. ⁴
I _{xy}	0	0.232158 in. ⁴	I _w	67.727584 in. ⁶	60.701714 in. ⁶
r _x	0	0.039188 in.	R	51.00 in.	51.075 in.
r _y	0.49292 in.	0.400655 in.	α ₁	90°	90°
I _p	201.176008 in. ⁴	203.484188 in. ⁴	ρ	0.000114 $\frac{\text{lb. sec.}^2}{\text{in.}^4}$	0.000114 $\frac{\text{lb. sec.}^2}{\text{in.}^4}$

stresses, hence it can be concluded that the chosen E_c value should be somewhere in between.

Static analysis of curved boxes under various loading conditions (12) indicate that the ratio between major in-plane stresses and flexural stresses varies appreciably with the location and with the loading condition. It seemed logical to compare with the case of distributed loads and take the average of the in-plane modulus of elasticity (421 KSI) and the flexure one (460 KSI) hence $E_c = 440$ KSI.

Poisson's ratio $\nu = 0.36$ is taken as an average of the experimental values obtained in section 3-1-2.

4-2 Natural Frequencies and Modal Shapes

Natural frequencies can be calculated directly from Eq.(23), given the numerical data of section 4-1. The relative amplitudes of modal shapes can be calculated from Eqs.(24), (25) and (28) in terms of the vertical amplitude, which is assigned a unit value.

The program given in Appendix II was used to calculate the coupled natural frequencies of the curved girder and the natural frequencies of an equivalent straight girder with no coupling. The relative amplitudes of modal functions in the u , v and ϕ directions and the tangential movement of the roller support are given in Tables 4-2, A and B for models A and B respectively. Since the modulus of elasticity after creep E_c was used in calculating the frequencies of Tables 4-2, these values must be corrected to account for the

Table 4-2, A

ANALYSIS OF MODEL A

THE COUPLED NATURAL FREQUENCIES AND AMPLITUDES OF MODAL FUNCTIONS

MODE	FREQUENCY CPS	VERT. AMPL.	HORZ. AMPL.	TORS. AMPL.	R.S AXIAL DISPL.
1	63.82949	1.00000	122.26070	0.70411	61.03673
1	106.77053	1.00000	-0.68661	1.23520	-0.50755
1	12.43012	1.00000	-0.00883	-0.03229	-0.00012
2	198.64483	1.00000	0.32415	0.93661	0.01877
2	286.79655	1.00000	-66.36014	1.33777	-16.67898
2	67.23980	1.00000	-0.00293	-0.04239	0.00209
3	300.13468	1.00000	0.07247	0.73861	-0.02066
3	656.28884	1.00000	-120.57751	1.59996	-20.16717
3	158.78449	1.00000	-0.00213	-0.05382	0.00203
4	411.62312	1.00000	0.02637	0.51525	-0.01383
4	1173.71697	1.00000	-143.59556	1.71838	-18.00657
4	284.71107	1.00000	-0.00228	-0.07717	0.00228
5	541.86423	1.00000	0.00966	0.28618	-0.00664
5	1838.99027	1.00000	-155.20311	1.77940	-15.56763
5	437.53220	1.00000	-0.00335	-0.13897	0.00336

THE UNCOUPLED NATURAL FREQUENCIES OF AN EQUIVALENT STRAIGHT BRIDGE

MODE	HORIZ. FREQ. CPS	VERT. FREQ. CPS	TORS. FREQ. CPS
1	0.738140 02	0.188620 02	0.935460 02
2	0.295260 03	0.754470 02	0.189180 03
3	0.664330 03	0.169760 03	0.288900 03
4	0.118100 04	0.301790 03	0.394600 03
5	0.184540 04	0.471540 03	0.507940 03

Table 4-2, B

ANALYSIS OF MODEL B

THE COUPLED NATURAL FREQUENCIES AND AMPLITUDES OF MODAL FUNCTIONS

MODE #	FREQUENCY CPS	VERT. AMPL.	HORZ. AMPL.	TORS. AMPL.	R,S AXIAL DISPL.
1	61.69741	1.00000	146.95978	0.79470	73.38416
1	106.37042	1.00000	-0.60848	1.26058	-0.45609
1	12.10491	1.00000	-0.00656	-0.03257	0.00064
2	197.28017	1.00000	0.33461	0.96011	0.02583
2	277.10761	1.00000	-59.45863	1.23838	-14.93925
2	65.64276	1.00000	-0.00138	-0.04296	0.00224
3	297.38043	1.00000	0.07301	0.76074	-0.01838
3	634.10730	1.00000	-106.47690	1.38855	-17.80191
3	155.09860	1.00000	-0.00067	-0.05457	0.00208
4	406.77876	1.00000	0.02737	0.53571	-0.01271
4	1134.05745	1.00000	-124.73648	1.45132	-15.63577
4	278.18146	1.00000	-0.00081	-0.07799	0.00225
5	533.70744	1.00000	0.01095	0.30268	-0.00620
5	1776.85941	1.00000	-133.58063	1.48253	-13.39378
5	427.76370	1.00000	-0.00181	-0.13907	0.00317

THE UNCOUPLED NATURAL FREQUENCIES OF AN EQUIVALENT STRAIGHT BRIDGE

MODE	HORIZ. FREQ. CPS	VERT. FREQ. CPS	TORS. FREQ. CPS
1	0.71334D 02	0.18442D 02	0.92870D 02
2	0.28534D 03	0.73766D 02	0.18760D 03
3	0.64201D 03	0.16597D 03	0.28598D 03
4	0.11413D 04	0.29506D 03	0.38969D 03
5	0.17833D 04	0.46104D 03	0.50027D 03

dynamic modulus of elasticity E_d .

Recalling Eqs.(17) for natural frequencies of a straight simply supported beam with uncoupled vibrations, it can be seen that the frequency ω is proportional to the square root of E . However, in the general case of coupled vibrations, this relationship is not identical as can be seen from Eq.(23). Nevertheless, the preceding approximation is probably adequate for the relatively small corrections involved. Eq.(39) is used, with α taken from Fig.3.10, to correct the frequencies of Tables 4-2, A and B.

Table 4-3
Corrected Theoretical Natural Frequencies
vs. Experimental Values

Model	Mode No.	Calculated Frequency	$\alpha^{1/2}$	Frequency cps.		Error %
				Theoretical	Experimental	
A	1	12.43	1.107	13.55	12.7	-5.53
	2	63.83	1.025	65.20	59.7	-8.42
	3	67.24	1.023	68.90	63.0	-8.6
	4	106.77	1.020	108.8	114.0	+4.78
B	1	12.10	1.10	13.3	12.5	-6.02
	2	61.70	1.026	63.20	58.65	-7.20
	3	65.64	1.024	67.10	60.50	-9.85
	4	106.37	1.02	108.30	115.0	+6.18

Table 4-3 shows the calculated frequencies obtained from Tables 4-2, A and B, the corresponding correction factors, the corrected

theoretical frequencies, the corresponding experimental values and the percentage of error.

Figs.4.1, 4.2, 4.3 and 4.4 show a perspective view of the first four modal shapes for the upper deck of model B as predicted by Eqs.(24), (25) and (28) with the amplitudes taken from Table 4-2, B. Vertical component of the modal shape of the exterior edge V_1 and interior edge V_2 of the upper deck are also shown with the corresponding experimental results. These Figures also show two positions of the cross-section at maximum amplitudes and the optimum location and orientation of the exciting force.

CHAPTER 5

DISCUSSION, SUMMARY AND CONCLUSIONS

5-1 Limitations of the Results

Experimental frequencies are within a margin of $\pm 5 - 9\%$ of calculated values. Some possible sources of error can be identified as follows:

(a) Theoretical solutions

- (i) The value of E_c used in calculating the natural frequencies, though reasonable, is not necessarily correct. The exact E_c value for plexiglas is hard to predict as was shown in section 3-1-2.
- (ii) The theoretical values obtained from Eq.(23) were based on the assumption of a beam-like behavior and thin walled cross-sectional dimensions. In fact the width/diameter ratio of the model (18/51), and the width/span ratio (18/80) are both relatively large for a reliable application of thin walled beam theory.
- (iii) The curvature of both models (1/51) is relatively high compared to real curved highway bridges. For very large curvatures the shift in the position of the neutral axis of the beam towards the center of curvature should be considered.
- (iv) The effects of diaphragms used in both models are not accounted for in the thin walled beam theory. Such diaphragms change the torsional stiffness of

the box, and so the natural frequencies.

(b) Experimental results

- (i) As mentioned previously (section 3-2) an infinite number of synchronized shakers is needed to excite a pure mode of a continuum. The smaller the number of shakers used the more error can be expected in natural frequencies and modal shapes.
- (ii) For a given number of shakers (one in our case), discrepancies from the correct modes will increase as the number of halfsine waves of the mode increases. This was experienced in the test results. For mode 3, which consists of two halfsine waves, it was found that there is a small amplitude of vibration at the theoretical nodal line located at midspan (Fig.4.3) in addition to incomplete symmetry of the modal shapes.
- (iii) Force orientation was considered taking into account the u , v and ϕ but not the w displacements. For mode 2 where the axial or tangential vibrations are significant, one might expect more error than in modes 1 and 4.

5-2 Summary

The objectives of this work were to obtain a solution to the general case of coupled free vibrations of curved simply-supported box girders of any cross-section, and to carry out laboratory tests to compare with theoretical natural frequencies and modal shapes.

An idealized model was developed in Chapter 2. The basic differential equations of motion of a curved thin walled beam element were derived for quadruple coupling between the radial, vertical, torsional and tangential vibrations. The cross-section was assumed non-deformable while damping, rotary inertia and shear deformations were neglected. It is important to state that this analysis cannot predict local vibrations of various parts of the girder. By neglecting axial inertia forces and assuming the axial force equal to zero, quadruple coupling was reduced to triple coupling between radial, vertical and torsional vibrations. The case of a simply-supported curved girder was solved assuming sinusoidal modal functions. Amplitudes of modal functions were determined relative to the vertical one and the amplitude of tangential motion of the roller support was calculated. The orthogonality condition of the coupled modal functions was established and satisfied for small amplitudes of vibration. A parametric study was performed to investigate the effect of various geometric parameters on coupled natural frequencies. The results of the parameter study are given in section 2-11.

Two simply-supported curved box girder models made of plexiglas were tested experimentally. The first model had a single cell section symmetric with respect to the vertical axis. The second model had a two-cell asymmetric cross-section. Both models have a central angle of 90° , radius of 51 inches, upper deck width of 18 inches, depth of 2.7 inches.

The models were excited by one concentrated dynamic force whose position, orientation, frequency and amplitude can be controlled. Probing of natural modes was done by a trial and error procedure until a nearly pure modal shape satisfying resonance criteria involving phase and amplitude was obtained. Vertical response at several points on the upper deck were measured for the first four modes. Reasonable agreement between the theoretical and experimental frequencies and modal shapes was obtained.

5-3 Conclusions

It can be concluded that thin walled beam theory, which is the basis of the given theoretical analysis, together with the other simplifying assumptions, can be used to estimate the natural modes and frequencies of a curved simply-supported girder of asymmetric multi-cell section, even in cases of high curvature, width/radius, width/span ratios.

REFERENCES

1. Aneja, I.K., *Experimental and Analytical Study of a Horizontally Curved Box-beam Highway Bridge Model.* Ph.D. Dissertation, Dept. of Civil Engr., Univ. of Pennsylvania, 1968.
2. Benscoter, S.U., *A Theory of Torsion Bending for Multi-cell Beams.* Jour. of Applied Mech., Trans. ASME, Vol.76, 1954.
3. Bishop, R.E.D. and Johnson, D.C., *The Mechanics of Vibration.* Cambridge Univ. Press, 1960.
4. Bleich, F., *Buckling Strength of Metal Structures.* McGraw-Hill Book Co.Inc., 1952.
5. Broch, J.T., *The Application of the Brüel and Kjaer Measuring Systems to Mechanical Vibration and Shock Measurements.* Brüel and Kjaer, Naerum, Denmark.
6. Christiano, P.P., *The Dynamic Response of Horizontally Curved Bridges subject to Moving Loads.* Ph.D. Dissertation, Dept. of Civil Engr., Carnegie-Mellon Univ., Oct. 1967.
7. Christiano, P.P. and Culver, C.G., *Horizontally Curved Bridges subject to Moving Load.* Jour. Struc. Div., ASCE, Aug. 1969.
8. Culver, C.G., *Natural Frequencies of Horizontally Curved Beams.* Jour. Struc. Div., ASCE, April 1967.
9. Dabrowski, R., *Equations of Bending and Torsion of a Curved Thin Walled Bar with Asymmetric Cross-section.* Archiwum Mechaniki, Stosowanej, Vol.12, 1960.

- 10.* Dabrowski, R., *Zur Berechnung von Gekrümmten Dünnwandigen Trägern mit Offenem Profil.* Der Stahlbau, Wilhelm Ernst und Sohn, Berlin-Wilmersdorf, Germany, Dec. 1964.
- 11.* _____ *Wölbkrafttorsion von Gekrümmten Kastenträgern mit Nichtverformbarem Profil.* Der Stahlbau, Wilhelm Ernst und Sohn, Berlin-Wilmersdorf, Germany, May 1965.
12. Fam, A.M., *Static and Free Vibrations Analysis of Curved Box Girders.* Ph.D. Dissertation in preparation, Dept. of Civil Eng. and Applied Mechs., McGill University.
13. Federhofer, K., Sitzber. Akad. Wiss. Wien, Abt. IIa, Vol.156, 1947.
14. Fine, I.M., *The Vibrations of Multi-girder Highway Bridges.* M.Eng. Thesis, Dept. of Civil Engr. and Applied Mechs., McGill Univ., Aug. 1966.
15. Fraeijs de Veubeke, R.M., *A Variational Approach to Pure Mode Excitation based on Characteristic Phase Lag Theory.* AGARD Report 39, April 1956.
16. Gauzy, H., *Vibration Testing by Harmonic Excitation.* AGARD, Manual on Aeroelasticity, Vol.1, 1961.
17. _____ *Measurement of Inertia and Structural Damping.* AGARD, Manual on Aeroelasticity, Vol.IV, 1961.
18. Gere, J.M. and Lin, Y.K., *Coupled Vibrations of Thin Walled Beams of Open Cross-section.* Jour. of Applied Mech., ASME, Vol.80, 1958.

* Translated in cooperation with the Translations Section, National Science Library, NRC, Ottawa - Technical Translations 1548 and 1549.

19. Harris, C.M. and Crede, C.E., *Shock and Vibration Handbook*.
McGraw-Hill Book Co. Inc., 1961.
20. Iyengar, K.T.S.R. and Iyengar, R.N., *Free Vibrations of Beam and Slab Bridges*. IABSE, pub.Vol.27, 1967.
21. Kennedy, C.C. and Pancu, C.D.P., *Use of Vectors in Vibration Measurement and Analysis*. Jour. of the Aeronautical Sciences, Vol.14, No.11, Nov. 1947.
22. Kollbrunner, C.F. and Basler, K., *Torsion in Structures*.
Springer-Verlag, New York, Heidelberg, Berlin, 1969.
23. Komatsu, S. and Nakai, H., *Study on Free Vibration of Curved Girder Bridges*. 19th Annual Conf., Japan Soc. of Civ. Engrs., May 1964.
24. Kuhn, P., *Stresses in Aircraft and Shell Structures*. McGraw-Hill Book Co. Inc., 1956.
25. Lang, T.E., *Vibration of Thin Circular Rings*. Tech. Rep. No.32-261, Jet Propulsion Laboratory, California Institute of Technology, July 1962.
26. Lewis, A.C. and Wrisley, D.L., *A System for the Excitation of Pure Modes of Complex Structures*. Jour. of the Aeronautical Sciences, No.11, 1950.
27. Love, A.E.H., *A Treatise on the Mathematical Theory of Elasticity*.
Dover Publications, New York.
28. Macfas Rendón, M.A. and Van Horn, D.A., *Structural Model Study of Load Distribution in Box Beam Bridges*. Report No.322.1, Fritz Engineering Laboratory, Lehigh Univ., Bethlehem, Penn.

29. Morrow, C.T., *Shock and Vibration Engineering.* John Wiley and Sons Inc., Vol.I, 1963.
30. Oden, J.T., *Mechanics of Elastic Structures.* McGraw-Hill Book Co. Inc., 1967.
31. Oestel, D.J., *Dynamic Response of Multispan Curved Bridges.* M.Sc. Thesis, Dept. of Civil Engr., Carnegie-Mellon Univ., Nov. 1968.
32. Ojalvo, I.U., *Coupled Twist-bending Vibrations of incomplete Elastic Rings.* Int.J.Mech.Sci., Pergamon Press Ltd., Vol.4, 1962.
33. Rayleigh, J.W.S., *The Theory of Sound.* Vol.I, Dover Publications, New York.
34. Reddy, M.N., *Lateral Vibrations of Plane Curved Bars.* Jour. Str.Div., ASCE, Vol.94, Oct. 1968.
35. Robinson, D.W., *An Apparatus for the Measurement of Dynamic Mechanical Properties of Polymers over a Wide Temperature Range.* Jour.Scientific Instruments, 32,2, 1955.
36. Tan, C.P. and Shore, S., *Dynamic Response of Horizontally Curved Bridges.* Jour.Str.Div., ASCE, Vol.94, March 1968.
37. Timoshenko, S.P., *Vibration Problems in Engineering.* Van Nostrand Co., New York, 1955.
38. Tinawi, R.A., *Behaviour of Orthotropic Bridge Decks.* Ph.D. Dissertation, Dept. Civ. Engr. and Applied Mechs., McGill University, 1972.

39. Vashi, K.M., *Dynamic Response of Simple Span Horizontally Curved Highway Bridges to Moving Vehicles.* Ph.D. Dissertation, Dept. of Civil Engr., Univ. of Maryland, 1970.
40. Vlasov, V.Z., *Thin Walled Elastic Beams.* 2nd. Edition, National Science Foundation, Washington D.C., 1961.
41. Volterra, E., *The Equations of Motion for Curved Elastic Bars deduced by the use of the Method of Internal Constraints.* Ingenieur-Archiv., Vol.23, 1955.
42. _____ *Eigenvibrations of Curved Elastic Bars according to the Method of Internal Constraints.* Ingenieur-Archiv., Vol.24, 1956.
43. _____ *The Equations of Motion for Curved and Twisted Elastic Bars deduced by the Method of Internal Constraints.* Ingenieur-Archiv., Vol.24, 1956.
44. Volterra, E. and Morell, J.D., *Lowest Natural Frequencies of Elastic Arcs.* Jour. of the Acoustical Soc. of America, Vol.33, No.12, Dec. 1961.
45. Volterra, E. and Morell, J.D., *Lowest Natural Frequency of Elastic Arc for Vibrations outside the Plane of Initial Curvature.* Trans. ASME, Vol.83, Jour. of Applied Mech., Dec. 1961.
46. Von Karman, T. and Chien, W.Z., *Torsion with Variable Twist.* Jour. of the Aeronautical Sciences, Vol.13, Oct. 1946.

47. Yonezawa, H., *Moments and Free Vibrations in Curved Girder Bridges.* Jour. of Engr. Mech. Div., ASCE, Vol.88, EMI, Feb.1962.
48. Zbirohowski - Koscia, K., *Thin Walled Beams.* Crosby-Lockwood and Son Ltd., 1967.

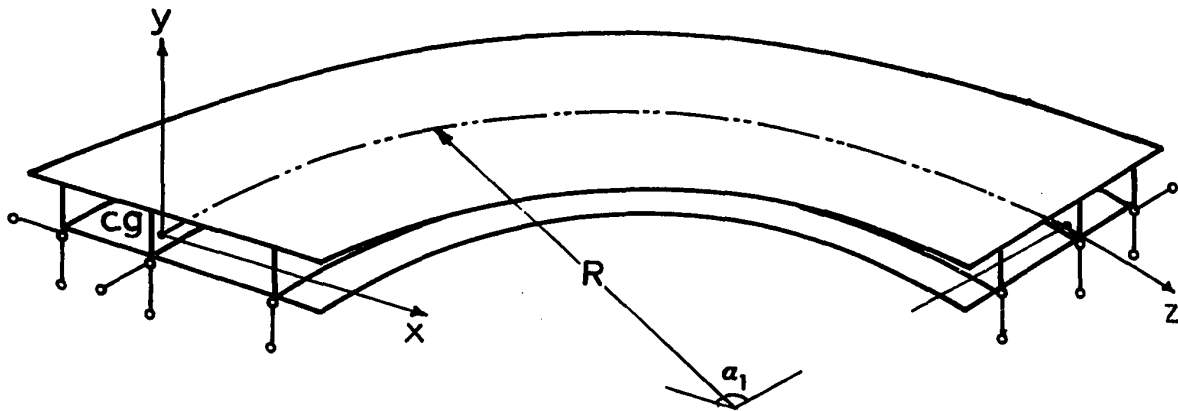


Fig. 2.1 Idealized model of a simply supported curved asymmetric box girder

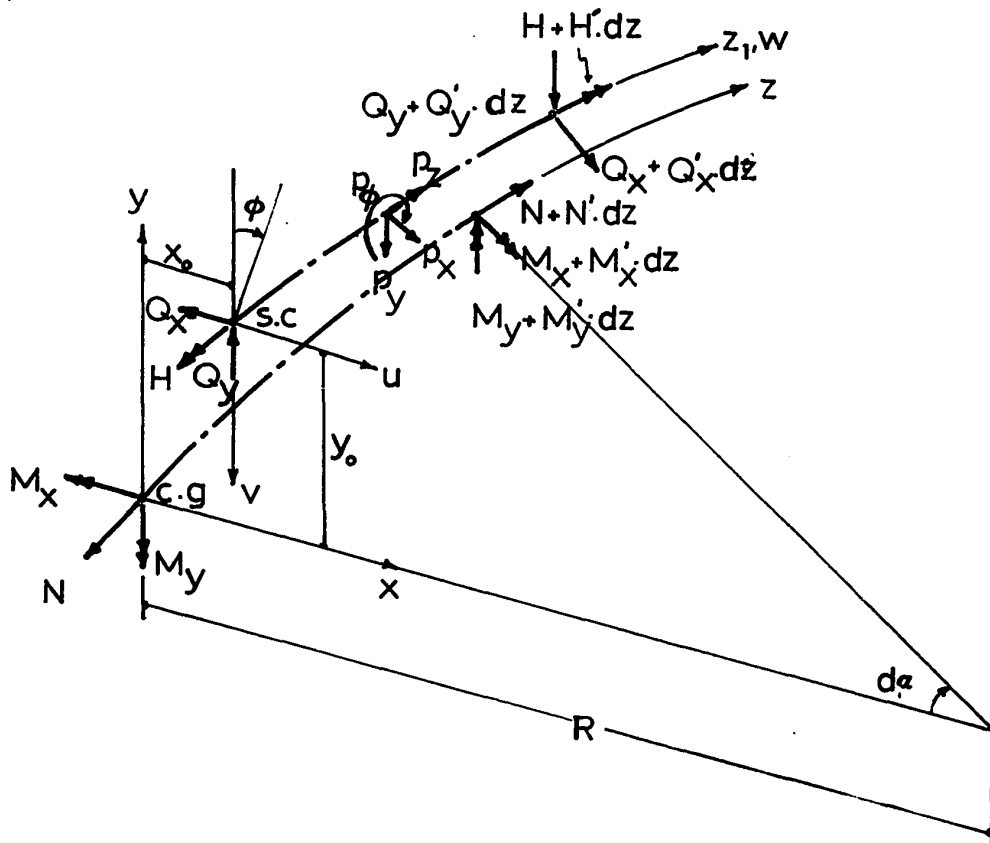
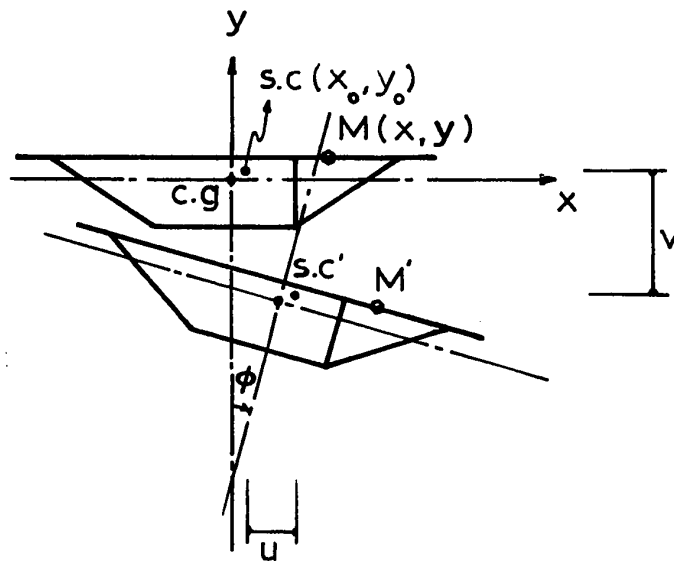


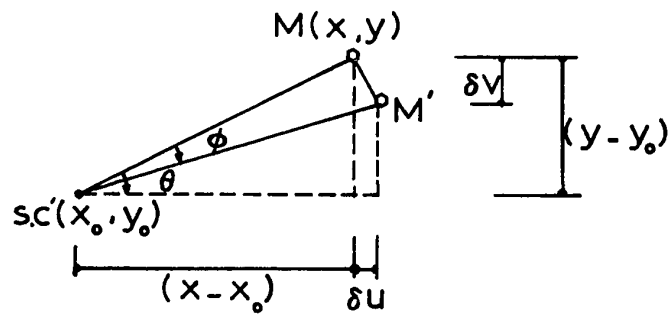
Fig. 2.2 Forces acting on an element of a curved girder

Vertical ($v - \phi x_0$)

Horizontal ($u - \phi y_0$)



(a) Net centroidal displacements



$$\delta u = (x - x_0)(\cos \phi - 1) + (y - y_0) \sin \phi$$

$$\delta v = (x - x_0) \sin \phi + (y - y_0)(1 - \cos \phi)$$

(b) Net displacement of a point on the wall
M due to an angle of twist ϕ only.

Fig.2.3

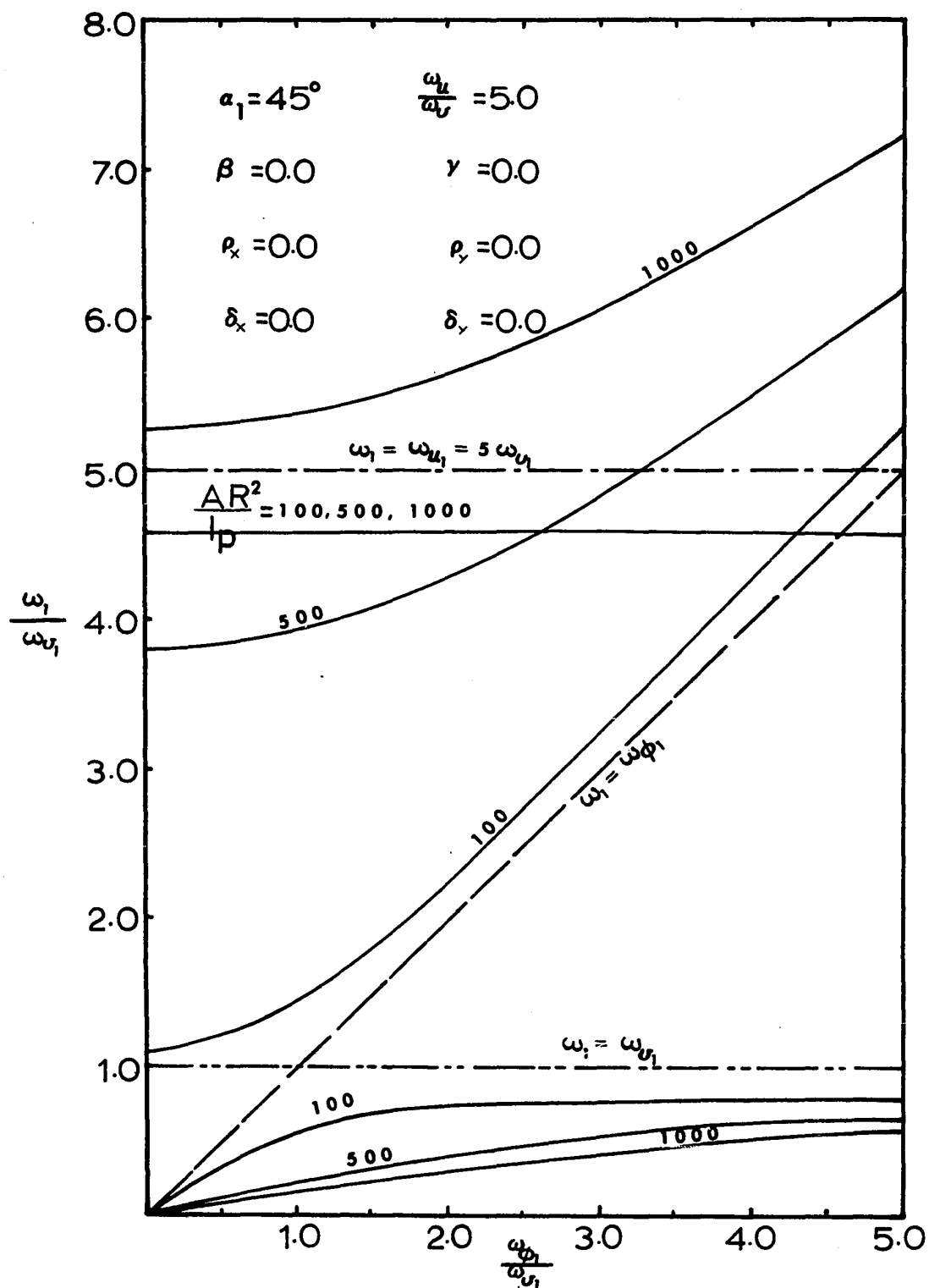


Fig.2.4 First Mode Natural Frequencies of Curved Girders
of a Symmetric Cross-Section
(Double Coupling between v and ϕ)

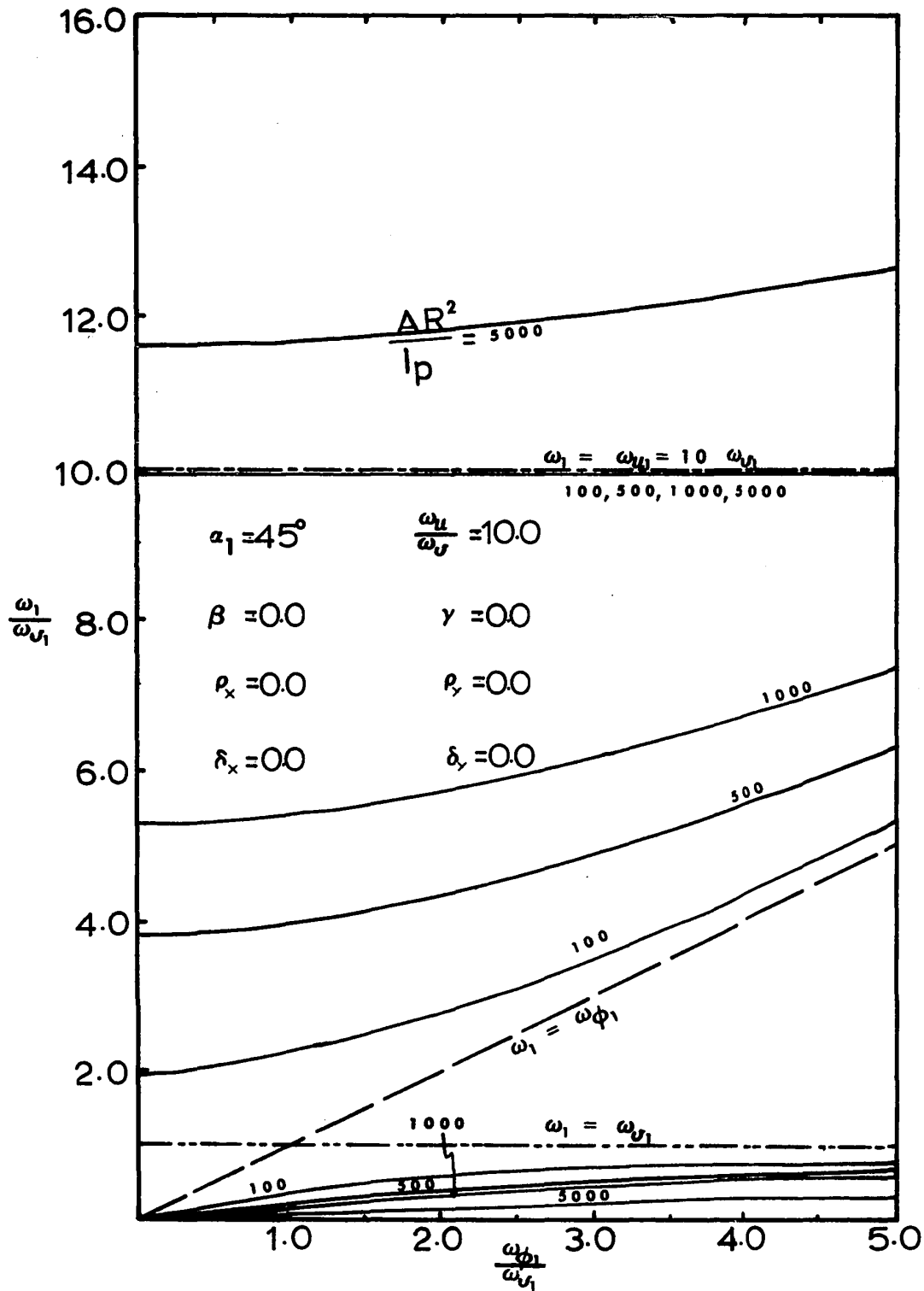


Fig.2.5(a) First Mode Natural Frequencies of Curved Girders of a symmetric Cross-section (Double Coupling between v and ϕ)

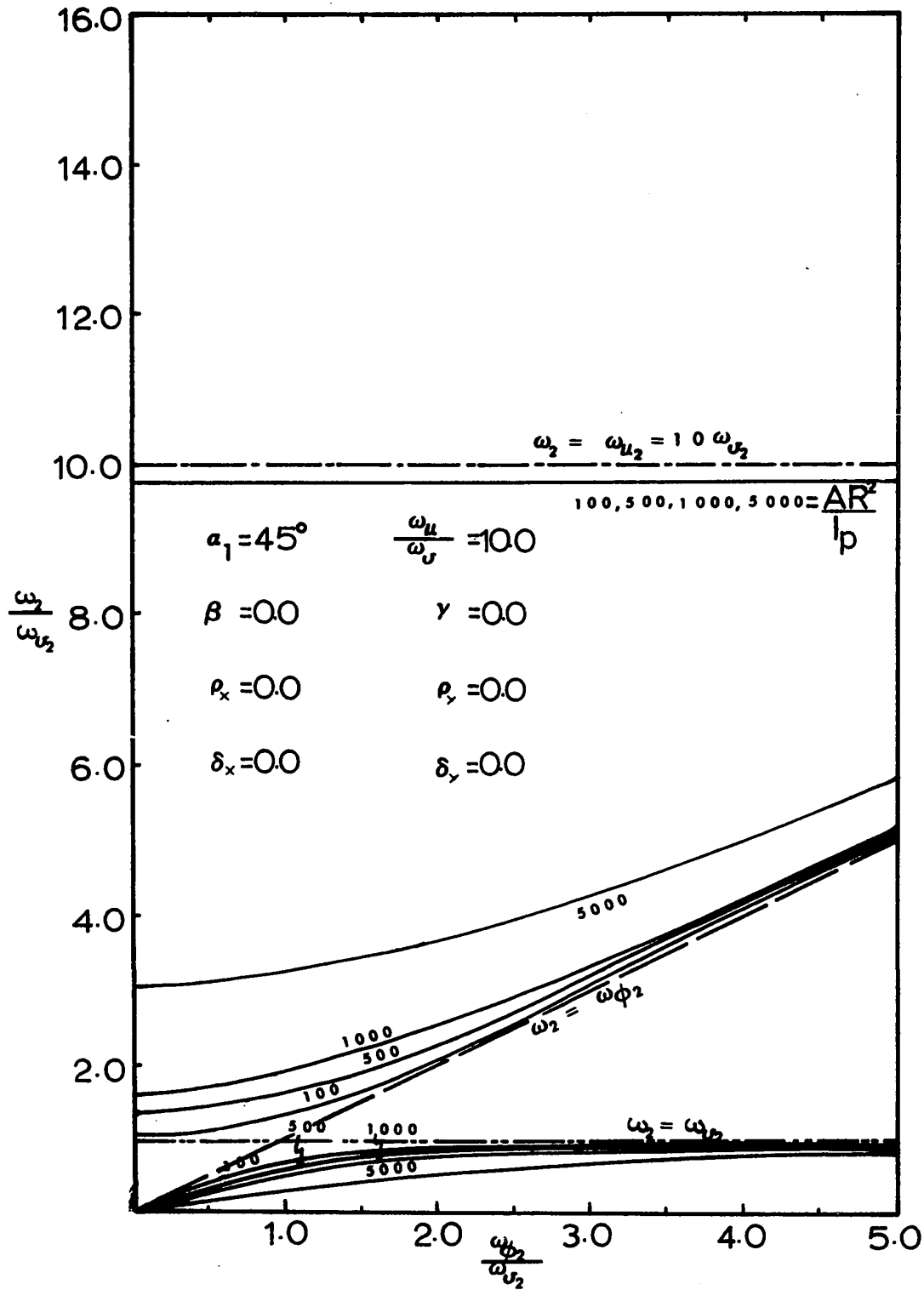


Fig.2.5(b) Second Mode Natural Frequencies of Curved Girders of a symmetric Cross-Section (Double Coupling between v and ϕ)

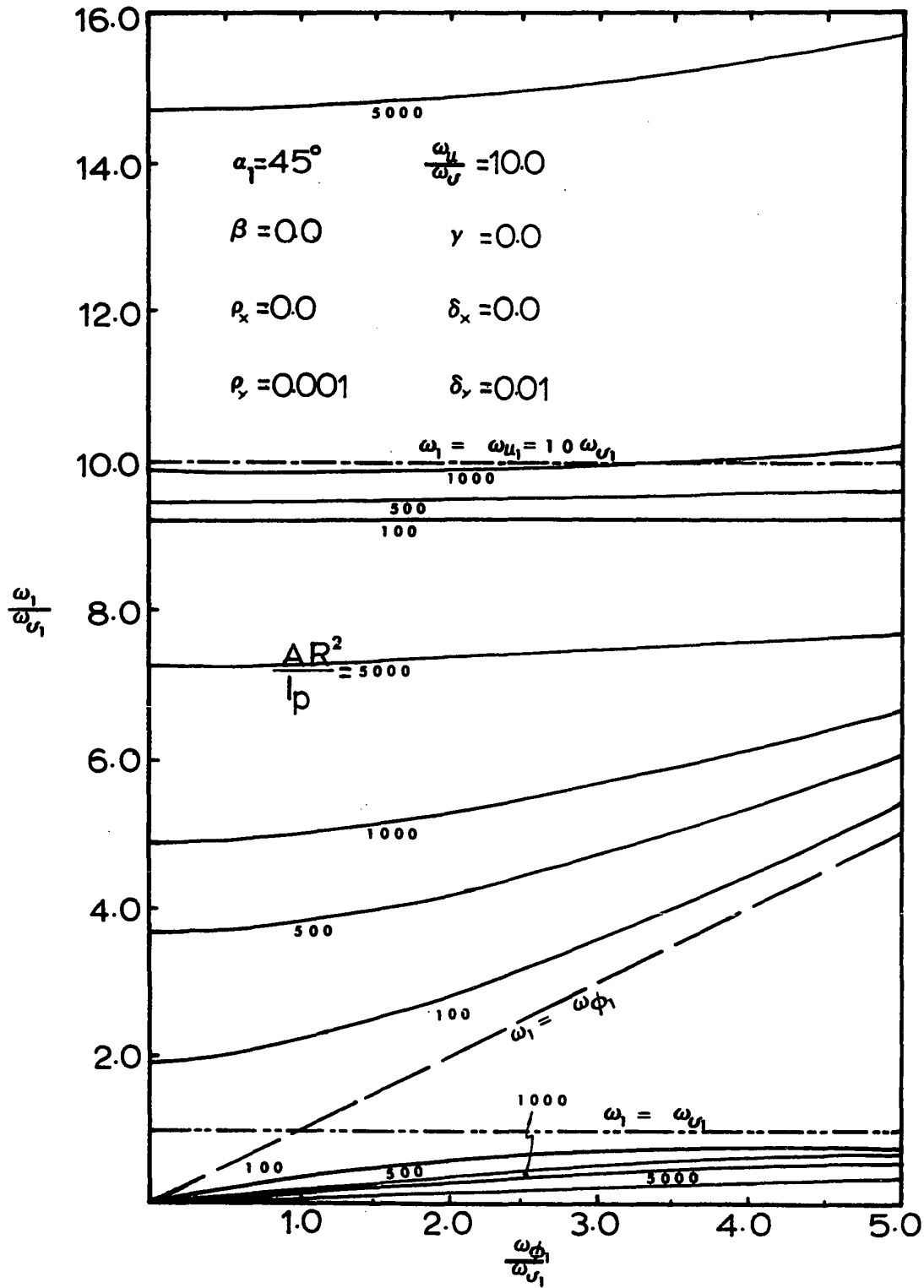


Fig.2.6(a) First Mode Natural Frequencies of Curved Girders of an Asymmetric Cross-Section (Triple Coupling between u, v and ϕ)

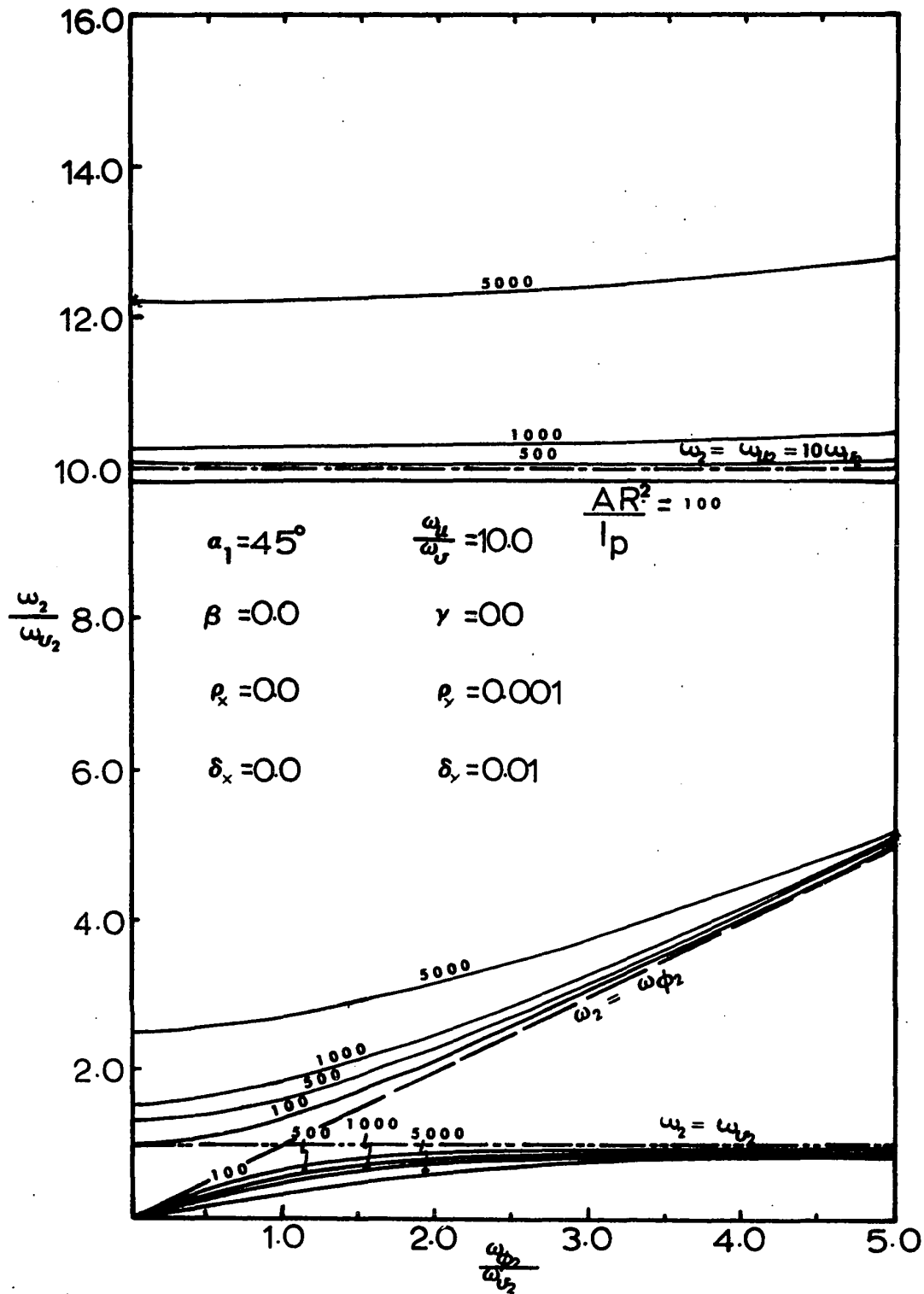


Fig.2.6(b) Second Mode Natural Frequencies of Curved Girders of an Asymmetric Cross-Section (Triple Coupling between u , v and ϕ)

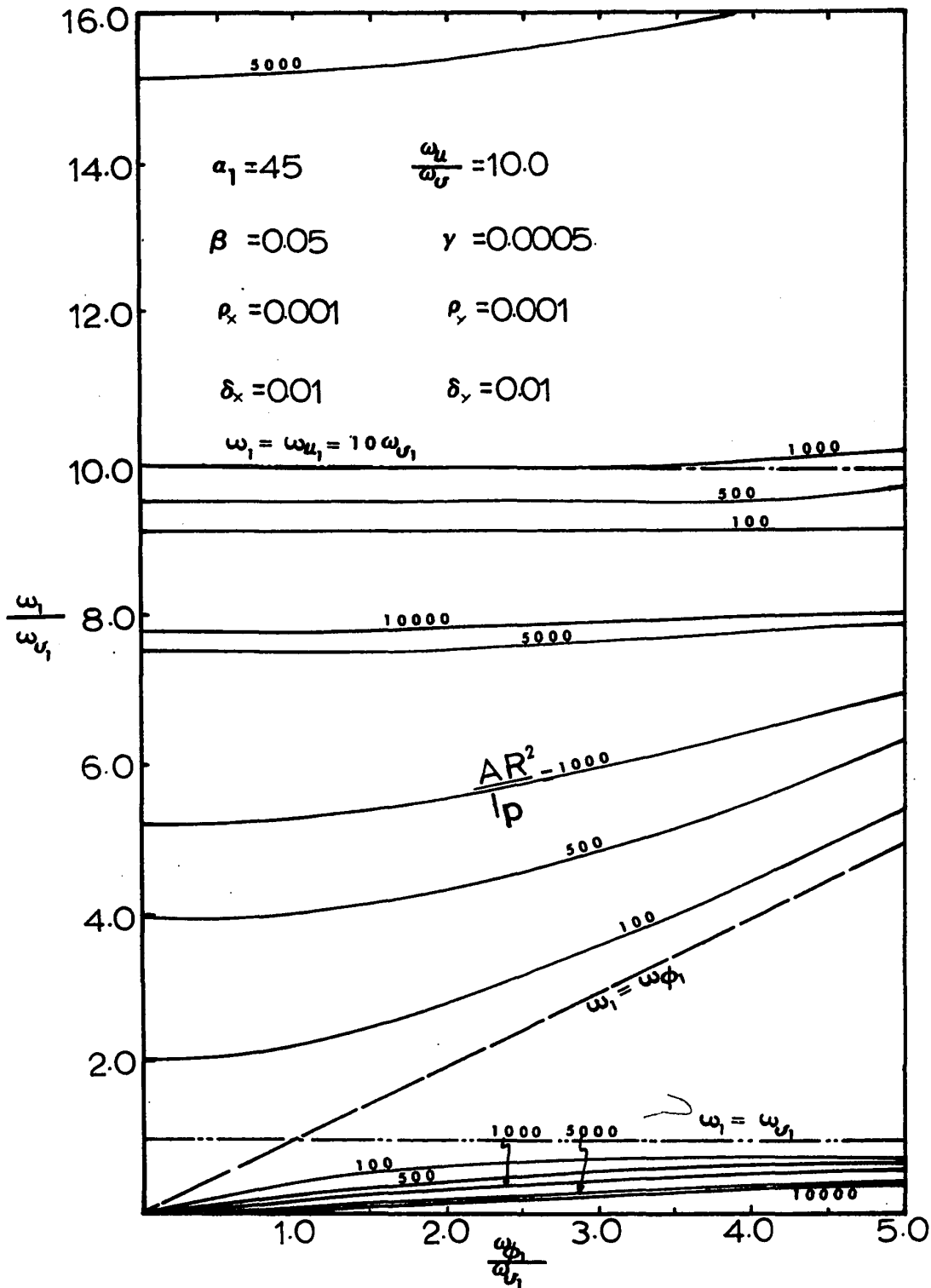


Fig.2.7(a) First Mode Natural Frequencies of Curved Girders of an Asymmetric Cross-Section (Triple Coupling between u , v and ϕ)

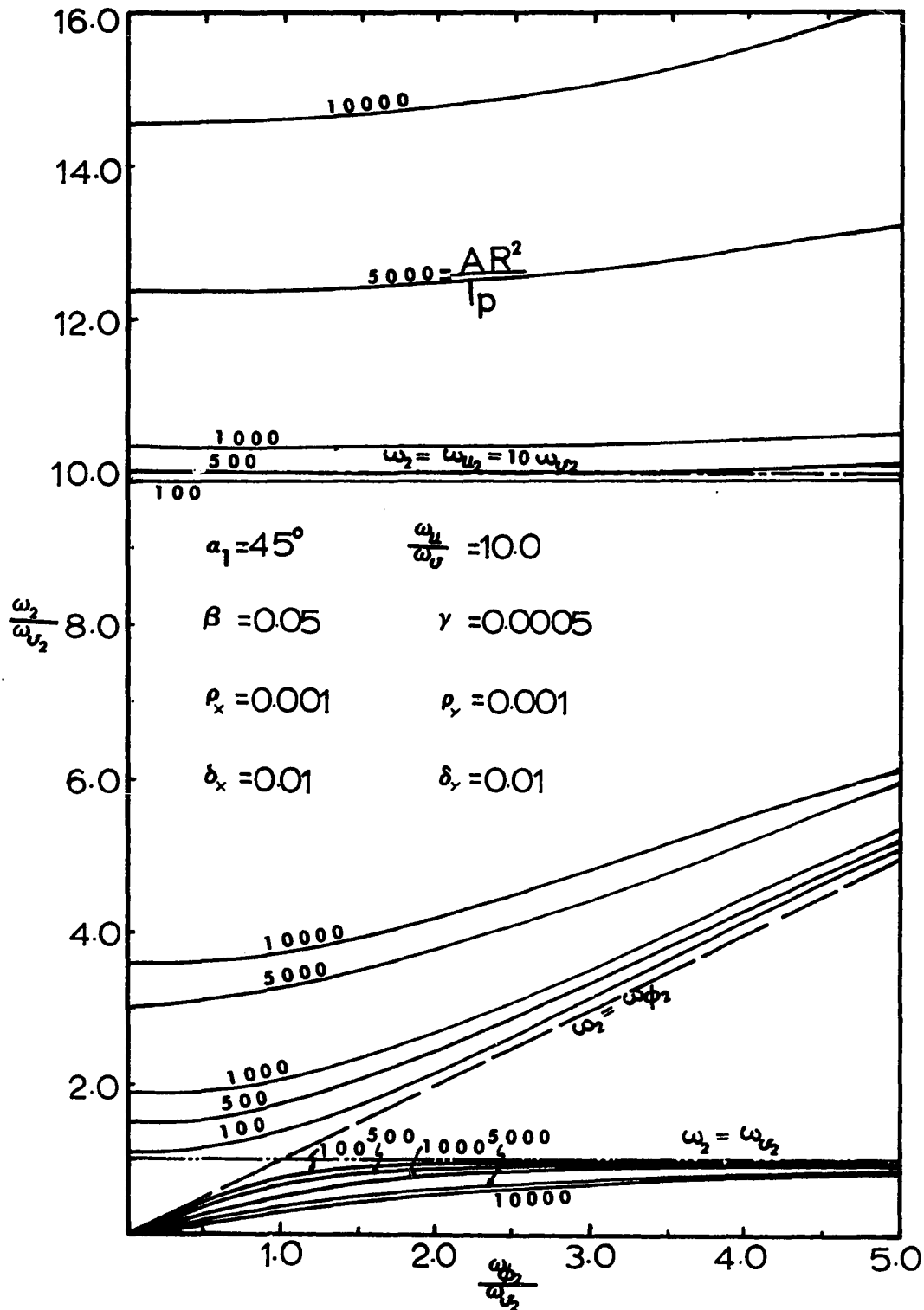


Fig.2.7(b) Second Mode Natural Frequencies of Curved Girders of an Asymmetric Cross-Section (Triple Coupling between u , v and ϕ)



•

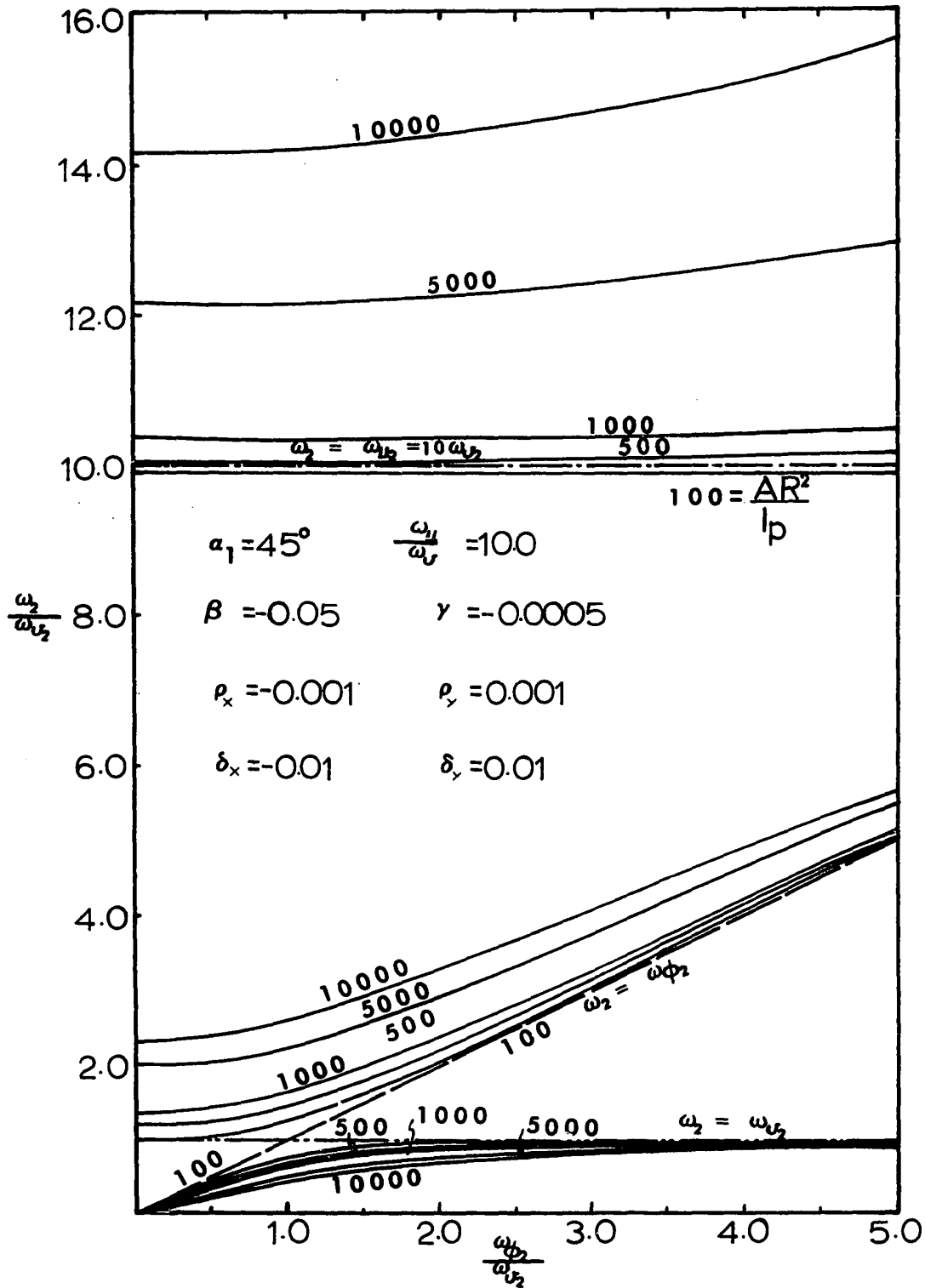


Fig.2.8(b) Second Mode Natural Frequencies of Curved Girders of an Asymmetric Cross-Section (Triple Coupling between u , v and ϕ)

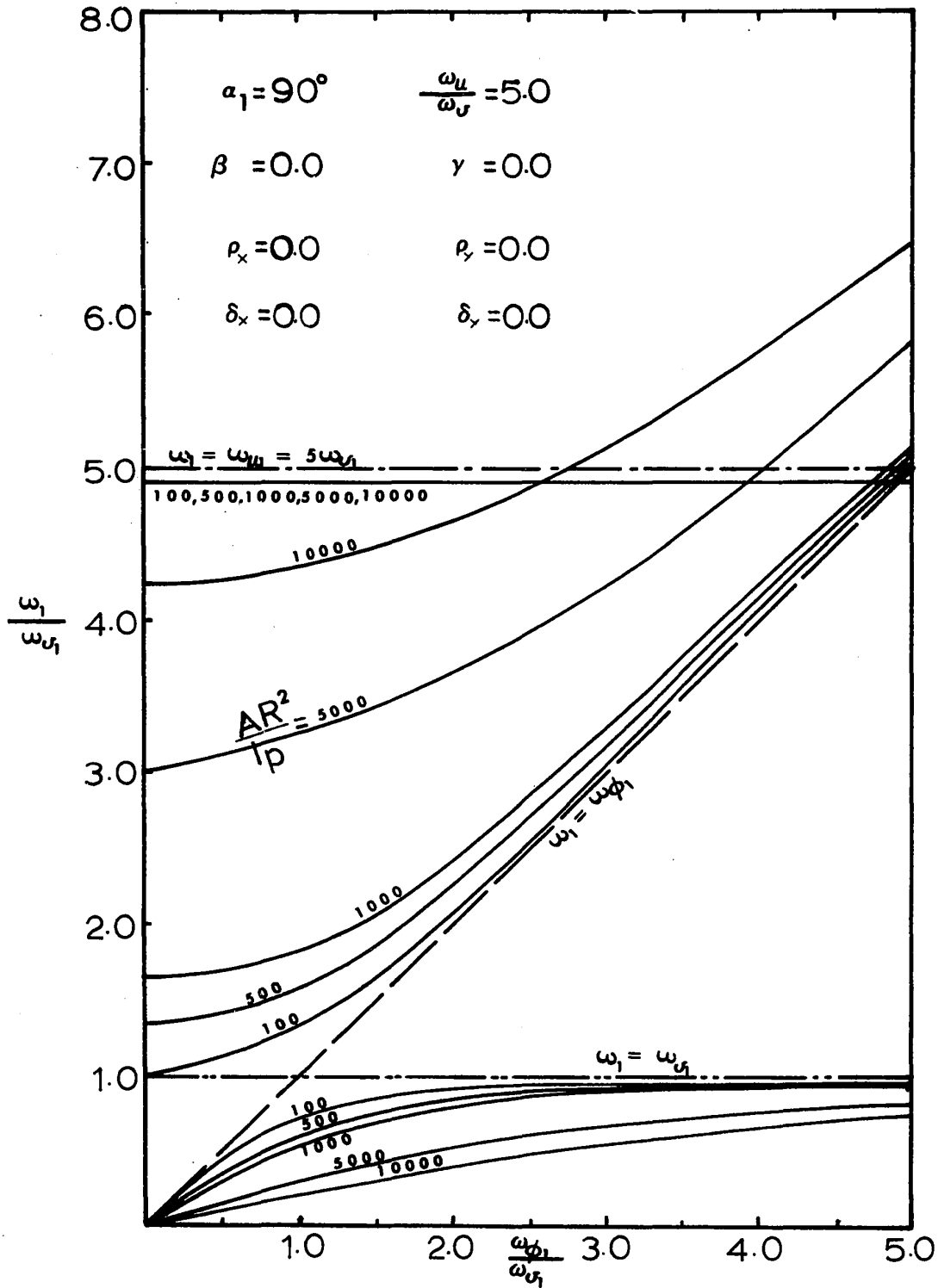


Fig.2.9(a) First Mode Natural Frequencies of Curved Girders of a symmetric Cross-Section (Double Coupling between v and ϕ)

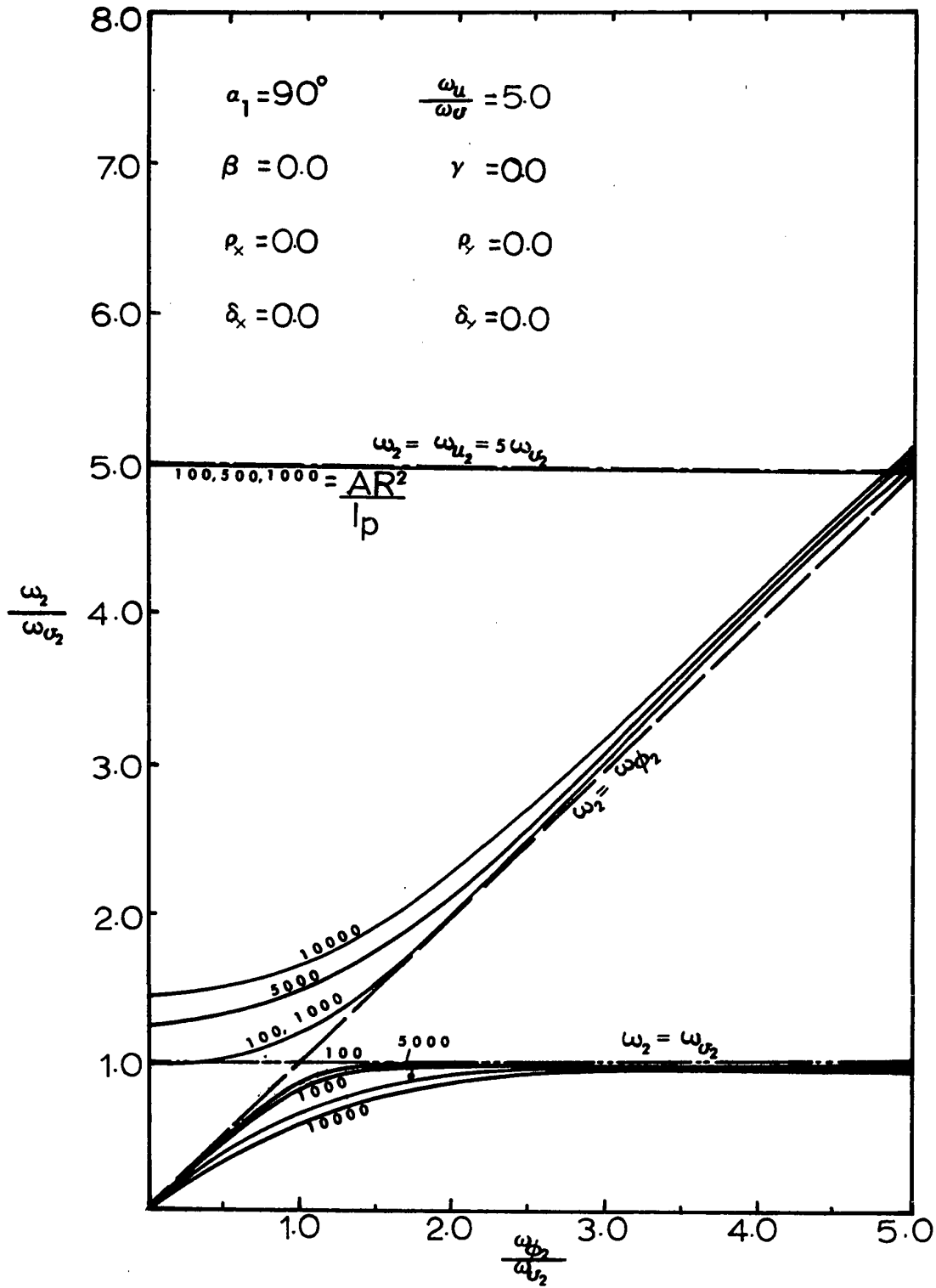


Fig.2.9(b) Second Mode Natural Frequencies of Curved Girders of a Symmetric Cross-Section (Double Coupling between v and ϕ)

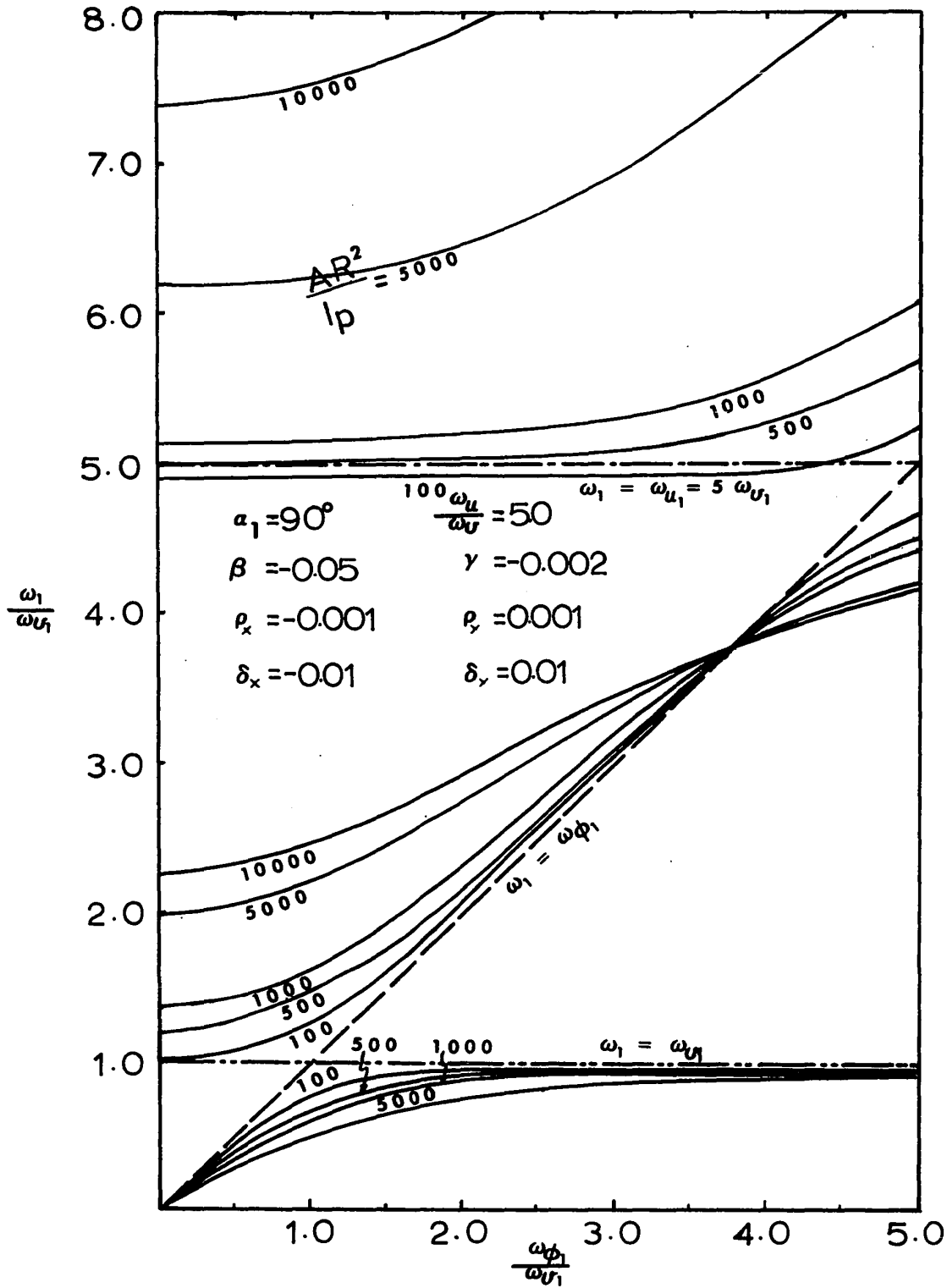


Fig.2.10(a) First Mode Natural Frequencies of Curved Girders of an Asymmetric Cross-Section (Triple Coupling between u , v , and ϕ)

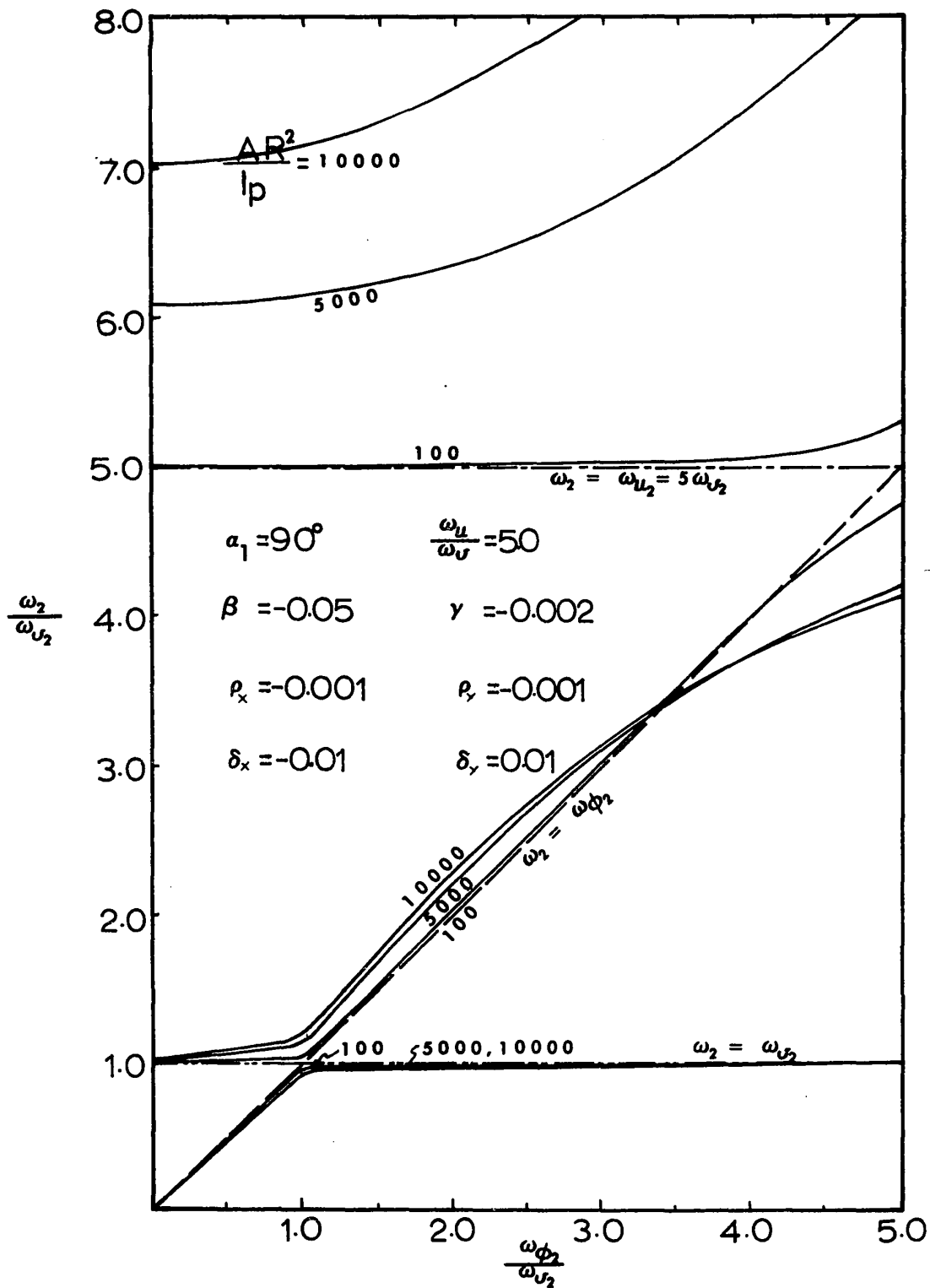


Fig.2.10(b) Second Mode Natural Frequencies of Curved Girders of an Asymmetric Cross-Section (Triple Coupling between u , v and ϕ)

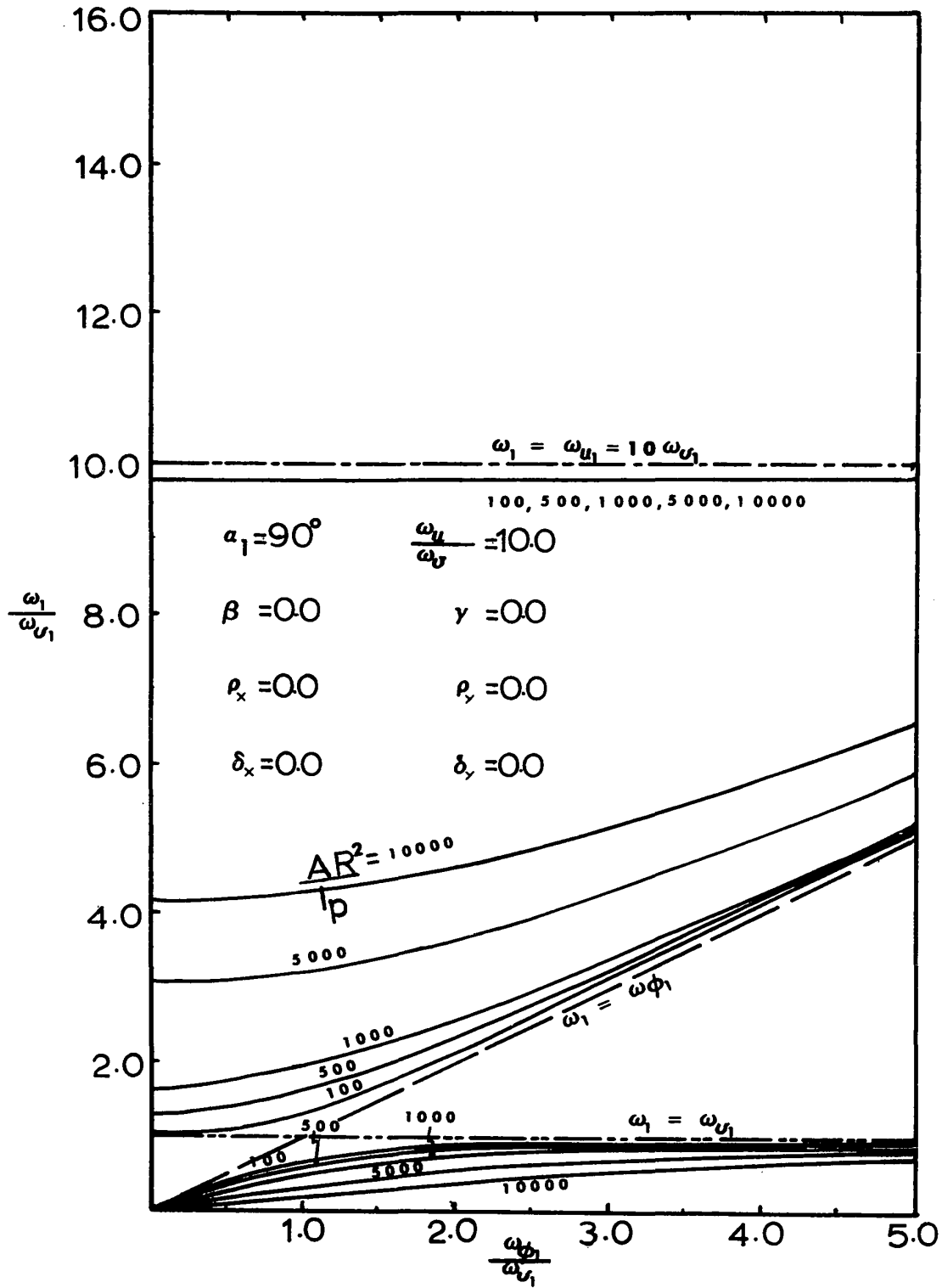


Fig.2.11(a) First Mode Natural Frequencies of Curved Girders of a Symmetric Cross-Section (Double Coupling between v and ϕ)

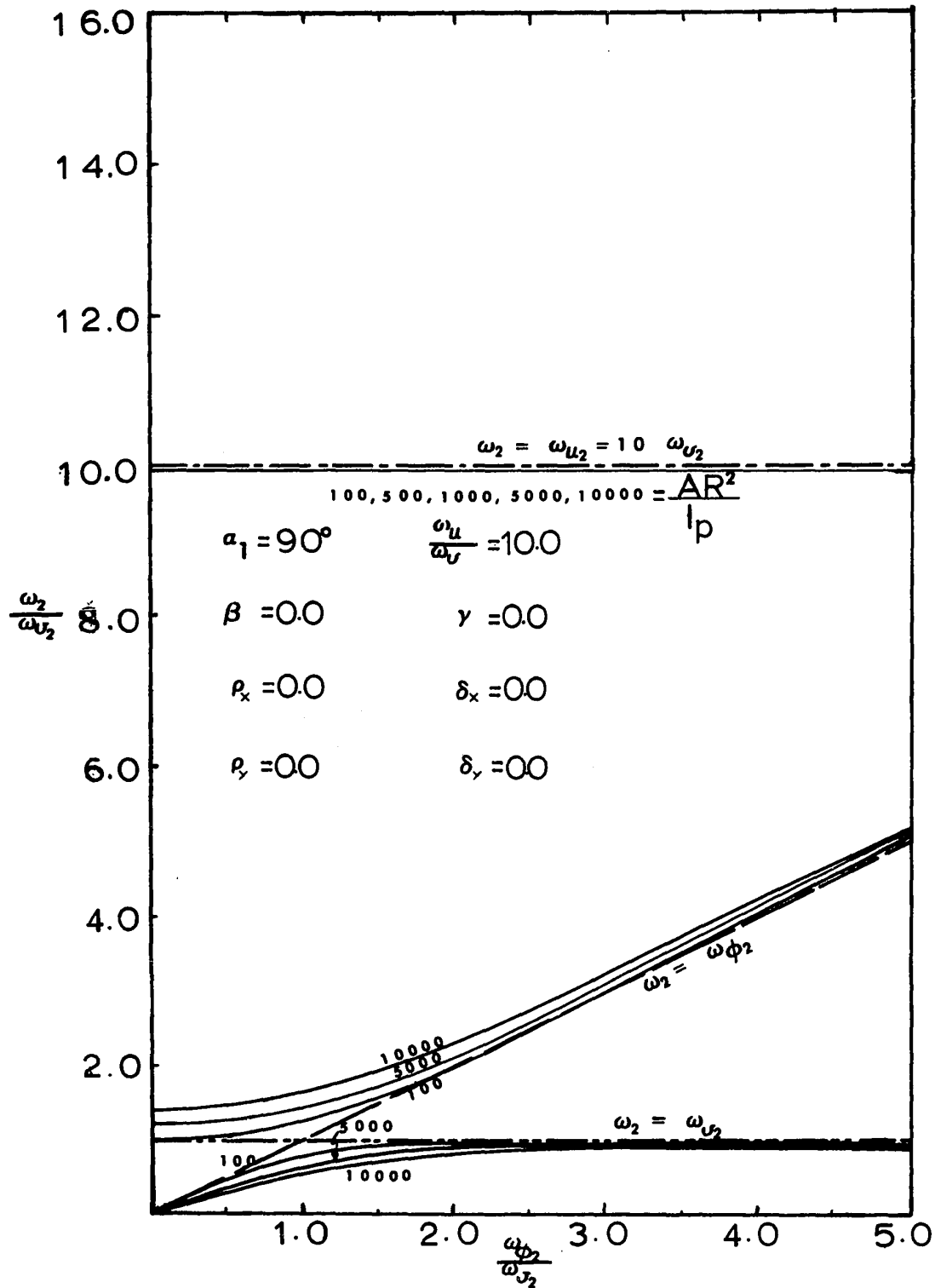


Fig.2.11(b) Second Mode Natural Frequencies of Curved Girders of a Symmetric Cross-Section (Double Coupling between v and ϕ)

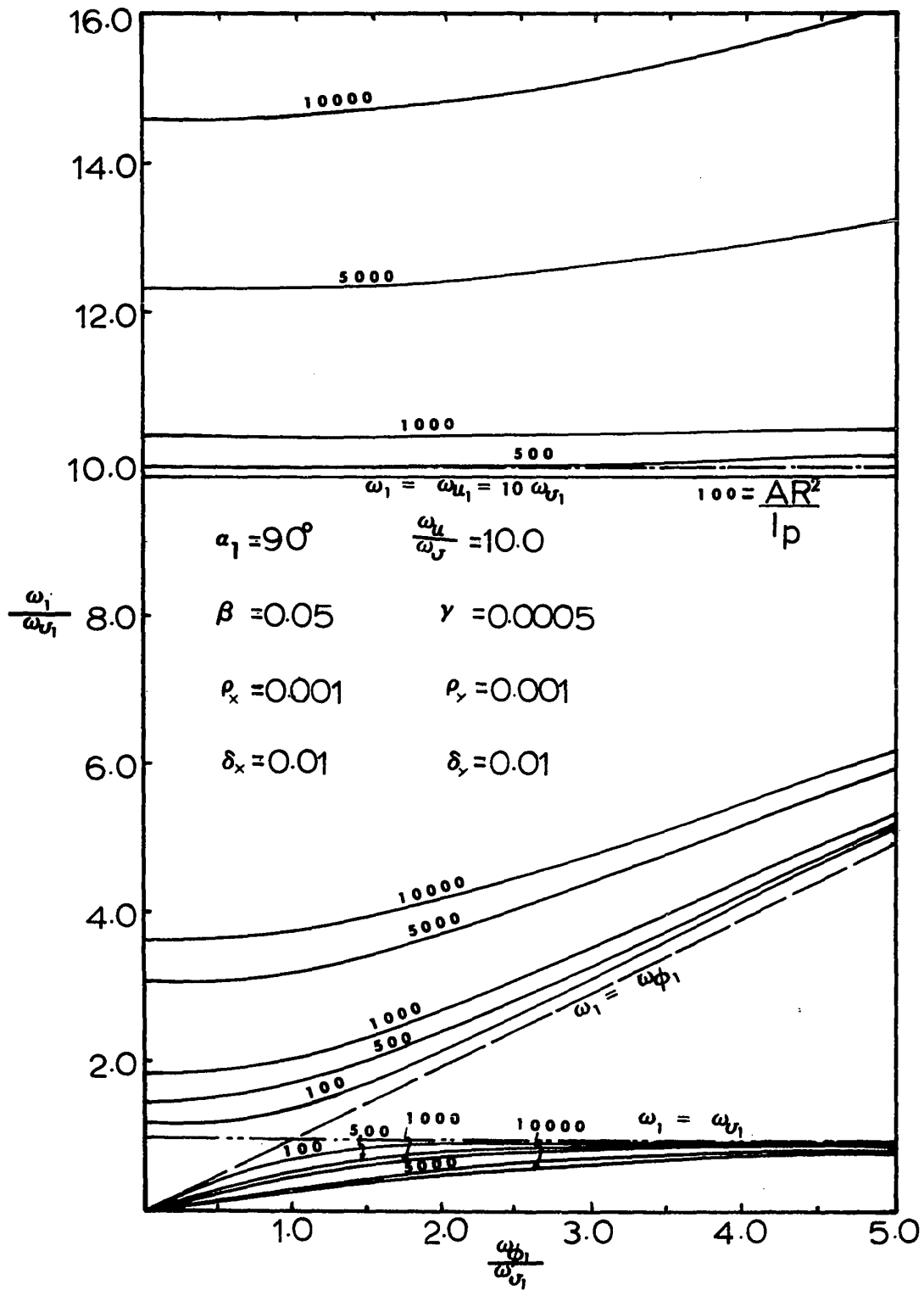


Fig.2.12(a) First Mode Natural Frequencies of Curved Girders of an Asymmetric Cross-Section (Triple Coupling between u, v and ϕ)

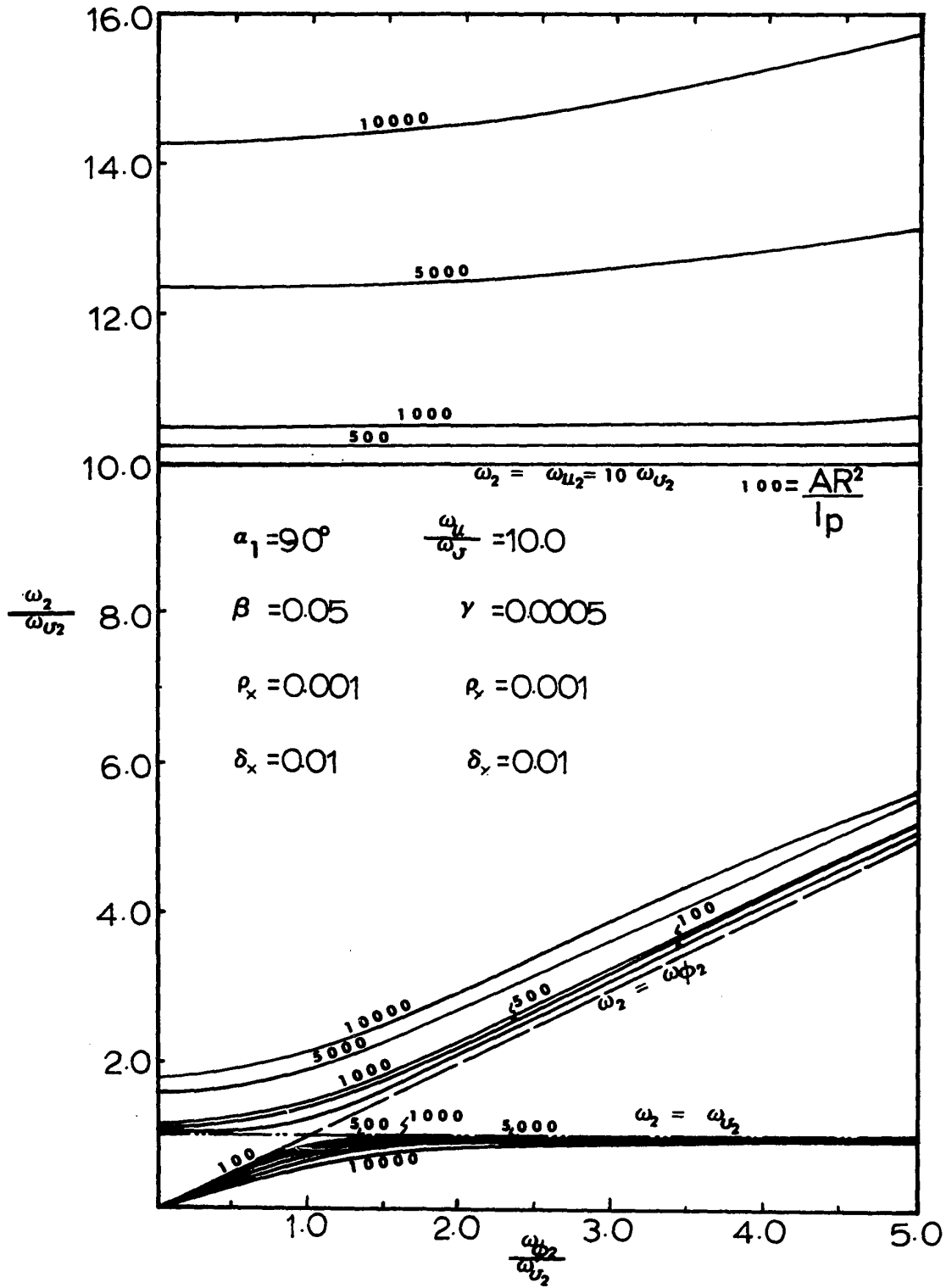


Fig.2.12(b) Second Mode Natural Frequencies of Curved Girders of an Asymmetric Cross-Section (Triple Coupling between u, v and ϕ)

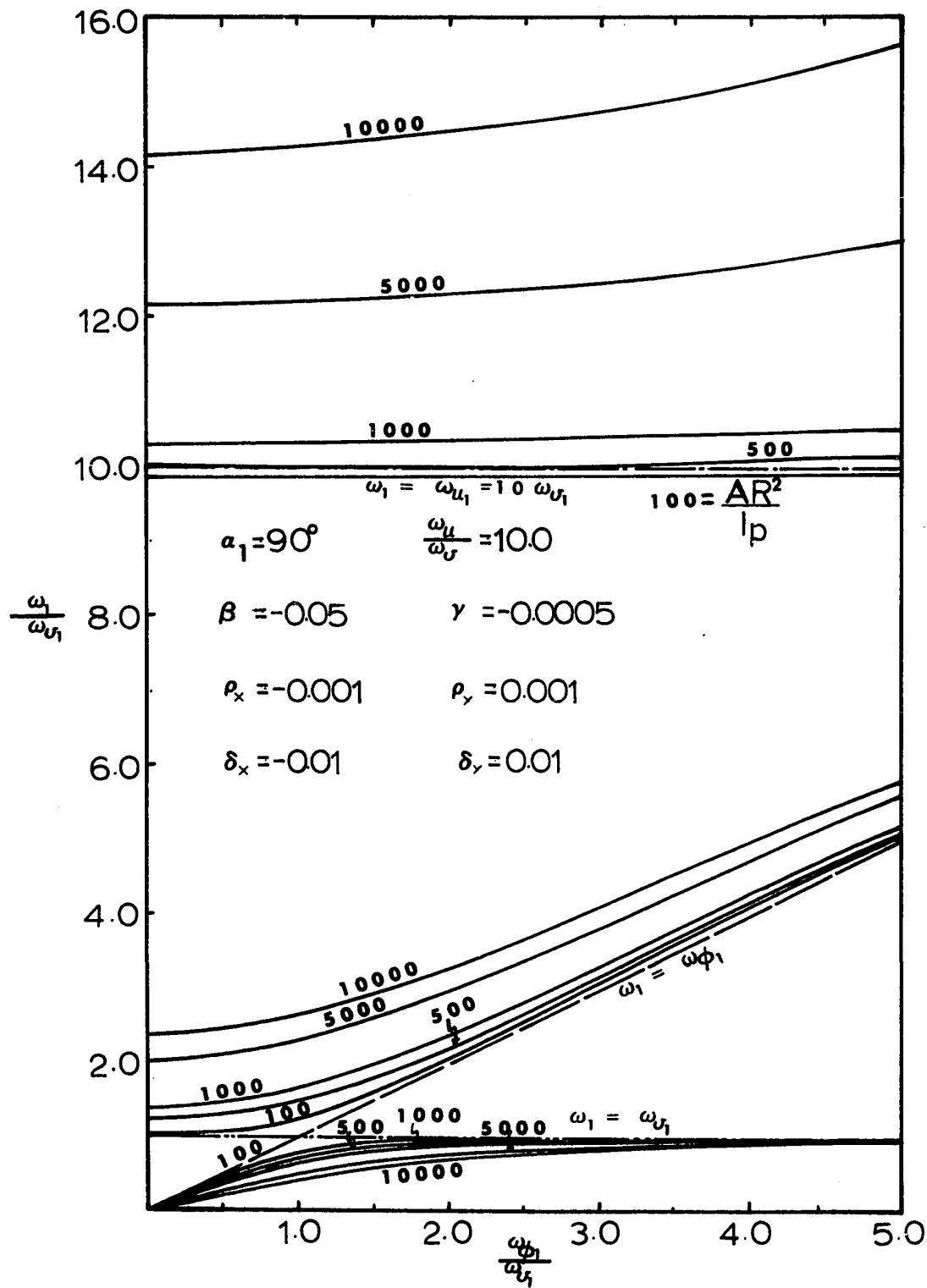


Fig.2.13(a) First Mode Natural Frequencies of Curved Girders of an Asymmetric Cross-Section (Triple Coupling between u , v and ϕ)

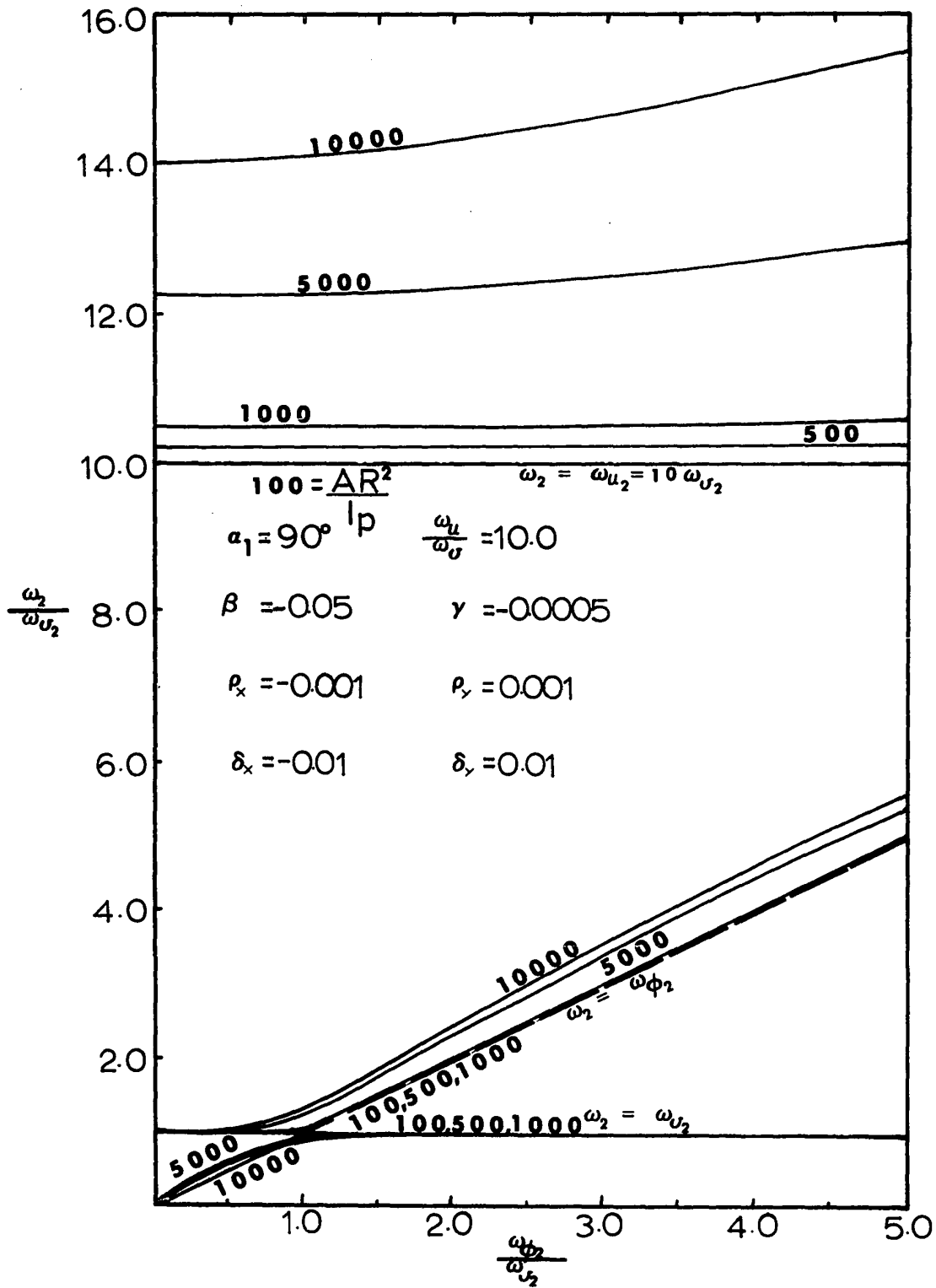


Fig.2.13(b) Second Mode Natural Frequencies of Curved Girders of an Asymmetric Cross-Section (Triple Coupling between u, v and ϕ)

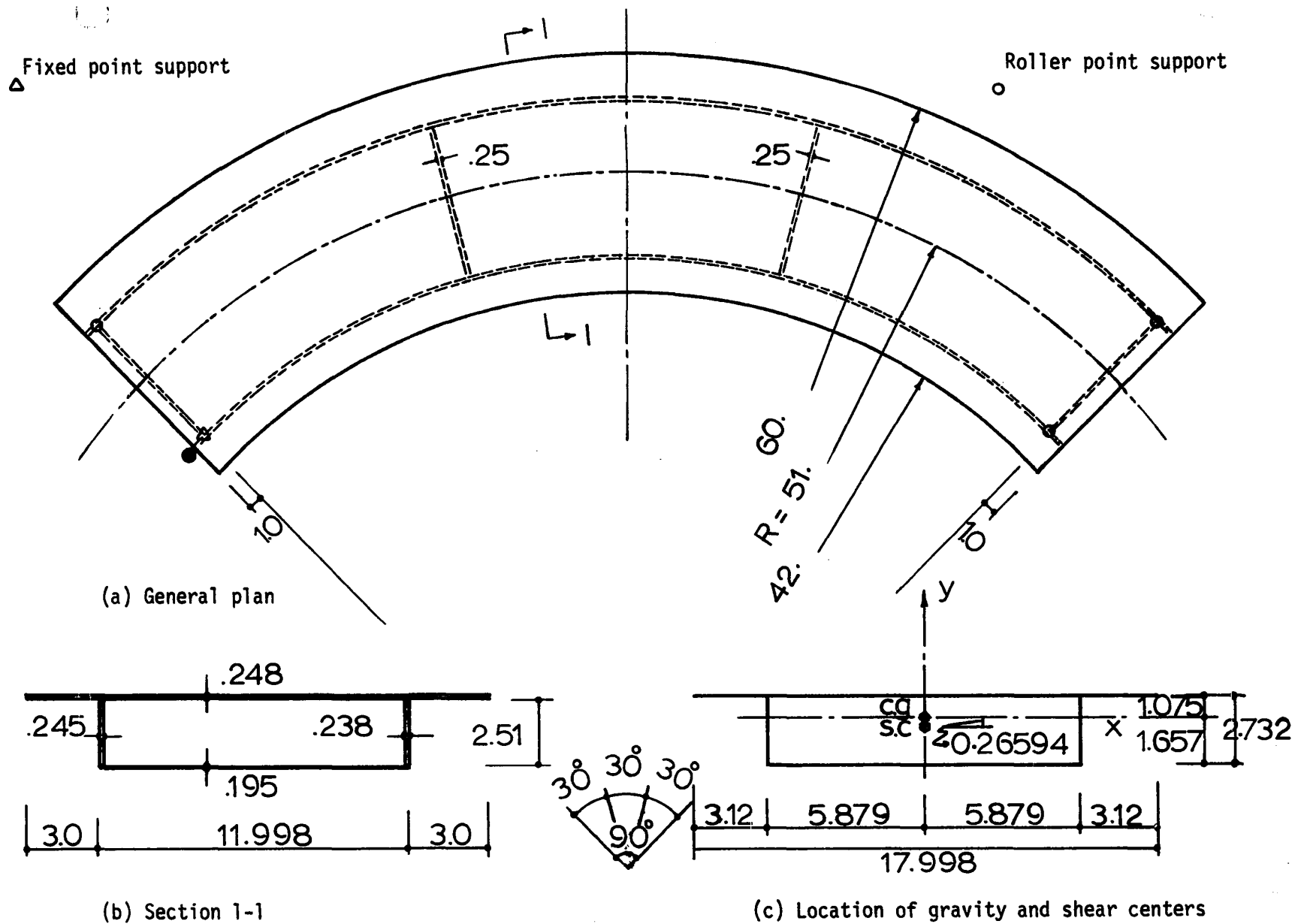
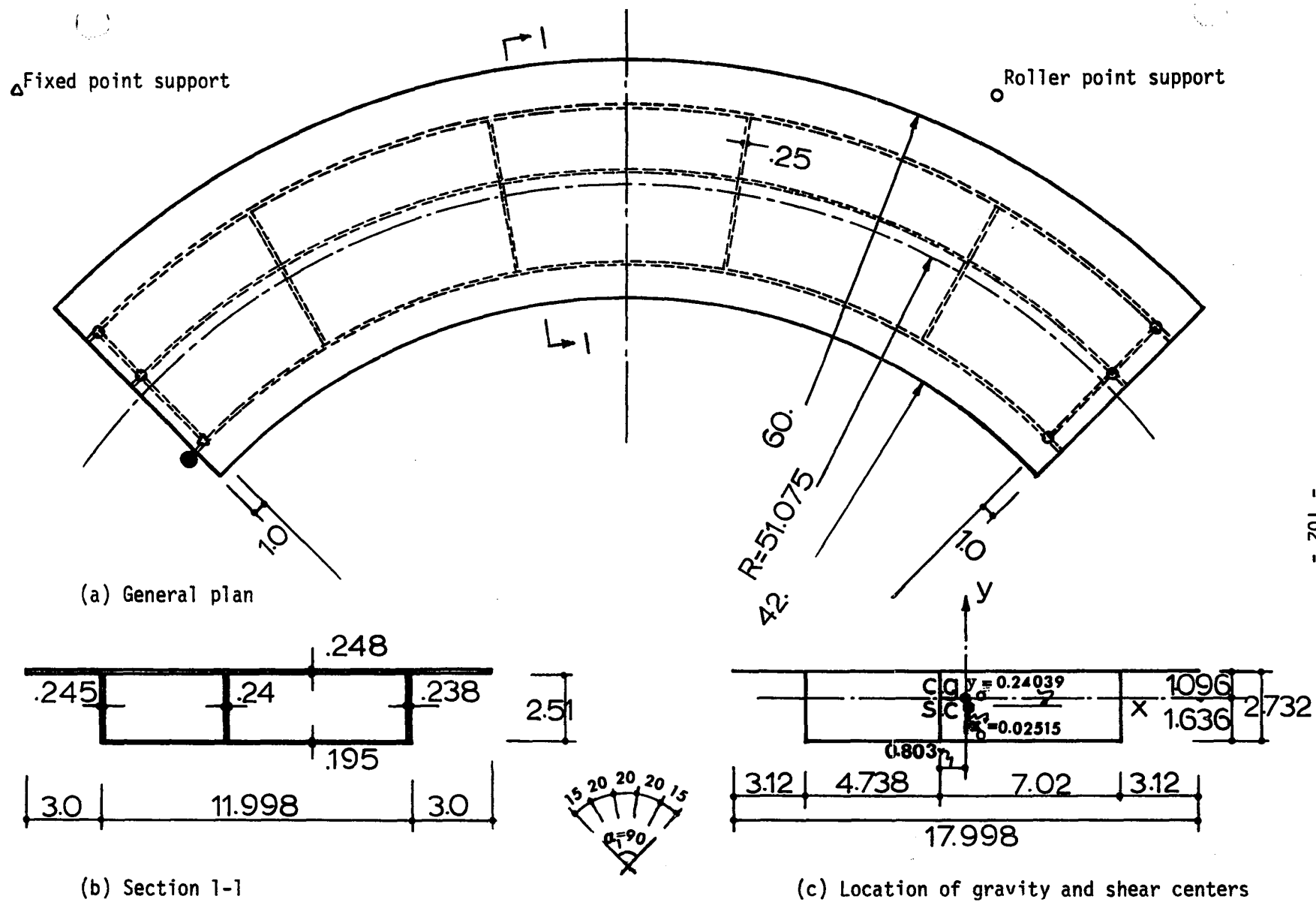


Fig.3.1 General plan and cross-sectional dimensions
(in inches) of Model A.



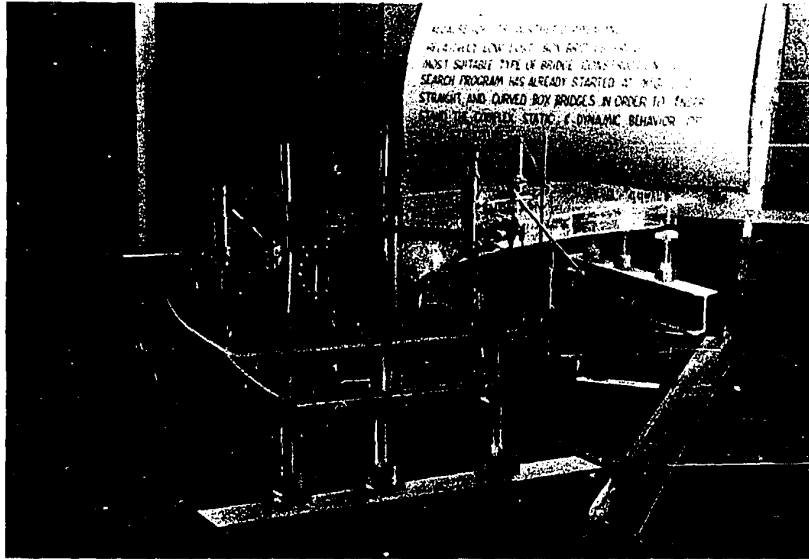


Fig.3.3 General View of Model B

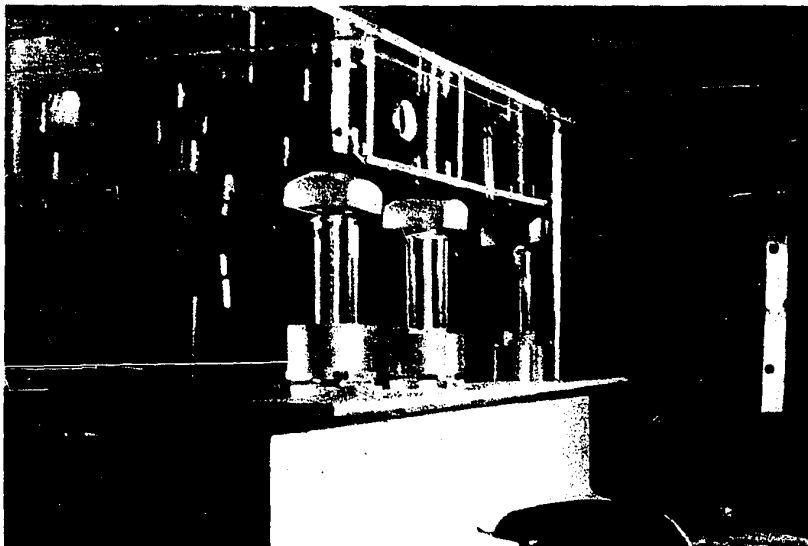


Fig.3.4 Left support of Model B.
Two Roller Point Support and
One Hinge Point Support.

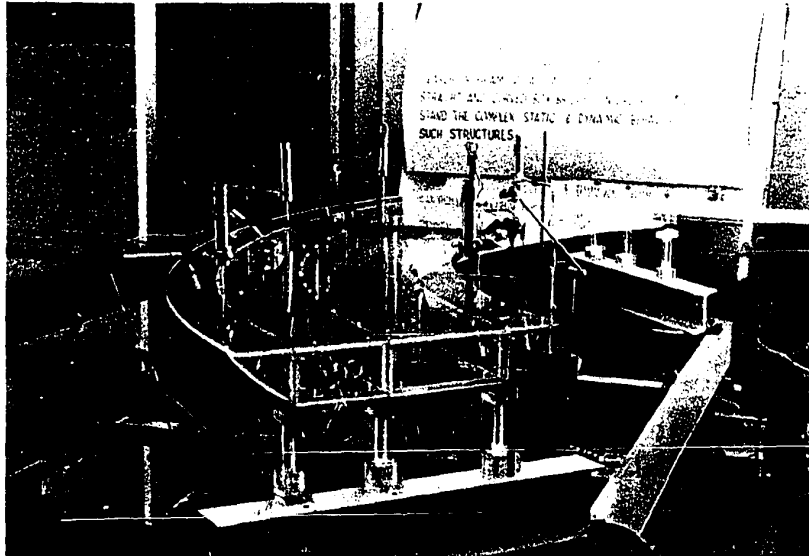


Fig.3.3 General View of Model B

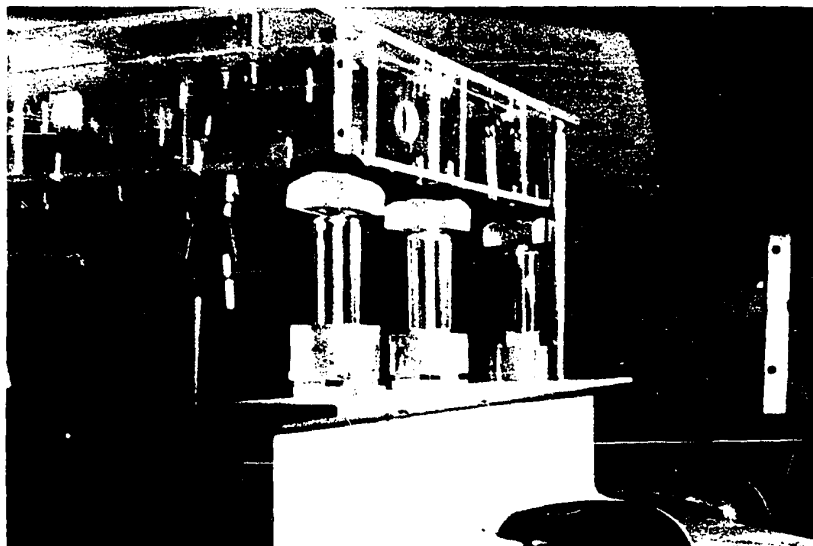


Fig.3.4 Left support of Model B.
Two Roller Point Support and
One Hinge Point Support.

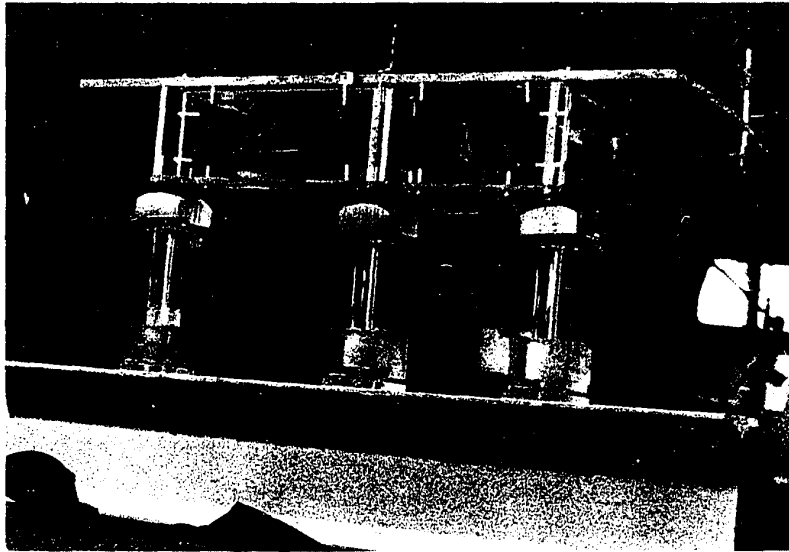


Fig.3.5 Right Support of Model B.
Three Roller Point Support.

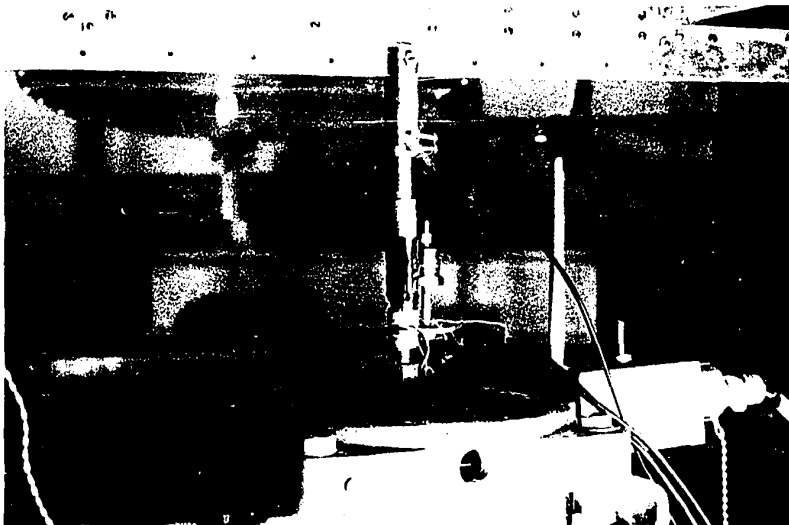


Fig.3.6 Shaker Head and Attachment to the Model.
Showing also Accelerometer and Load Cell

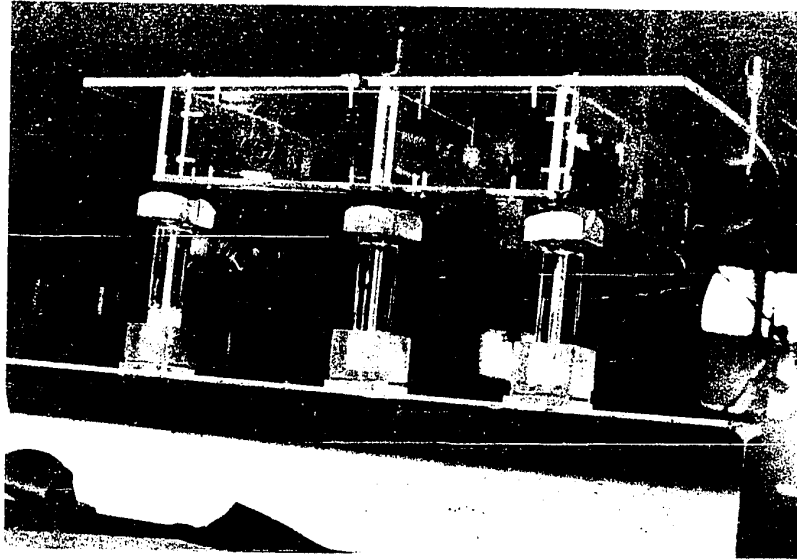


Fig.3.5 Right Support of Model B.
Three Roller Point Support.

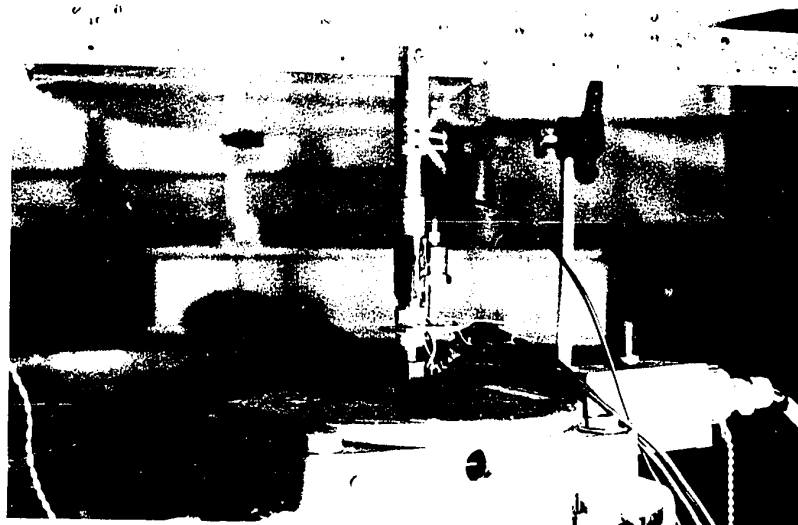


Fig.3.6 Shaker Head and Attachment to the Model.
Showing also Accelerometer and Load Cell

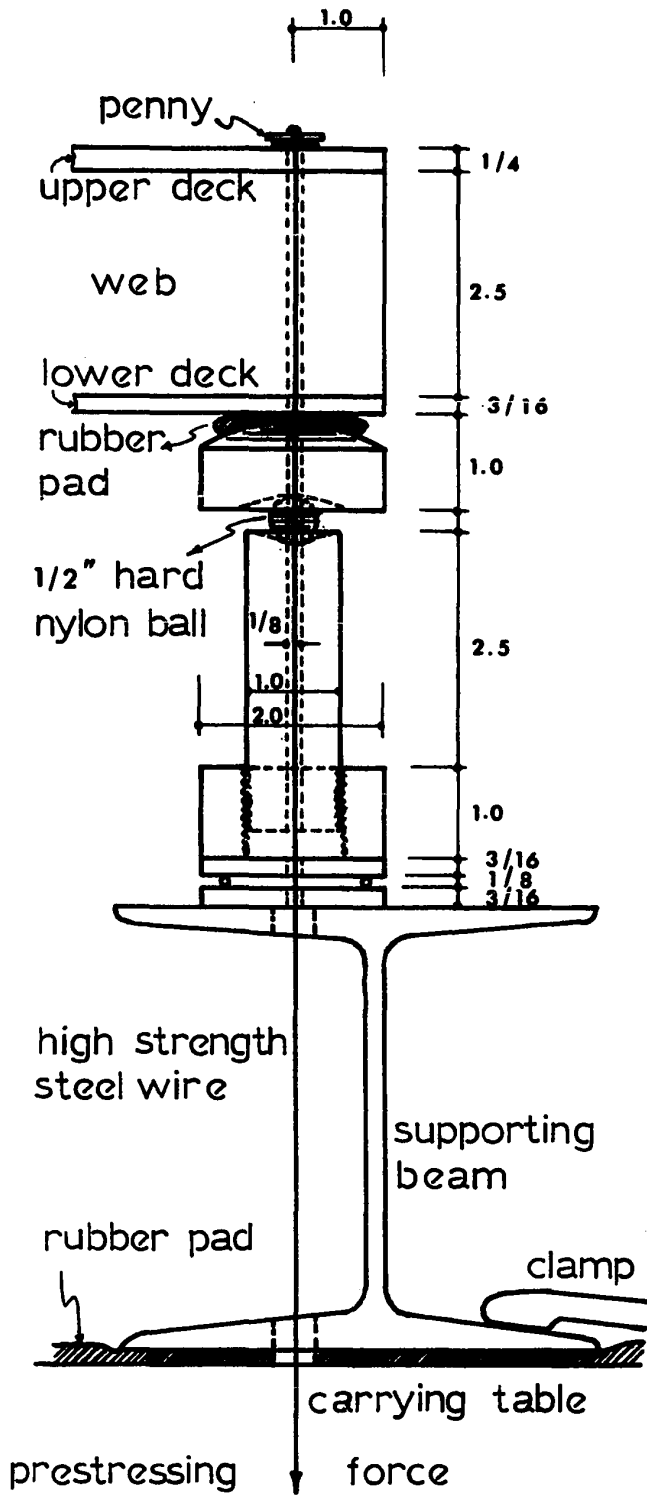


Fig.3.7 Roller point support

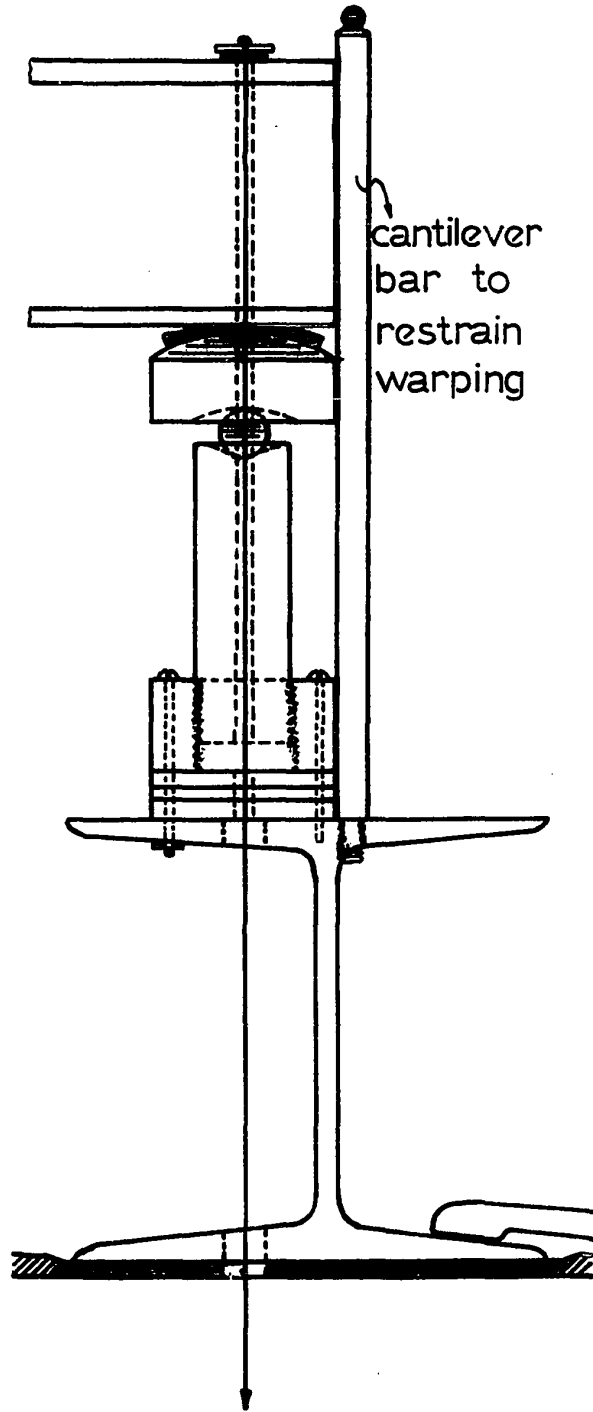


Fig.3.8 Fixed point support

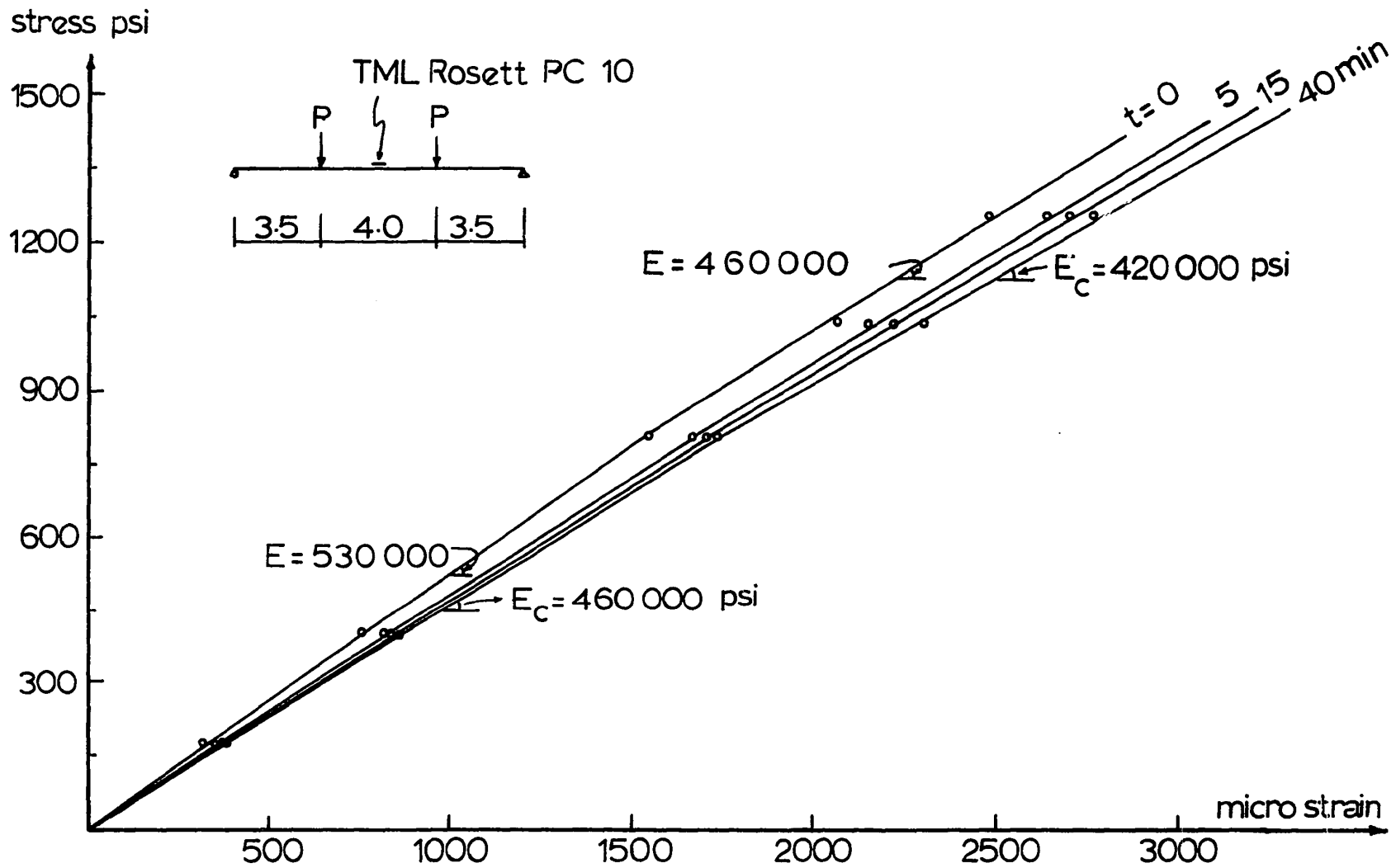


Fig.3.9 Stress strain creep diagrams of plexiglas.

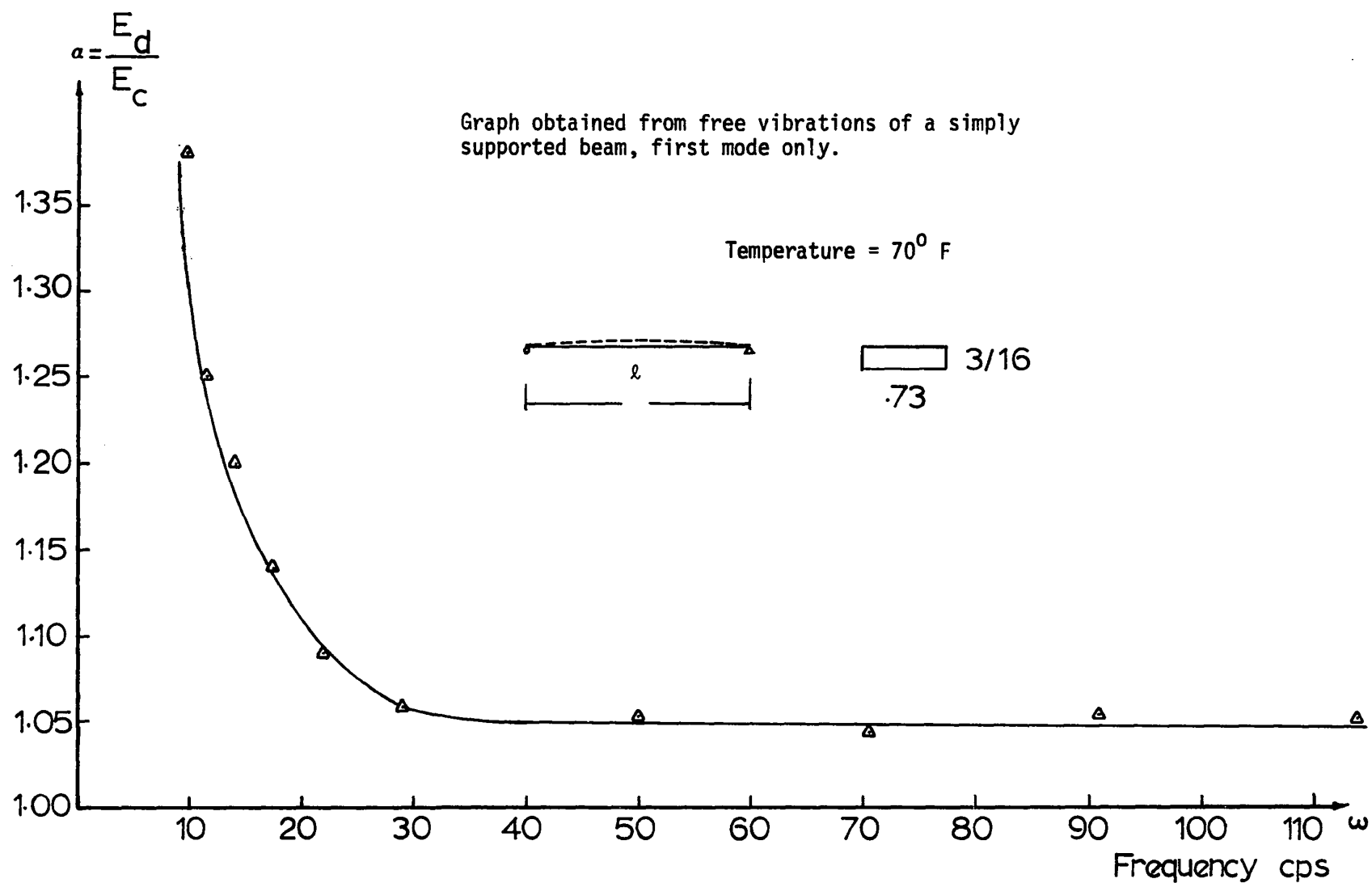


Fig.3.10 Correction factor α of the modulus of elasticity vs. frequency for plexiglas.

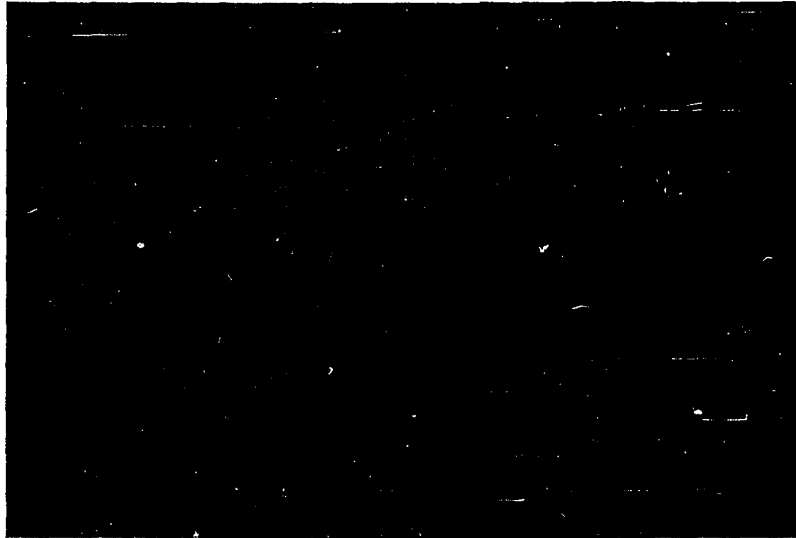


Fig.3.11 Curved Webs mounted on Special
Aluminum Frameworks



Fig.3.12 Curved Webs glued to the Upper Deck.
Wooden Studs used for Web Alignment

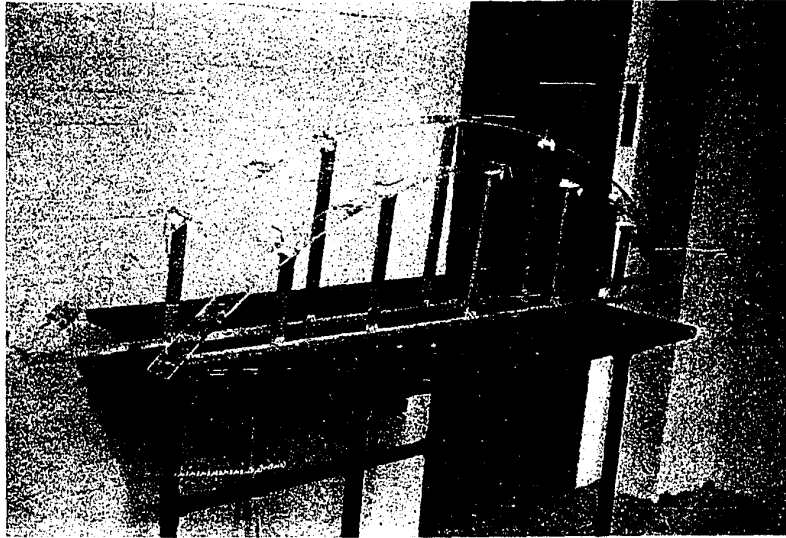


Fig.3.11 Curved Webs mounted on Special Aluminum Frameworks

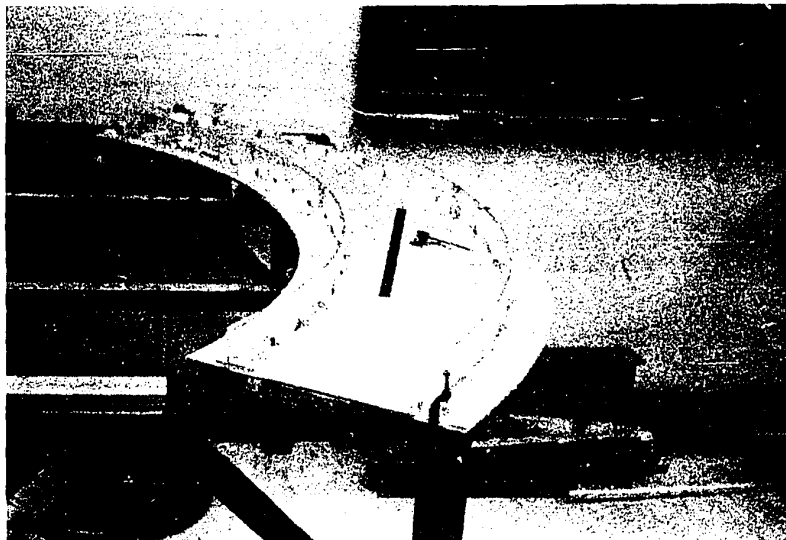


Fig.3.12 Curved Webs glued to the Upper Deck.
Wooden Studs used for Web Alignment

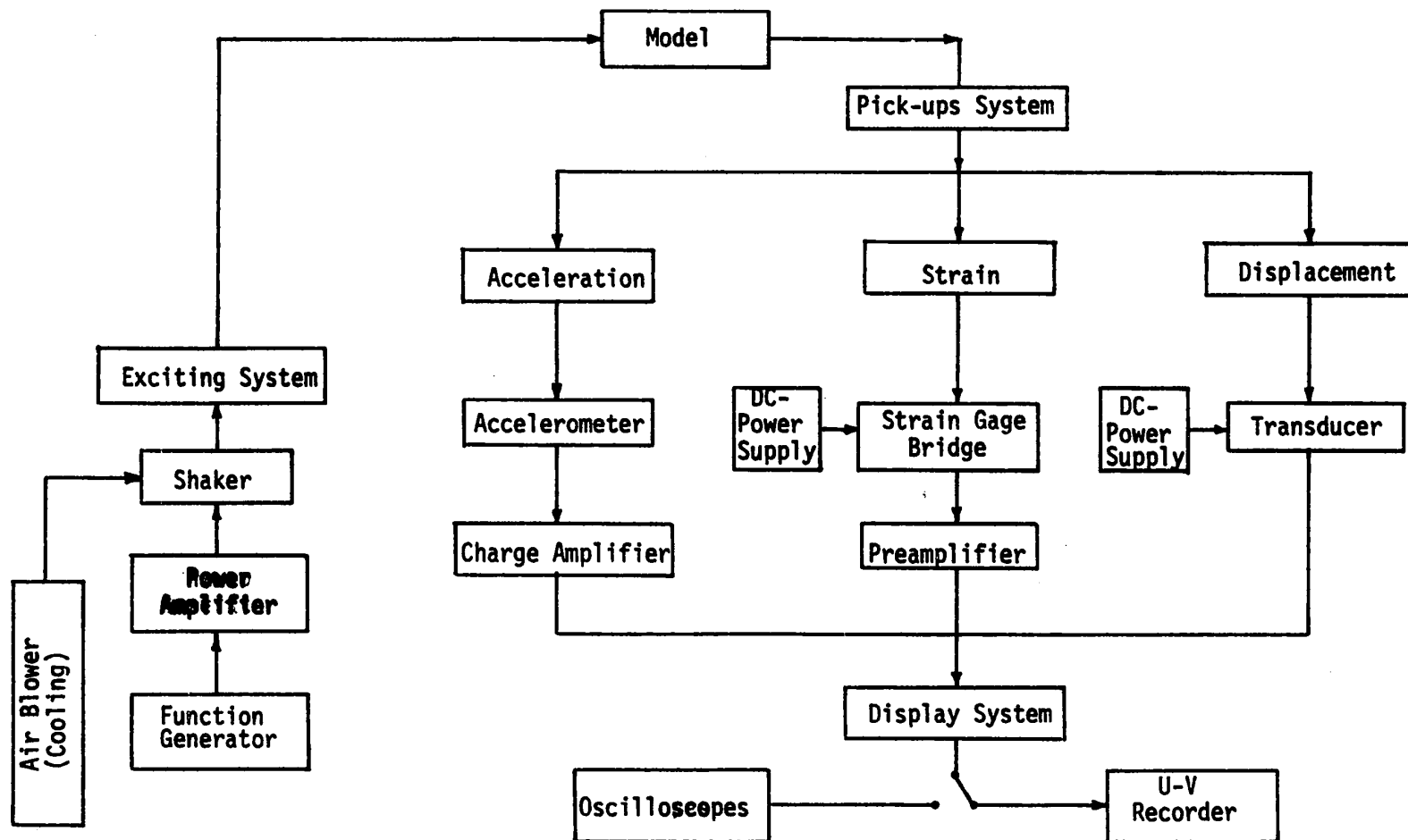


Fig.3-13 - Block Diagram of Experimental Setup

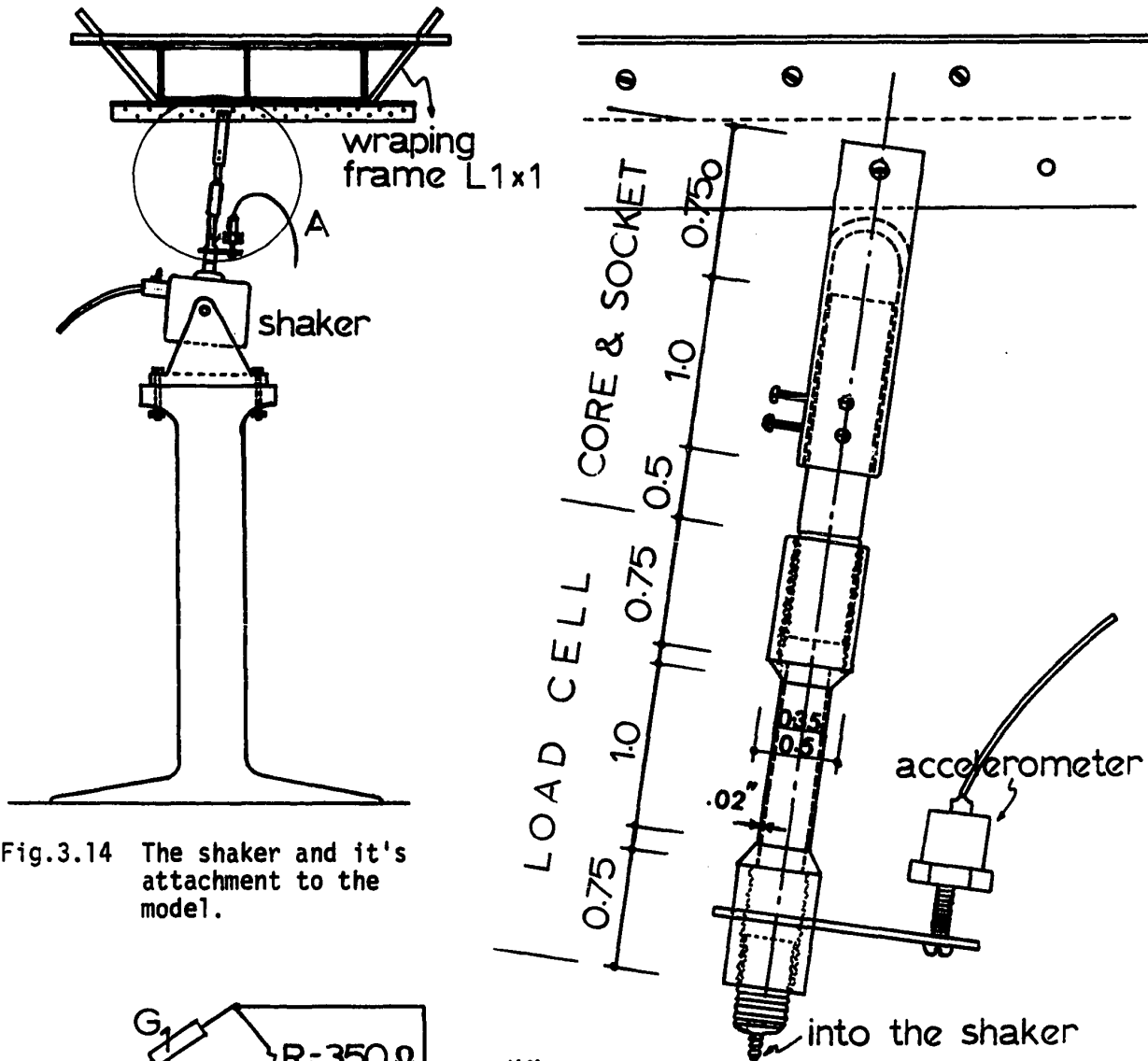


Fig.3.14 The shaker and it's attachment to the model.

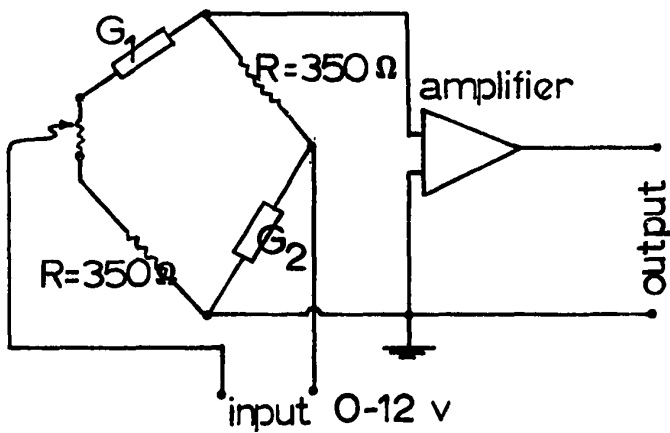


Fig.3.15 Circuitry of load cell.

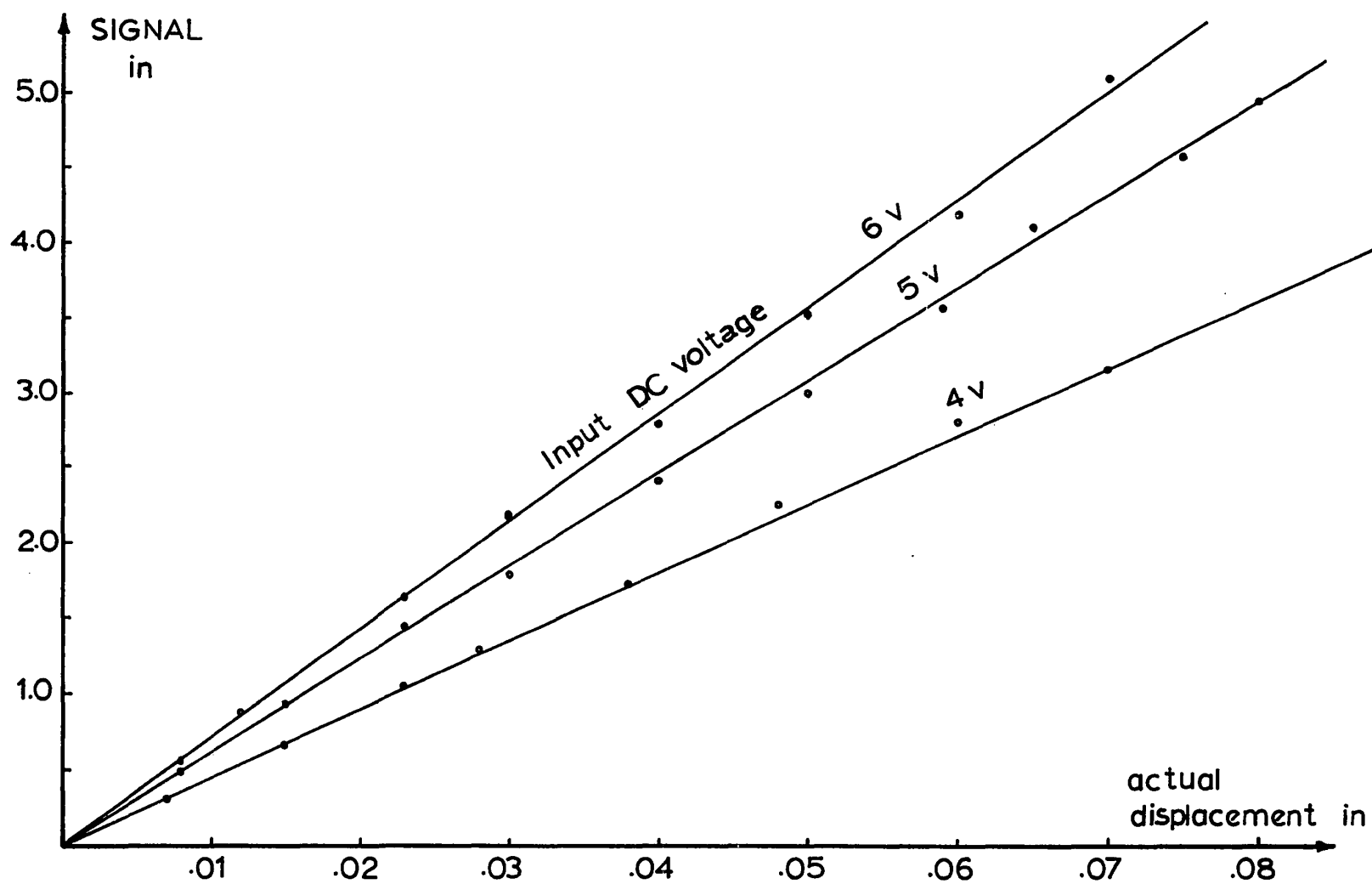


Fig.3.16 Calibration of Transducer T-3 with Channel 6 of the U-V Recorder

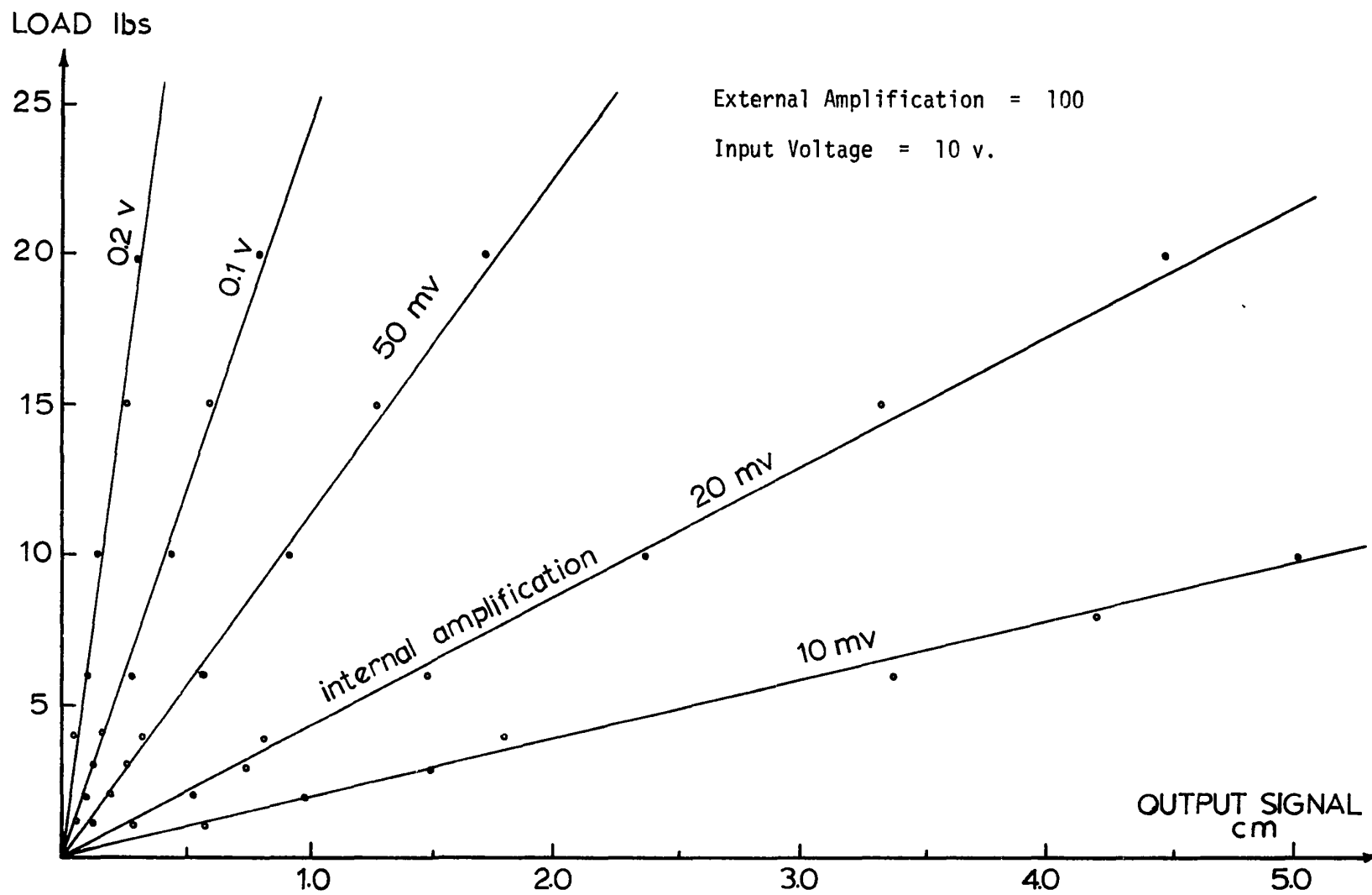


Fig.3.17 Load cell calibration graph.

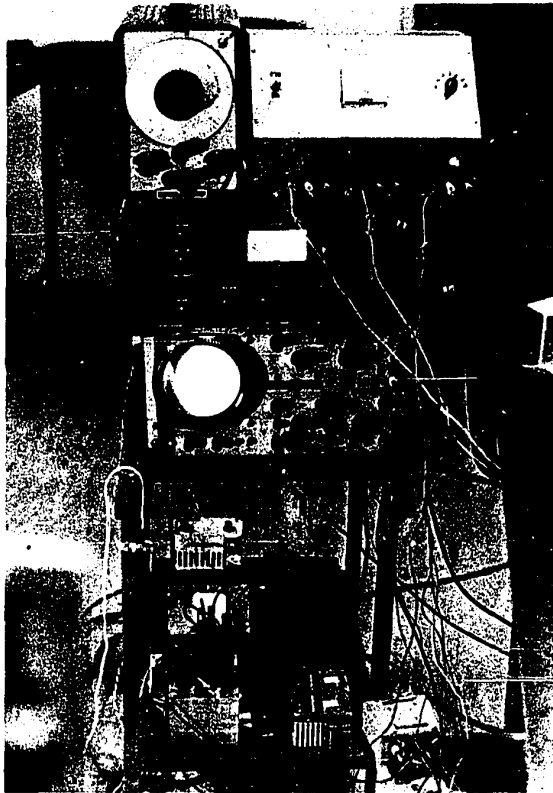


Fig.3.18 Top left to right, Oscillator, DC Power Supply, Shaker's Power Amplifier, Oscilloscope, Load Cell's Bridge and Amplifier.

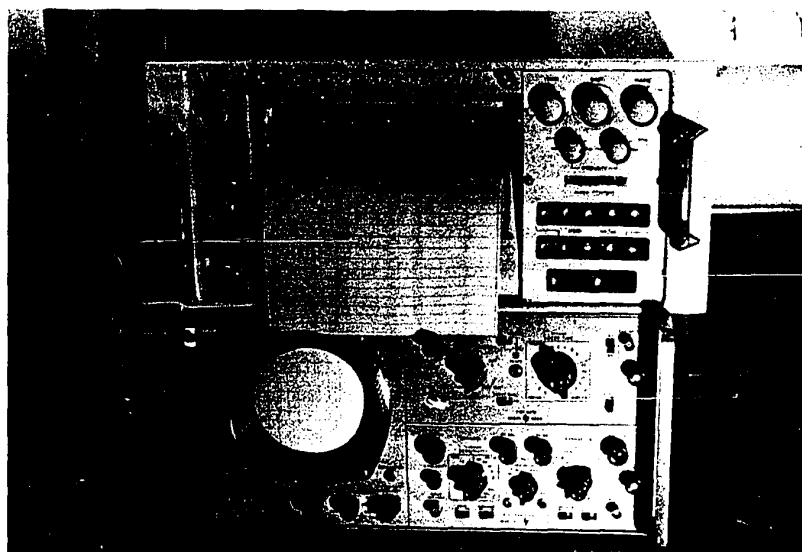


Fig.3.19 Display System U.V. Recorder and Memoscope

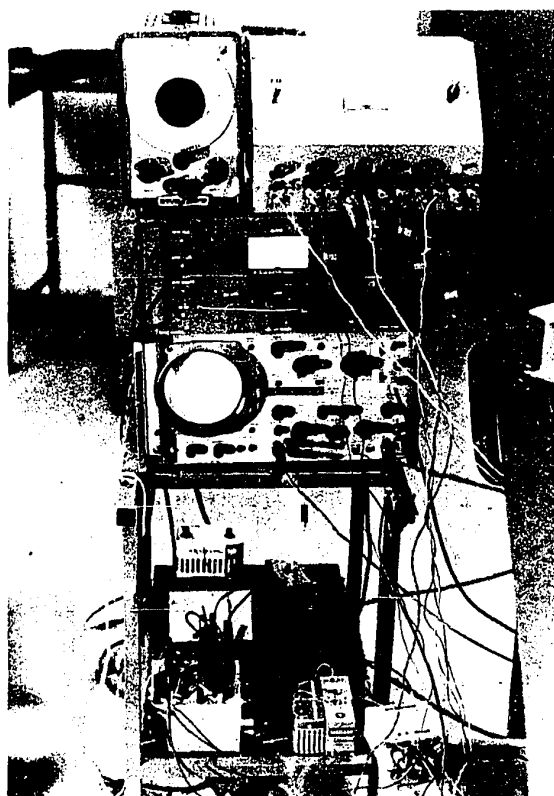


Fig.3.18 Top left to right, Oscillator, DC Power Supply, Shaker's Power Amplifier, Oscilloscope, Load Cell's Bridge and Amplifier.

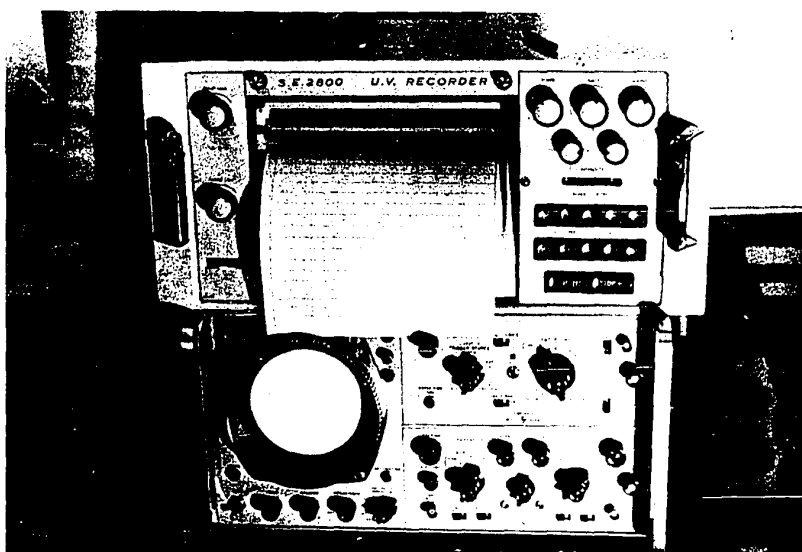
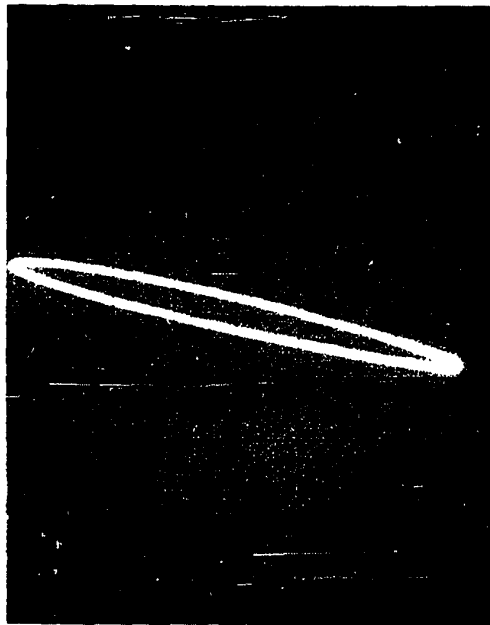


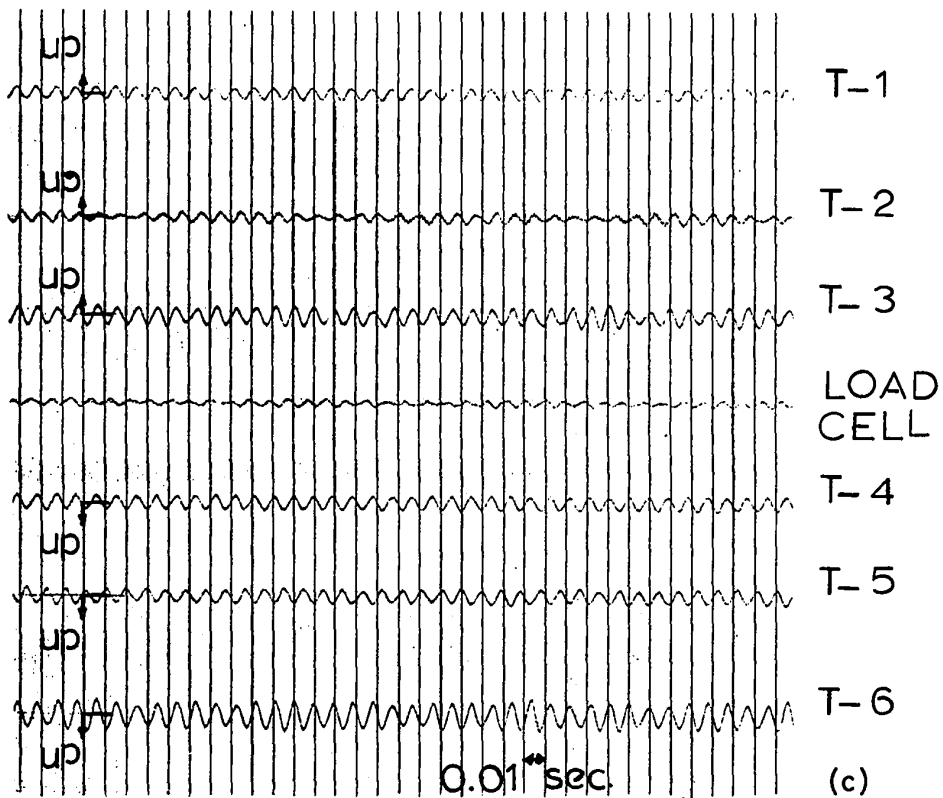
Fig.3.19 Display System U.V. Recorder and Memoscope



(a)



(b)



(c)

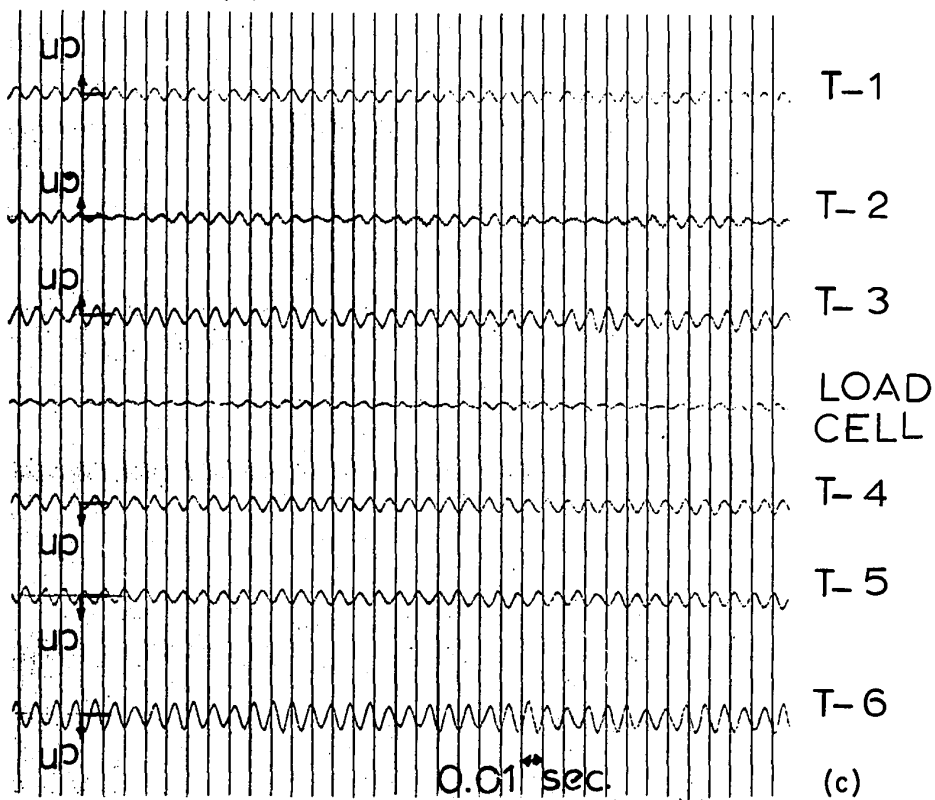
Fig.3.20 (a) Lissajous Figure, signals not in phase.
 (b) Two signals perfectly in phase.
 (c) Typical Forced Vibration record, near 4th mode of Model B.
 $\omega = 110$ cps.



(a)

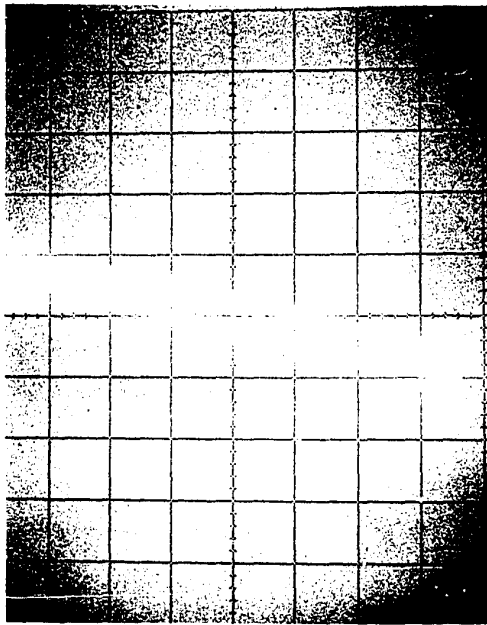


(b)



(c)

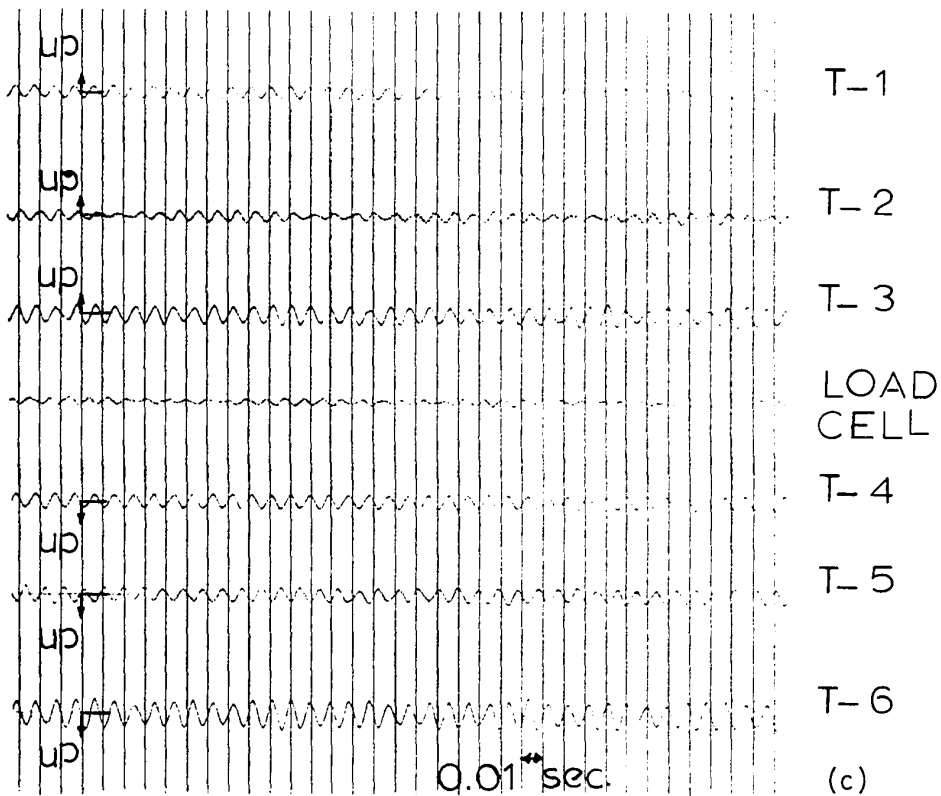
Fig.3.20 (a) Lissajous Figure, signals not in phase.
 (b) Two signals perfectly in phase.
 (c) Typical Forced Vibration record, near 4th mode of Model B.
 $\omega = 110$ cps.



(a)

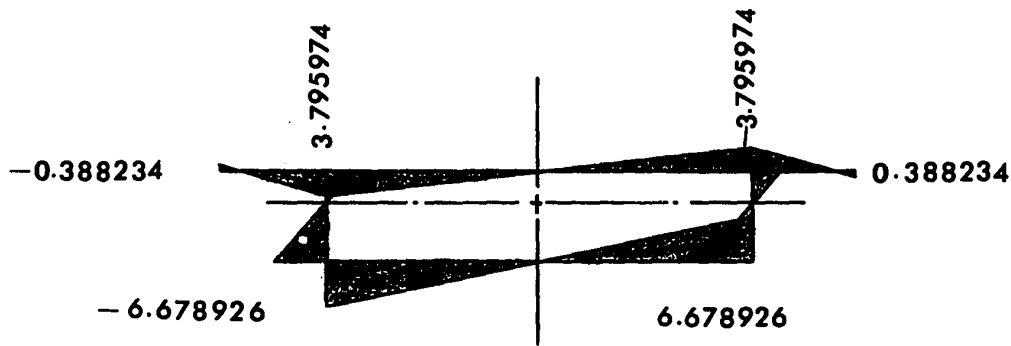


(b)

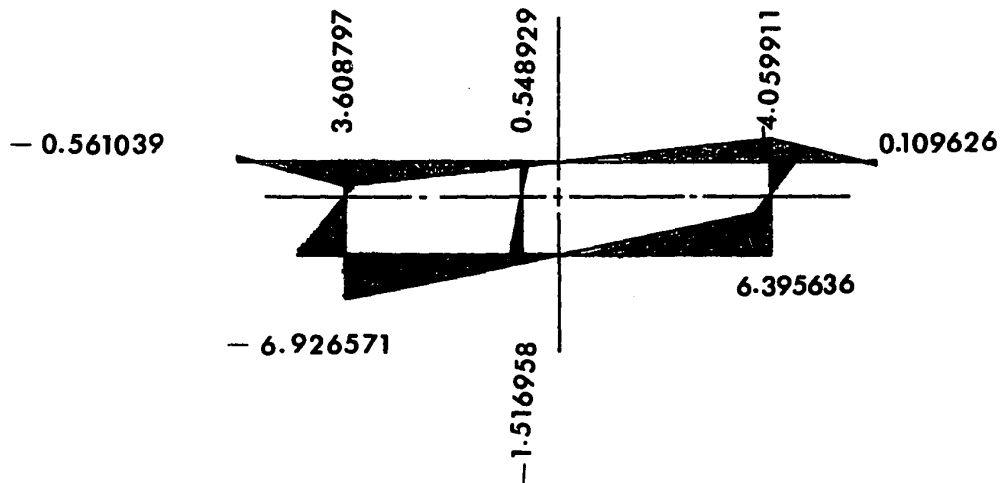


(c)

Fig.3.20 (a) Lissajous Figure, signals not in phase.
 (b) Two signals perfectly in phase.
 (c) Typical Forced Vibration record, near 4th mode of Model B
 $\omega = 110$ cps.



(a) Model A



(b) Model B

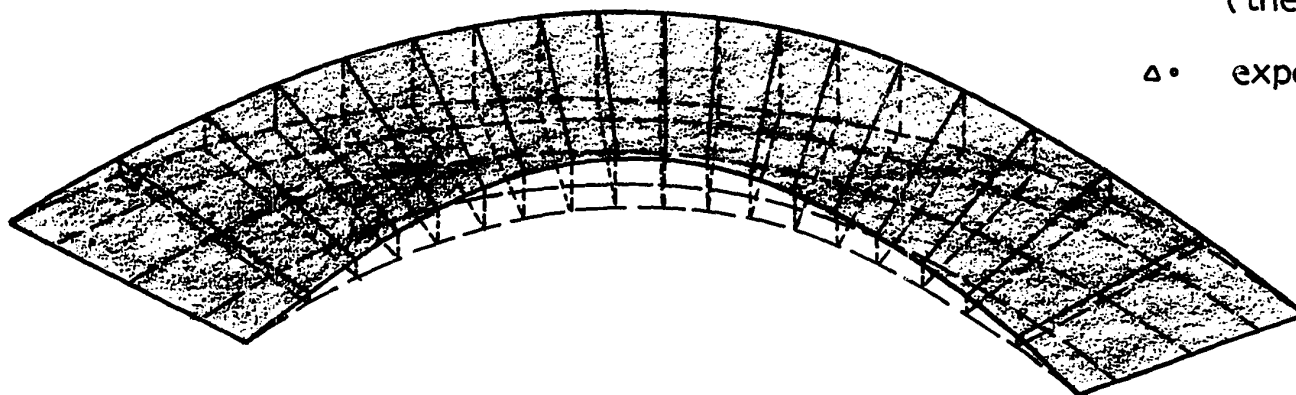
Fig.4.1 Warping displacement diagrams (sectorial coordinates) of box models.

↗ position & direction of optimum
excitation

--- static

— vibrating
(theory)

Δ• experiment



$$U_1 = -0.00656$$

$$V_1 = 1.0$$

$$\omega_1 = 13.3 \text{ cps Theory}$$

$$\phi_1 = -0.03256 \text{ rad.}$$

$$W_{rs} = 0.00064$$

$$\omega_1 = 12.5 \text{ cps Experiment}$$

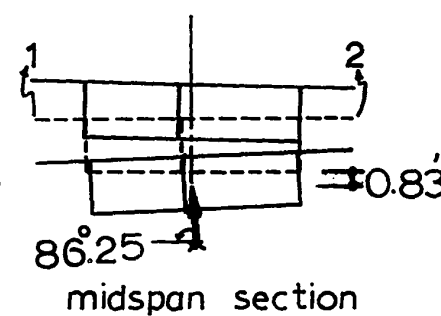
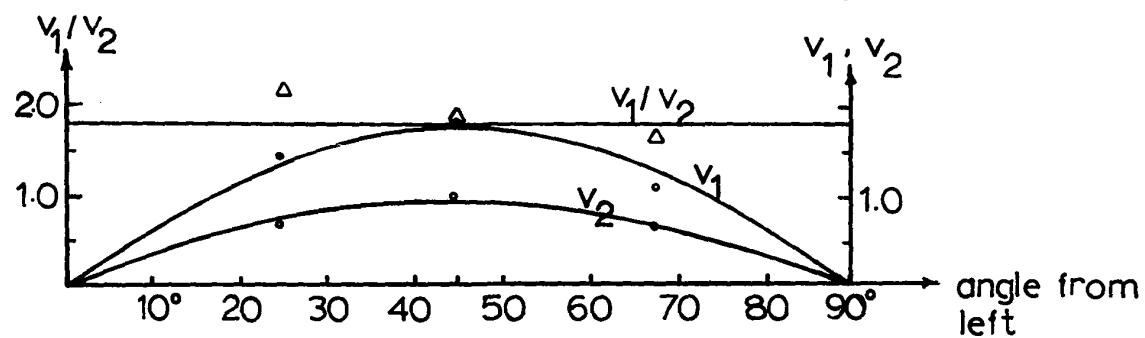

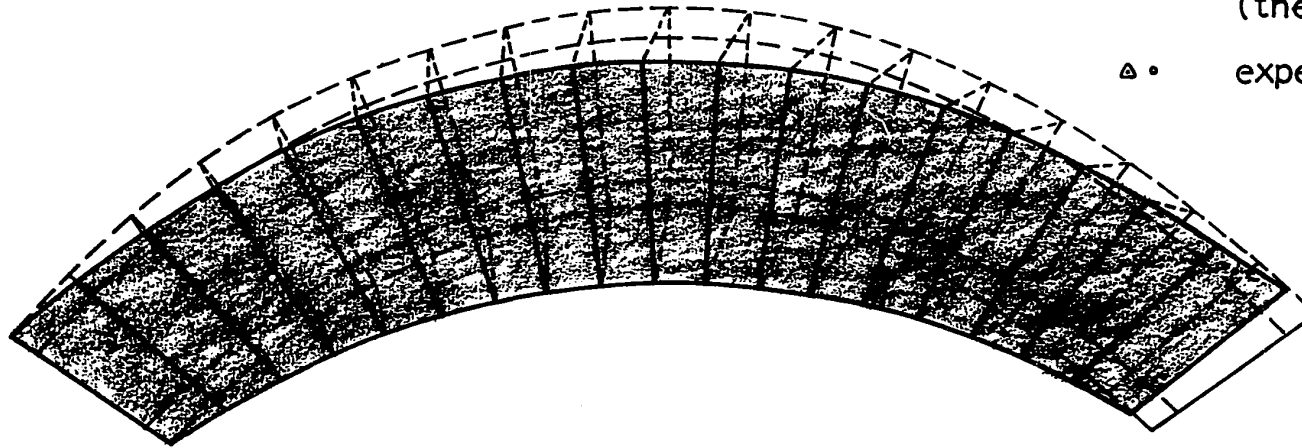


Fig.4.2 First Modal Shape of the upper deck of model B.

 position & direction of optimum
excitation

----- static
 ----- vibrating
 (theory)
 Δ • experiment



$$U_2 = 146.96$$

$$V_2 = 1.0$$

$$\omega_2 = 63.2 \text{ cps Theory}$$

$$\phi_2 = 0.79 \text{ rad.}$$

$$W_{rs} = 73.38$$

$$\omega_2 = 58.65 \text{ cps Experiment}$$

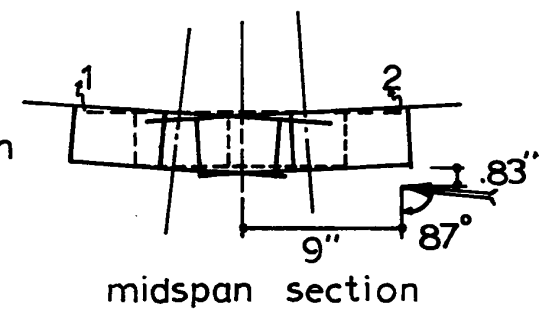
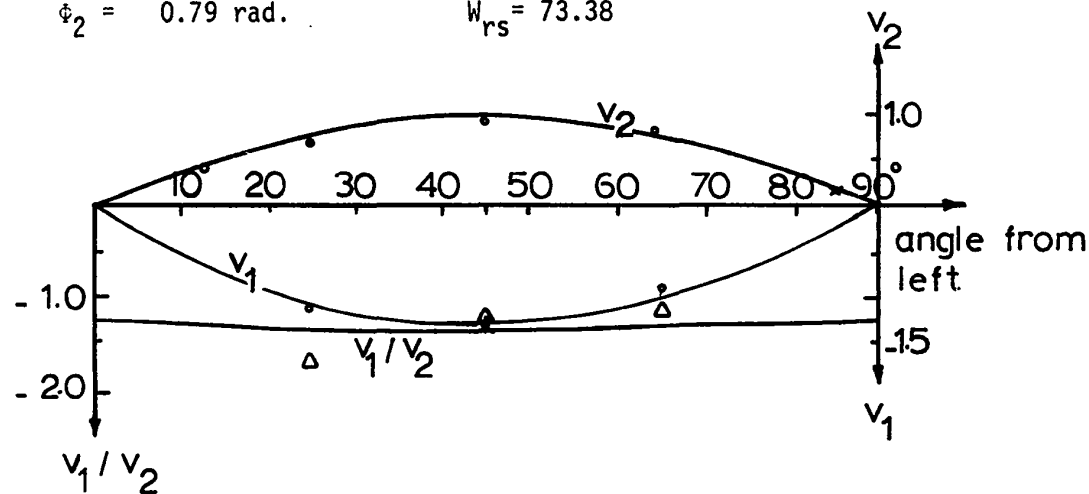

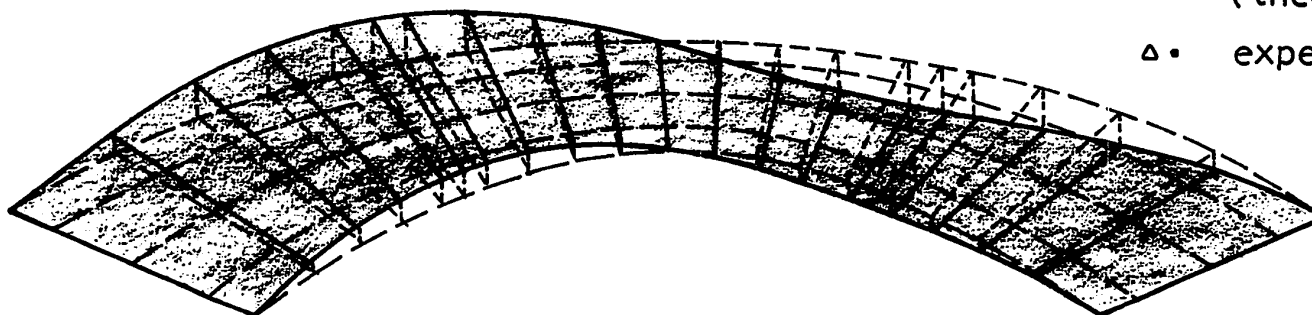


Fig.4.3 Second Modal Shape of the upper deck of model B.

 position & direction of optimum
excitation

--- static
 — vibrating
 (theory)
 Δ • experiment



$$U_3 = -0.00138$$

$$V_3 = 1.0$$

$$\omega_3 = 67.10 \text{ cps Theory}$$

$$\phi_3 = -0.0429 \text{ rad.}$$

$$W_{rs} = 0.00224$$

$$\omega_3 = 60.50 \text{ cps Experiment}$$

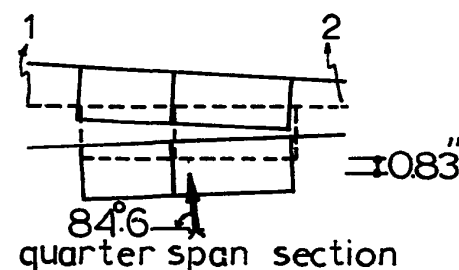
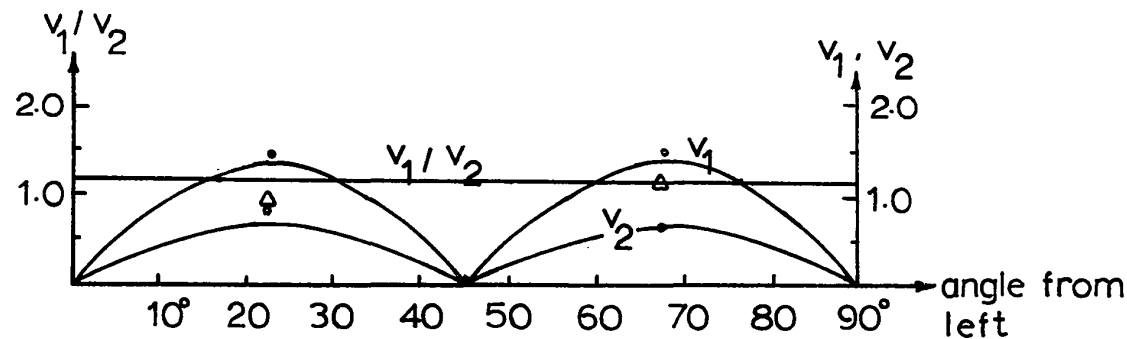

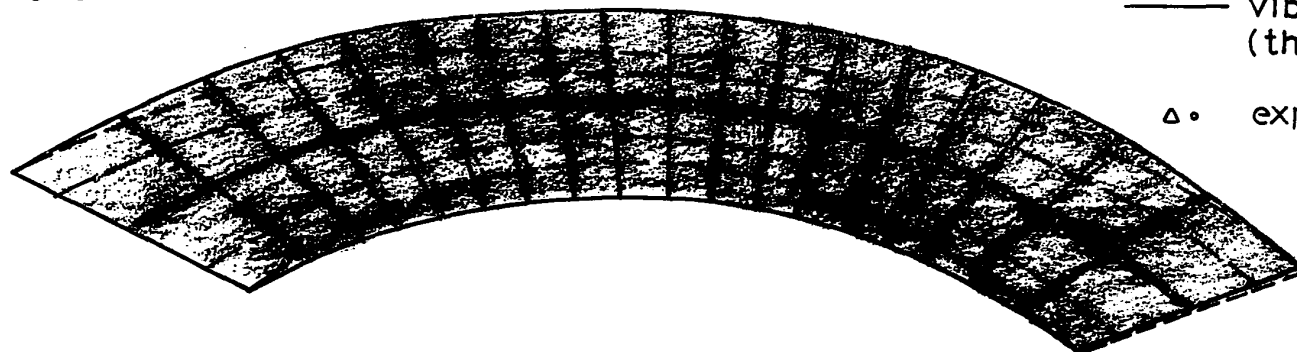


Fig.4.4 Third Modal Shape of the upper deck of model B.

 position & direction of optimum excitation

--- static
 — vibrating (theory)
 Δ • experiment



$$U_4 = -0.608$$

$$\phi_4 = 1.261 \text{ rad.}$$

$$V_4 = 1.0$$

$$W_{rs} = -0.456$$

$\omega_4 = 108.30$	cps	Theory
$\omega_4 = 115.0$	cps	Experiment

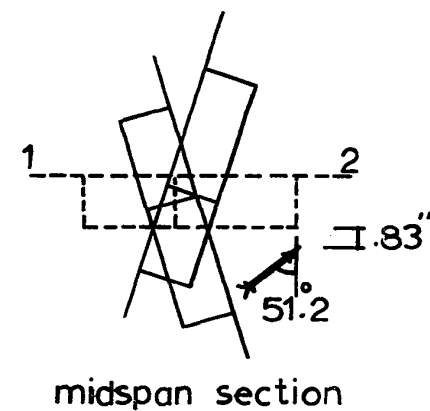
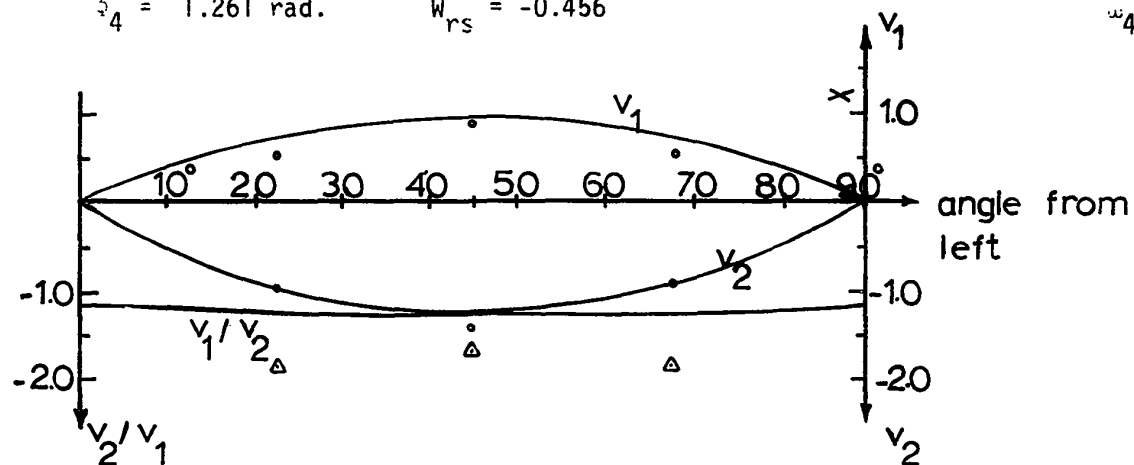


Fig.4.5 Fourth Modal Shape of the upper deck of model B

APPENDIX I

WARPING IN BOX GIRDERS WITH OVERHANGS

Engineering beam theory assumes that plane sections remain plane when the beam deforms under loads. Although this assumption leads to reliable prediction of the behavior of solid girders, nevertheless, it is not adequate for thin walled beams, (30, 40, 48). The longitudinal displacement in the x-direction (Fig.1.a) caused by a torque and/or (for cases where there is coupling between the bending and twisting moments) bending moments or bimoments is defined as the warping displacement. Vlasov (40) introduced the concept of the bi-moment which consists of two parallel, equal and opposite moments about one axis acting a distance apart to describe the warping phenomenon. The effects of such bimoments can be superimposed on the results of engineering beam theory to obtain the total behavior.

The distribution of warping displacements in the overhangs as obtained from Eq.(44) and shown in Fig.4.1 is open to question. Dabrowski (11) reported almost the same distribution for a single cell box with two overhangs similar to the cross-section of model A. It is not obvious that the absolute value of warping displacement should decrease in magnitude between the joint with the web and the free end of the overhang. If the overhang is thought of as an extension fixed to the upper deck, warping should increase as one proceeds away from

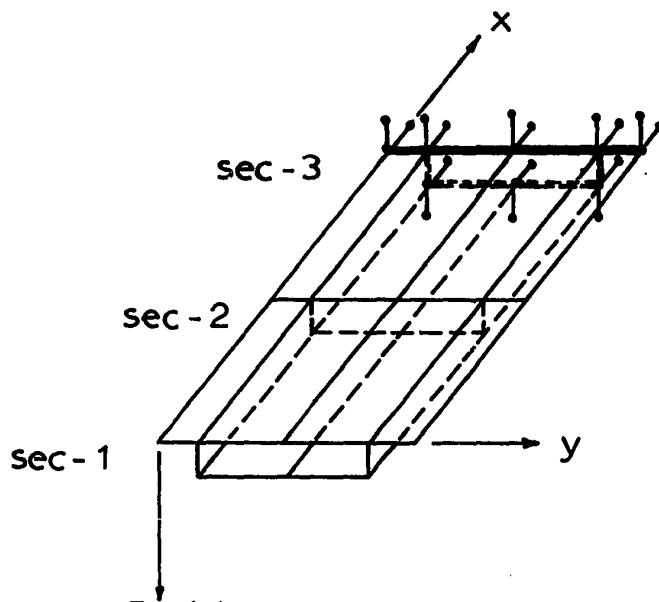
the center of twist. It follows that one might expect an increase of the absolute value of the warping displacement as one proceeds towards the free end of the upper deck.

A three-dimensional finite element program (38) which assumes six degrees of freedom at each node (three displacements and three rotations) and takes into account both bending and in plane stresses, was used to analyze the warping behavior of a box with overhangs. A straight girder with cross-section similar to that of model A was idealized as shown in Fig.I.a. The end conditions were such that sec-1 was completely free in all directions, sec-3 was constrained at the nodes against x and z displacements, and no rotations with respect to the y and z axes were permitted. No relative movements along the sides connecting two adjacent nodes were allowed.

Two loading conditions were used - the first a torque applied at the free end 'sec-1' Fig.I.b, and the second a bimoment idealized as four equal forces acting as shown in Fig.I.e at sec-1 as well.

Warping displacements in the x -direction obtained from the program are shown for both loading conditions at two sections 1 and 2 in Figs.I.c, I-d, I-f, I-g. It can be seen that the absolute values of warping displacements in the overhangs are always greater than those at the joint with the box, for both sections under both loading conditions.

This difference in distribution of the warping displacements in the overhangs should not significantly affect the girder's natural frequencies and modal shapes, since the effect of warping in boxes is generally small as compared to other effects. However, in some cases such as restrained warping the inadequacy of the theory might cause some undesirable results. It can be concluded that a re-examination of thin walled beam theory as given by Vlasov (40) is indicated in this case.

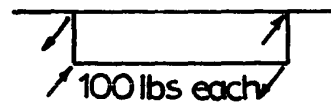


restricted rotations
at sec-3

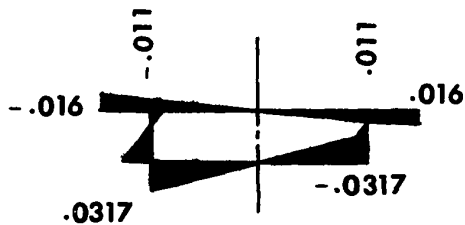
(a) Finite Element Idealization of a straight box girder. Cross-sectional dimensions are identical to those of Model A.



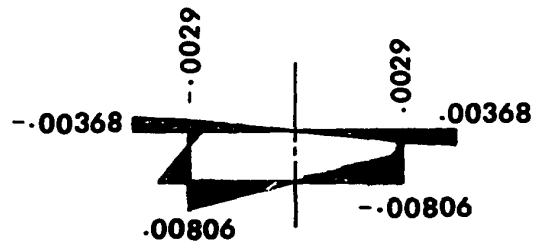
(b) Loading Condition 1
Torque



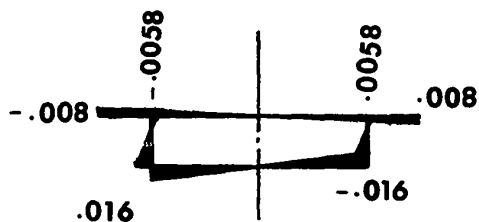
(e) Loading Condition 2
Bimoment



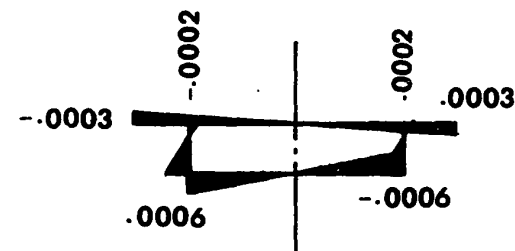
(c) Warping Displacement Sec-1



(f) Warping Displacement Sec-1



(d) Warping Displacement Sec-2



(g) Warping Displacement Sec-2

Fig.I Finite Element Analysis of warping displacements (in the x-direction) in a box girder with overhangs.

APPENDIX II

COMPUTER PROGRAM

```

C
C *****
C FREE VIBRATIONS OF CURVED THIN WALLED GIRDERS
C *****
C
C PURPOSE-CALCULATES NATURAL FREQUENCIES AND AMPLITUDES OF MODAL
C FUNCTIONS FOR A CIRCULARLY CURVED SIMPLY SUPPORTED GIRDER.
C THE CROSS SECTION CAN BE SOLID OR THIN WALLED ASYMMETRICAL
C UNISYMMETRICAL OR DOUBLY SYMMETRICAL W.R.T. CENTROIDAL
C AXES X & Y.
C
C ALPHABETICAL INDEX OF PARAMETERS
C
C A -CROSS SECTIONAL AREA
C ALFA -CENTRAL ANGLE IN DEGREES
C DPRQD -IBM'S SSP PACKAGE SUBROUTINE, FINDS ROOTS OF A POLYNOMIAL
C E -MODULUS OF ELASTICITY
C I -MODE NUMBER OR NUMBER OF SINE WAVES LONGITUDINALLY
C M -NUMBER OF MODES DESIRED
C QI -POLAR MOMENT OF INERTIA W.R.T. SHEAR CENTER
C PHI -TORSIONAL AMPLITUDE OF MODAL FUNCTION
C PI -POLAR MOMENT OF INERTIA W.R.T. CENTROID
C PIE -3.1415926535898
C POIS -POISSON'S RATIO
C R -RADIUS OF CURVATURE MEASURED TO CENTROID
C RD -MASS PER UNIT VOLUME OF MATERIAL IN USE
C RSW -AMPLITUDE OF RIGHT SUPPORT MOTION
C RX - $\int X*(Y**2)*DA/XI$ 
C RY - $\int Y*(X**2)*DA/YI$ 
C TK -ST-VENANT'S TORSION CONSTANT
C UU -HORIZONTAL AMPLITUDE OF MODAL FUNCTION
C VE -VERTICAL AMPLITUDE OF MODAL FUNCTION
C W(I,J) -ROOT J OF THE I-TH COUPLED NATURAL FREQUENCIES IN CYCLES
C PER SECOND
C WI -WARPING MOMENT OF INERTIA
C WT -UNCOUPLED TORSIONAL NATURAL FREQUENCY OF AN EQUIVALENT
C STRAIGHT GIRDER
C WU -UNCOUPLED HORIZONTAL NATURAL FREQUENCY OF AN EQUIVALENT
C STRAIGHT GIRDER
C WV -UNCOUPLED VERTICAL NATURAL FREQUENCY OF AN EQUIVALENT
C STRAIGHT GIRDER
C XI -MOMENT OF INERTIA W.R.T. A HORIZONTAL CENTROIDAL AXIS
C XO -X-COORDINATE OF SHEAR CENTER
C XYI -PRODUCT OF INERTIA W.R.T. AXES X&Y
C YI -MOMENT OF INERTIA W.R.T. A VERTICAL CENTROIDAL AXIS
C YO -Y-COORDINATE OF SHEAR CENTER
C
C IMPLICIT REAL*8(A-H,O-Z)
C DIMENSION CDF(4),US(4),Z(4),V(4),W(5,3),WUS(5),WVS(5),WTS(5)
C DATA PIE/3.1415926535898/
C READ(5,130)M
C READ(5,140)E,RD,POIS
C READ(5,140)R,ALFA
C READ(5,140)A,XI,YI,XYI

```

```

READ(5,140)XQ,YQ,RX,RY
READ(5,140)WI,TK,PI
WRITE(6,136)E,RQ,POIS
WRITE(6,137)R,ALFA
WRITE(6,138)A,XI,YI,XVI
WRITE(6,139)XQ,YQ,RX,RY
WRITE(6,141)WI,TK,PI
DPIE=2.*PIE
G=E/(2.*(1.+POIS))
SL=ALFA*PIE*R/(180.)
DI=PI+A*(XQ*XQ+YQ*YQ)
CO=1.-TK/PI
C1=XVI/XI
C2=XVI/YI
C3=RX/R
C4=RY/R
C5=XQ/R
C6=YQ/R
C7=(A*R*R)/PI
C8=1.+C7*(C5*C5+C6*C6)
DO 40 I=1,M
WUS(I)=0.
WVS(I)=0.
WTS(I)=0.
DO 40 J=1,3
W(I,J)=0.
40 CONTINUE
PRINT 132
PRINT 200
DO 90 I=1,M
C9=((DFLOAT(I))*PIE)/SL)**2
C10=1./(R*R*C9)
C11=1.-C10
C12=1.-C1*C2
C13=C7*C10
WUS(I)=(C9*C9*E*YI)/(RQ*A)
WVS(I)=(C9*C9*E*X1)/(RQ*A)
WTS(I)=C9*(G*TK+CO*C9*E*WI)/(RQ*DI)
RA1=WUS(I)/WVS(I)
RA2=WTS(I)/WVS(I)
CDF(1)=C8*C11*C11*(C3*C10-C1*C4*C10-C11*C12)*RA1*RA2
CDF21=C8*C11*C12*2.*C13*C5*C11*C12+C13*C2*C11*C3*C6-C13*C1*C11*C4*
a(C5+C10)-C13*C4*C6*C11+C10*C13*C11*C12+C13*C3*C11*(C5+C10)
CDF22=C8*C11*C11*(1.+C1*C6)-C8*C10*C11*(C3-C1*C6)
CDF23=C8*C11*(2.*C5-C6*C6+1.+(C8/C7))
CDF(2)=CDF21*RA1+CDF22*RA2+CDF23*RA1*RA2
CDF31=C2*C6*(C8-C7*C6*C6)+C7*C5*C6*C2*(1.+C10)-C7*C5*C6*(C6-C4*C10
a)+C13*C2*C6*C13*C6*(C6-C4)-C11*(C8-C7*C5*C5)
CDF32=C8*(1.+2.*C5*(C8/C7)-C6*C6)
CDF33=C7*C1*C5*C6-(C8-C7*C6*C6)-C13*(-C1*C6+2.*C5+C10+C3*(C5+C10))
CDF(3)=CDF31*RA1-CDF32*RA2+CDF33
CDF(4)=1.
CALL DPRQD(CDF,4,US,Z,V,3,IER)
DO 80 J=1,3

```

```

C      W(I,J)=(DSQRT(US(J)*WVS(I)))/DPIE
C
C      CALCULATION OF AMPLITUDES OF MODAL FUNCTIONS
C
      D11=C1*C11-C6*US(J)
      D12=-1.-(C8/C7)*RA2+US(J)
      D13=R*((-C8/C7)*RA2-C10*(1.+C3)+C1*C6*C10+(C6*C6-C3)*US(J))
      D21=C11*RA1-US(J)
      D22=-C2*RA1
      D23=R*(-C2+C6-C4)*C10*RA1+YD*US(J)
      D31=R*(C1*C10*C11-C6*US(J))
      D32=-R*((C8/C7)*RA2+C10+C5*US(J))
      D33=R*R*((C8/C7)*(-RA2+US(J))-C10*C10*(1.+C3-C1*C6))
      VE=1.
      PHI=VE*(D31*D22-D32*D21)/(D21*D33-D31*D23)
      UU=(-D22*VE-D23*PHI)/D21
      C14=1./(DSQRT(C9))
      RSW=UU*C14/R-PHI*C14*(XYI/(A*R*R)=C6)
      WRITE(6,210) I, W(I,J), VE, UU, PHI, RSW
80  CONTINUE
      DO 85 K=1,4
      CDF(K)=0.
      US(K)=0.
      Z(K)=0.
      V(K)=0.
85  CONTINUE
90  CONTINUE
      PRINT 220
      DO 100 I=1,M
      WU=(DSQRT(WUS(I)))/DPIE
      WV=(DSQRT(WVS(I)))/DPIE
      WT=(DSQRT(WTS(I)))/DPIE
      WRITE(6,250) I, WU, WV, WT
100 CONTINUE
130 FORMAT(I2)
132 FORMAT(1H1,T20,'ANALYSIS OF MODEL  A')
136 FORMAT(1H0,'E =' ,F 8.0,' PSI',2X,'DENSITY= ',F8.6,2X,'LB,SEC2/IN4'
      @ ,2X,'POIS= ',F4.2)
137 FORMAT(1H0,'RADIUS OF CURVATURE= ',F7.3,5X,'CENTRAL ANGLE= ',F6.2,
      @ ' DEGREES')
138 FORMAT(1H0,'A =' ,F 8.5,6X,'XI= ',F10.6,3X,'YI= ',F10.6,3X,'XYI= ',
      @ F8.6)
139 FORMAT(1H0,'XD= ',F8.6,5X,'YD= ',F9.6,4X,'RX= ',F8.6,6X,'RY= ',F8.
      @ 6)
140 FORMAT(4F15.6)
141 FORMAT(1H0,'WI= ',F10.6,3X,'TK= ',F10.6,3X,'PI= ',F10.6)
200 FORMAT(///1H0,'THE COUPLED NATURAL FREQUENCIES AND AMPLITUDES OF
      @MODAL FUNCTIONS',//2X,'MODE #',3X,'FREQUENCY CPS',3X,'VERT. AMPL.'
      @ ,2X,'HORIZ. AMPL.',3X,'TORS. AMPL.',2X,'R,S AXIAL DISPL.',//)
210 FORMAT(1H0,4X,12,5X,5(F10.5,4X))
220 FORMAT(///1H0,1X,'THE UNCOUPLED NATURAL FREQUENCIES OF AN EQUIVALE
      @NT STRAIGHT BRIDGE ',//1X,'MODE',3X,'HORIZ. FREQ. CPS',2X,
      @VERT. FREQ. CPS',4X,'TORS. FREQ. CPS')
250 FORMAT(2X,12,5X,3(F13.5,5X))
      STOP
      END

```